Flattening the slab: Farallon plate subduction and the Laramide orogeny

by

Sibiao Liu

A thesis submitted in partial fulfillment of the requirements for the degree of

Master of Science
in
Geophysics

Department of Physics
University of Alberta

Abstract

The Laramide orogeny (~80-50 Ma) was an anomalous period of mountain-building in the western United States that took place >1000 km inboard of the Farallon Plate subduction margin. The orogeny was preceded by the development of the Western Interior Seaway and eastward migration of the volcanic arc. Thus, it is believed that this marked a time of flat (subhorizontal) subduction. However, the factors that caused the Farallon Plate geometry to evolve from a steep geometry to flat subduction are not well-understood. Three mechanisms have been proposed: (1) a westward (trenchward) increase in North America plate motion, (2) an increased slab suction force owing to the presence of thick Colorado Plateau lithosphere, and (3) subduction of a buoyant oceanic plateau. This study uses 2D upper-mantle-scale numerical models to investigate these mechanisms. The models show that trenchward continental motion provides the primary control on subduction geometry, with decreasing slab dip as velocity increases. However, this can only create low-angle subduction, as the Farallon Plate was old (>100 Ma) and therefore much denser than the mantle. A transition to flat subduction requires: (1) subduction of a buoyant oceanic plateau which does not undergo eclogitization, and (2) a slab break-off at the landward side of the plateau. The break-off removes the dense frontal slab, and flat subduction develops as the oceanic plateau pulls the slab upward to a subhorizontal trajectory. These results are confirmed through a quantitative comparison of the models based on the slab dip and oceanic plate buoyancy. In the preferred model, the oceanic plateau is 400 km wide with 18 km thick metastable crust and an underlying

layer of depleted, harzburgitic mantle. With a continental velocity of 4 cm/yr, flat subduction develops within 14 Ma of plateau subduction. The flat slab segment underthrusts the continent at ~200 km depth and removes the lower ~40 km of the Colorado Plateau mantle lithosphere. It extends >1500 km inboard of the trench to underlie the Rocky Mountain foreland region, which was the locus of Laramide deformation. Overall, the models show that the Farallon Plate could have developed a flat slab geometry in the Late Cretaceous. This is also the first study to demonstrate the importance of a slab break-off in creating flat subduction of an old, dense oceanic plate.

Acknowledgements

It is with immense gratitude that I acknowledge the support and help of my supervisor, Dr. Claire Currie. The transition from a fresh undergraduate inquiring interesting things in Geoscience to a Master candidate keen on exploring more would not occur without her skillful guidance and encouragement. I am very privileged to work with Claire throughout my two years at University of Alberta. I would like to thank my supervisory committee: Dr. Vadim Kravchinsky, Dr. Moritz Heimpel, and Dr. Mauricio Sacchi, for reviewing my thesis and providing valuable comments. I also thank Huilin Wang, Juan Rosas and other colleagues for scientific discussions as well as sharing wonderful student life in UofA. A big thank-you to my family, especially my wife Lingxiu, without whose constant encouragement and support I would never go abroad and carry on chasing my dream.

Table of Contents

List of Tables

List of Figures

CHAPTER 1

Introduction

1.1 Subduction zones

Subduction zones are the largest recycling systems in the Earth and form the descending branch of the large-scale mantle convection system (Stern, 2002). At subduction zones, oceanic lithosphere covered with sediments descends into the mantle, modifying its composition. At the same time, subduction induces mantle melting and magmatism, and thus subduction zones are important locations of continental crust generation. Oceanic lithosphere forms at a mid-oceanic ridge. As the lithosphere moves away from the ridge, it cools and thickens, and its density increases due to thermal contraction. If the cold oceanic plate converges with a rigid continental plate or less dense oceanic plate, it will sink (subduct) into the hot mantle owing to its negative buoyancy (e.g., Turcotte and Schubert, 2002). During subduction, the descending lithosphere experiences higher pressures and temperatures, which induce metamorphic phase changes that further increase the density of the oceanic plate. Typically, the oceanic plate continues to subduct as long as the rocks remain denser than the adjacent mantle rocks at a given depth. Therefore, the descending plate can cross the transition zone (410-660 km depth) and penetrate into the lower mantle. The subduction zones in Central America and Central Japan are best-known examples of regions where the slab enters the lower mantle (e.g., Kárason and van der Hilst, 2000).

Most geodynamicists agree that the tectonic plates that cover Earth's surface move primarily as a result of lithosphere sinking at subduction zones (e.g., Davies and Richards, 1992). The oceanic plate is dense due to its cool temperature and metamorphic phase changes, creating the slab pull force as it descends. This is the most important force that

drives plate tectonics (e.g., Turcotte and Schubert, 2002). This body force transfers stress along the oceanic plate, causing the plate to move laterally. Furthermore, the interaction between the oceanic plate and the overlying plate can cause deformation of the overlying plate. For example, orogeny (mountain-building) is the result of compressive stresses in the overlying plate (e.g., Lallemand et al., 2005; Kearey et al., 2008).

Fig. 1.1 shows a schematic cross-section through a subduction zone in which an oceanic plate subducts below a continental plate (e.g., Turcotte and Schubert, 2002; Kearey et al., 2008). The seaward limit of a subduction zone is the trench, which marks the position where the subducting oceanic plate starts to descend into the mantle. In some cases, the trench is filled with sediments that have been scraped off the subducting plate and accreted to the edge of the continent. Another distinctive feature of a subduction zone is the volcanic arc. This is a chain of volcanoes that lies approximately parallel to the trench and is typically about 100 km above the surface of the subducted oceanic plate (Syracuse and Abers, 2006). The volcanic arc divides the subduction zone into the forearc (between the trench and arc) and backarc (the region landward side of the arc). Arc volcanism is generated through melting of the mantle wedge (the triangular region of mantle above the oceanic plate and below continental plate). As the oceanic plate subducts, hydrous minerals within the plate undergo metamorphism, which releases water into the overlying mantle. The addition of water lowers the solidus temperature of the mantle wedge, generating partial melt. It is generally believed that a temperature greater than 1200°C is needed for melting to occur (Schmitt and Poli, 1998). The melt then rises upward to form the volcanic arc (Grove et al., 2006). This process is how continental crust is generated at present day (e.g., Turcotte and Schubert, 2002).
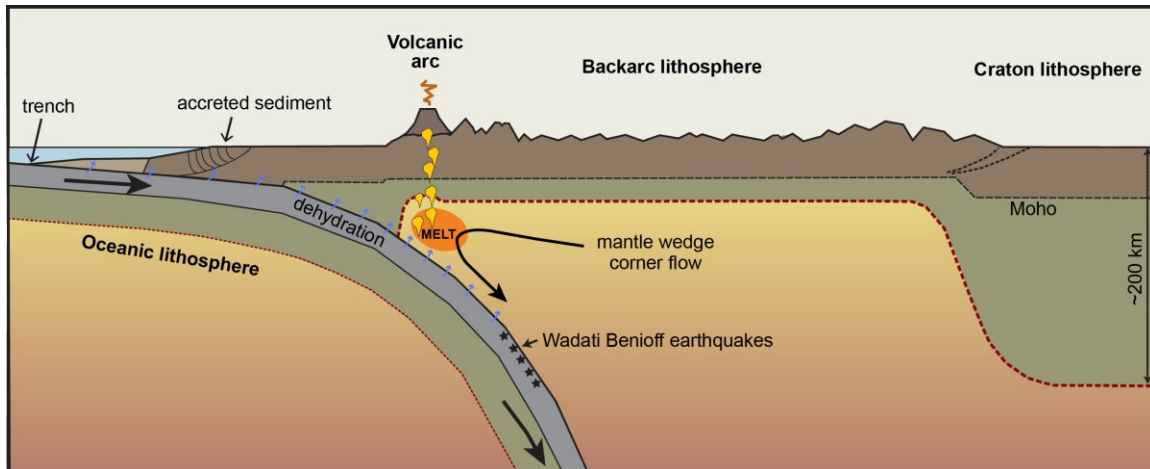
Fig. 1.1. Schematic cross-section through a subduction zone with a continental upper plate, showing the general features including the trench, volcanic arc, partial melting of hydrated mantle wedge, and the inclined Wadati-Benioff seismic zone.

The subduction zone system is the most extensive and pervasive feature of the Earth. The majority of modern subduction zones are located around the edge of the Pacific Ocean, with several other subduction zones in the Indian Ocean, Mediterranean and Atlantic Ocean (Fig. 1.2). In addition to playing a central role in plate tectonics and continental crust generation, subduction zones are also sites of societal hazards, such as explosive volcanism, large earthquakes and tsunamis. Examples of devastating earthquakes are the 1960 Chilean earthquake (Kanamori and Cipar, 1974), the 2004 Indian Ocean earthquake and tsunami (Lay et al., 2004), and the 2011 Tōhoku earthquake and tsunami (Ozawa et al., 2011). All of these are megathrust earthquakes, which occurred on the interface between the oceanic plate and overlying plate. Earthquakes can also occur within the interior of the oceanic plate, as a result of plate bending and metamorphism. These earthquakes form the Wadati-Benioff zone, which is an inclined band of earthquakes. The location of these earthquakes can be used to determine the geometry of the subducting plate in the upper mantle (e.g., Syracuse and Abers, 2006).
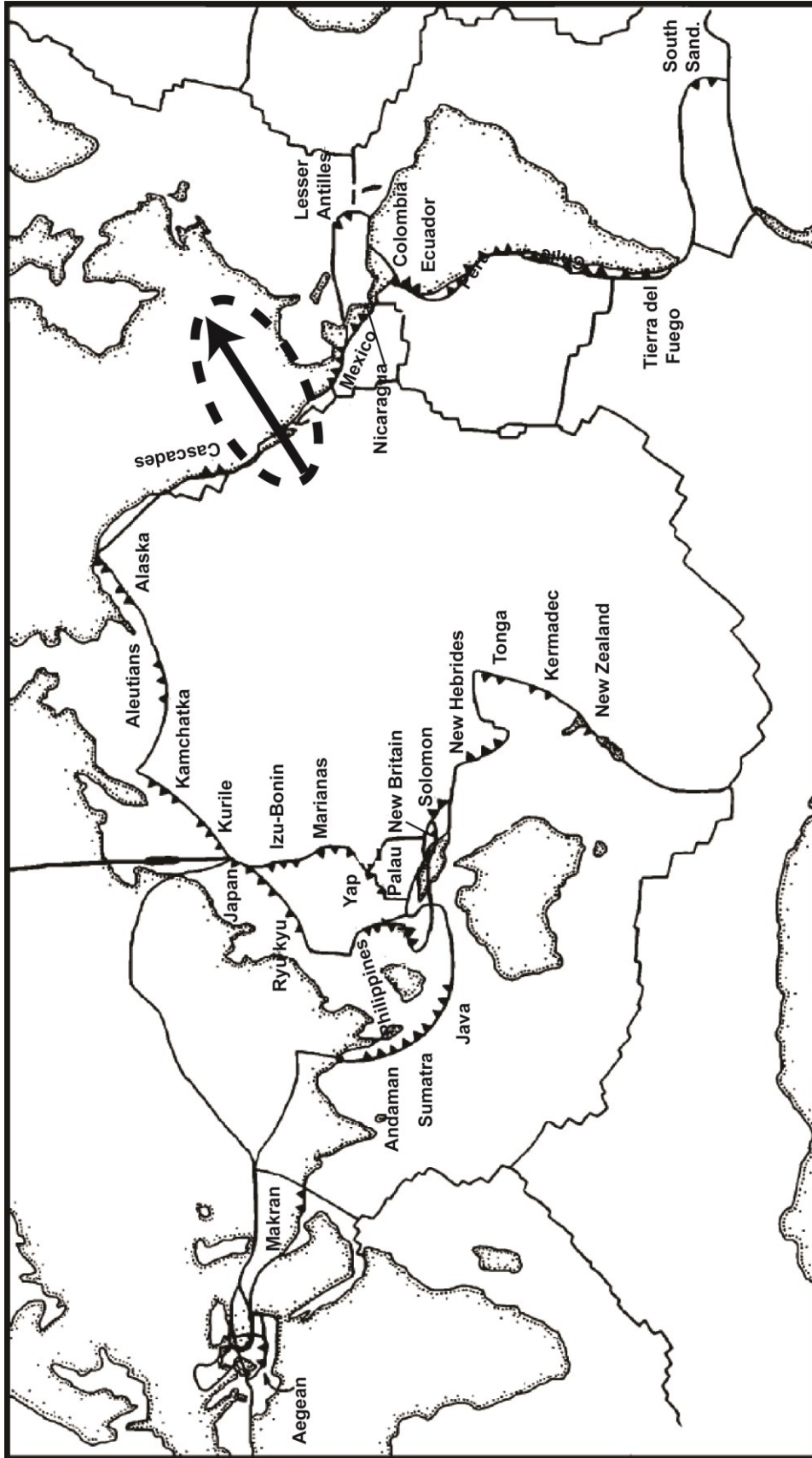
Fig. 1.2. Global distribution of major plate boundaries (lines) with present-day ubduction zones indicated by solid triangles on the over-riding plate (modified from Jarrad, 1986). The dashed ellipse and arrow indicate the former region of Farallon Plate subduction that is focus of this study.

This thesis addresses the factors that control the geometry of the subducting plate (or slab). As discussed above, oceanic plates tend to be negatively buoyant, and therefore they should descend into the mantle at a relatively steep angle. Fig. 1.3 shows the slab geometry at a number of subduction zones. The average slab dip is ~45° at 50-300 km depth (Turcotte and Schubert, 2002). However, there is significant variability between subduction zones. For example, the dip angle is greater than 70° in Marianas subduction zone, whereas it is less than 30° in several regions of western North and South America. There are also a few subduction zones in which the oceanic plate is subhorizontal at 50-100 km depth, such as the central Mexico subduction zone, the Peru and central Chile parts of the South America subduction zone, and the eastern Alaska subduction zone (Fig. 1.3). In some areas, the slab dip is correlated with the age of the oceanic plate, with a steeper dip where the plate is older. This is consistent with the idea that old plates are cooler and denser. This may explain the steep dip in the Marianas where the plate age is ~170 Ma. However, in other areas, the slab dip and age are not well correlated, indicating that slab dip is affected by other factors (e.g., Lallemand et al., 2005).
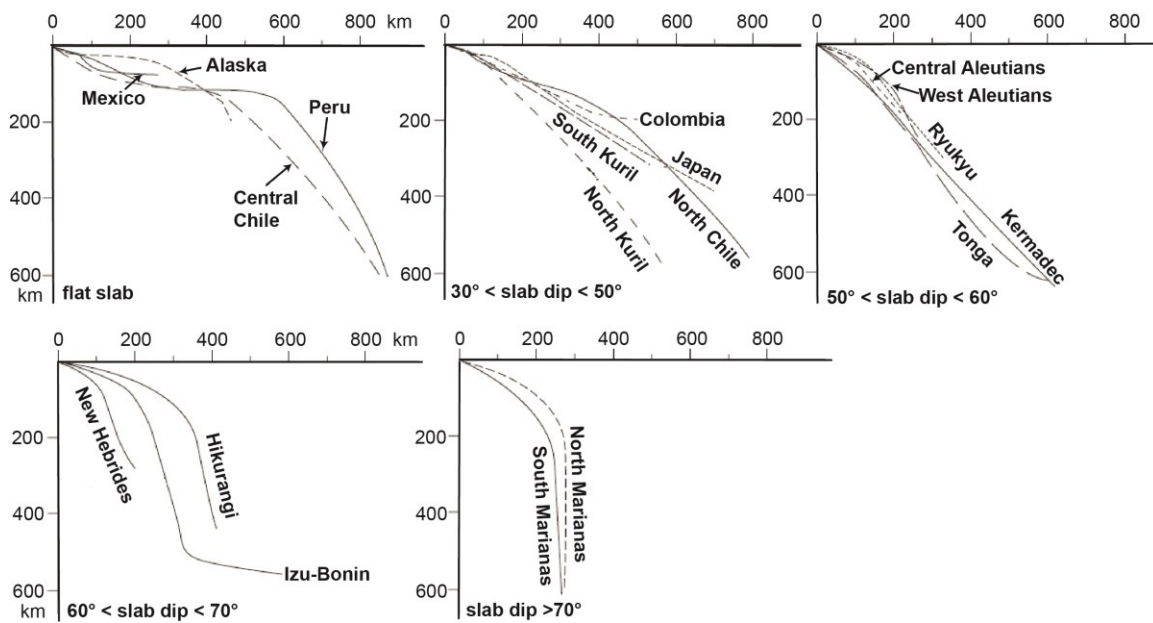
Fig. 1.3. Geometry of the top of the oceanic plate at subduction zones around the Pacific Ocean modified from Lallemand et al. (2005).

In previous studies, laboratory and numerical methods have been widely applied to determine the behavior of subducted oceanic lithosphere. Laboratory experiments on the structure of the slab have demonstrated the importance of density and viscosity changes in the mantle (i.e., the presence of the transition zone at 410-660 km depth), as well as properties of the slab (e.g., high viscosity, negative buoyancy) and the kinematics of the slab motion (e.g., subduction rate, trench migration) on the subduction dynamics (e.g., Guillou-Frottier, et al., 1995; Schellart, 2005). Analogue models of 3D subduction show a link between slab dynamics and the evolution of subduction-induced mantle flow around the slab edge, with potential implications for the source of intraplate volcanism (Strak and Schellart, 2014). 2D and 3D numerical models have also demonstrated that the slab geometry has a strong connection with the physical parameters of subduction zones (e.g., Christensen, 1996; van Hunen, et al., 2002b, 2004; Manea et al., 2012; Arrial and Billen, 2013).

In this thesis, the geometry of a subduction zone is characterized by the slab dip between 100 and 200 km depth: (1) steep or normal-angle subduction (dip>45°), (2) low-angle subduction (dip between 15° and 45°), and (3) flat or subhorizontal subduction (dip<15°). The angle of subduction influences the stress state and deformation in the overriding plate, as well as the location of the volcanic arc (e.g., Lallemand et al., 2005; Skinner and Clayton, 2011). A study of present-day backarc deformation shows that backarc extension is observed for slab dips greater than 50°, and conversely, backarc compression is commonly associated with shallower dips (Lallemand et al., 2005). In addition, a low-angle or subhorizontal slab is associated with a cooler mantle wedge, which can cause either migration of the volcanic arc away from the trench or the complete extinction of the arc (e.g., Chen and Moore, 1982; Manea et al., 2012).

It is estimated that approximately 10% of modern subduction zones exhibit a subhorizontal geometry (e.g., Jarrard, 1986; Gutscher et al., 2000). As shown below, there is also evidence that flat subduction has occurred in the past. The development of this geometry is puzzling, as it requires that the dense oceanic plate must first bend downward to enter the mantle and then unbend to form the flat geometry. One idea is that flat subduction at modern subduction zones may be due to the young age and

anomalously low density of the oceanic plates (e.g., van Hunen et al., 2004). However, this does not explain all flat-slab areas, and it is still not well-understood how flat subduction develops (e.g., van Hunen et al., 2004; Manea and Gurnis, 2007).

This thesis addresses the factors that lead to the development of flat subduction below the western United States (US) in the Late Cretaceous. In this area, the Farallon plate subducted beneath the North America Plate, creating the Laramide Orogeny (e.g., Dickinson and Snyder, 1978; Bird, 1988; Spencer, 1996). This was an anomalous period of mountain-building that started at ~80 Ma and produced deformation in Wyoming and adjacent regions. It is anomalous because the deformation took place more than 1000 km inboard of the Farallon subduction margin. It has been proposed that this orogeny was the result of flat/subhorizontal subduction of the Farallon plate (e.g., Dickinson and Snyder, 1978; Bird, 1988). Below, the geological history of the western US is briefly reviewed, and the evidence for flat-slab subduction is presented.

1.2 Western US subduction history

The North America continental plate is the product of a very long and ongoing geologic evolution that began early in the Archean. The core of North America is the ancient Laurentia craton. The stable craton occupies the majority of central North America, including Precambrian outcrops on the Canadian and Greenland Shields and their subsurface extension (Bally et al., 1989; Dalziel, 1992b). In the southwestern US, the craton and its cover have been deformed and are involved in local basement uplifts, such as Colorado Plateau, Rocky Mountain foreland and parts of Great Plains (e.g., Fig. 1.4; Spencer, 1996; English et al., 2003). The western edge of North America, from Alaska to Mexico, is an active plate margin, which comprises the North America Cordillera mountain chain (e.g., Bally et al., 1989; Oldow, et al., 1989; Dickinson, 2004).

Subduction of the Farallon plate below the western margin of North America began by the Early Jurassic (~180 Ma), transporting terranes to the continental margin and thus forming the Cordillera (e.g., Goes, 2013). The Farallon plate was a single continuous

plate along the entire margin until approximately 90 Ma, when it broke into two independent plates along an east-west fracture (Figge, 2009). The northern part became the Kula plate and the southern part is the Farallon plate. Both plates continued to subduct below North America (Fig 1.4). The Kula plate has since been completely subducted. The Farallon plate decreased in size as its western margin approached the subduction zone. At present, the last pieces of the Farallon plate can be found at the Cascadia subduction zone (the modern Juan de Fuca plate) and offshore Central America and South America (the modern Cocos and Nazca plates). The subducted Farallon plate can be observed in seismic tomography images of the mantle. These show that the plate has fragmented into several blocks that are found beneath northwestern Canada to the eastern USA (e.g., Bunge and Grand, 2000; Sigloch et al., 2008) and parts of the Farallon plate are in the lower mantle at depths of 800-2000 km (Sigloch and Mihalynuk, 2013).
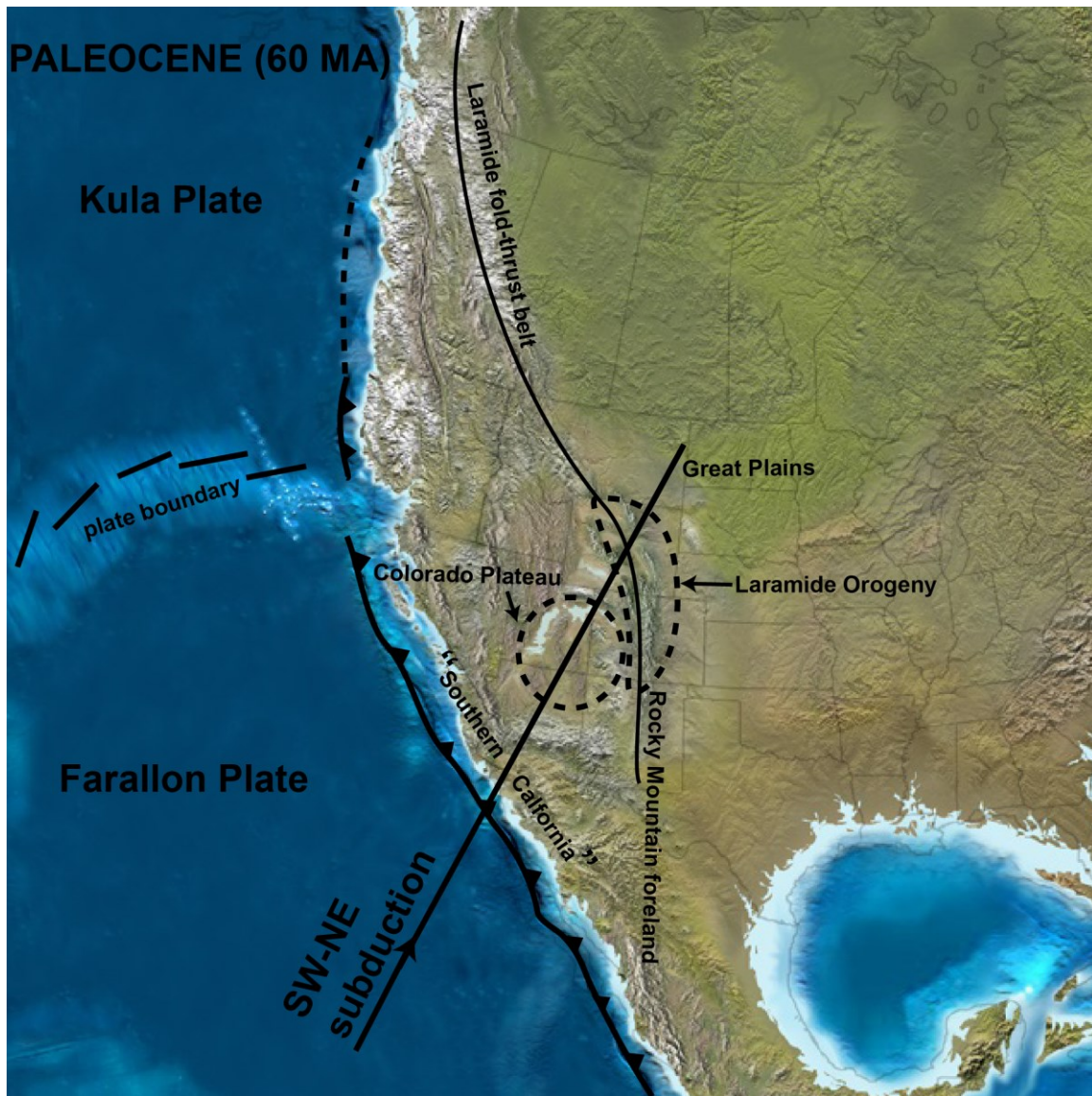
Fig. 1.4 Paleogeography and tectonic features associated with Farallon plate subduction at 60 Ma (the late stages of the Laramide Orogeny), based on the map of Ron Blakey (http://jan.ucc.nau.edu/~rcb7/nam.html). The solid line (with arrow) indicates the approximate location of the numerical models in this study.

Much of the continental deformation in the western US since 180 Ma is directly linked to Farallon plate subduction (e.g., Coney, 1978, Dickinson and Snyder, 1978; DeCelles, 2004). The Nevadan orogeny (~180-140 Ma) resulted in a narrow fold-and-thrust belt and foreland basin system from western Mexico through Alaska. This evolved into the Sevier orogeny, which produced thin-skinned deformation from southern Mexico to

northern Canada until the Late Cretaceous (e.g., Ward, 1995 and reference therein). A volcanic arc along the entire length of the margin was also formed during these orogenies (e.g., Coney and Reynolds, 1977; Chen and Moore, 1982). The crustal deformation and volcanism associated with the Nevadan-Sevier orogeny are consistent with normal (steep-angle) subduction (DeCelles, 2004).

The Laramide orogeny (80-50 Ma) marked a significant change in the style of deformation in western North America (e.g., DeCelles, 2004; English and Johnston, 2004; Jones, et al, 2011). In this orogeny, compressional deformation localized adjacent to the Great Plain region, more than 1000 km inboard of the plate boundary (Fig. 1.4); the previous orogenies were ~500 km closer to the plate margin. In addition, Laramide deformation is characterized by basement-core uplifts that involve much of the continental crust, as well as the overlying sedimentary cover (i.e., thick-skinned deformation). The overall orientation of Laramide shortening is northeast-southwest, which is subparallel to the direction of Farallon plate subduction below North America (Erslev, 1993; Bird, 1998). The orogeny was localized in the area northeast of the Colorado Plateau, which appears to be a strong block of continental crust (Saleeby et al., 2003). The Laramide block uplifts are the most dramatic features in the southern Rocky Mountain foreland. Here, the basement-involved deformation contrasts strongly with the Colorado Plateau that has little deformation (Fig. 1.4).

The Laramide orogeny coincides with a change in magmatism in western North America. During the Sevier orogeny, magmatism was localized in a narrow volcanic arc near the plate boundary (DeCelles, 2004). Igneous rock records indicate that the magmatic arc expanded eastward from the Aptian to Ypresian (~120-50 Ma) (Coney and Reynolds, 1977). In addition, several volcanic centers in California became extinct during this time. For example, isotopic dating of volcanism at the Sierra-Nevada batholith shows the cessation of volcanism at ~80 Ma (Chen and Moore, 1982). The Laramide orogeny and anomalous magmatism lasted until ~50 Ma. Following this, extensive volcanism occurred across much of the western US, including large-volume felsic eruptions (the "ignimbrite flare-up") at 50-20 Ma (e.g., Coney, 1978; Humphreys, 1995). The western US also

experienced widespread extension, which formed the Basin and Range extensional province from the Late Paleocene to late Middle Miocene (Dickinson, 2002).

In addition to the regional-scale Laramide orogeny, sedimentation records document continental-scale subsidence of North America, and the formation of the Western Interior Seaway starting at ~115 Ma (Currie and Beaumont, 2011). The sediment distribution is consistent with westward tilting of the North America plate, with a vertical deflection of 500-1000 m (not including sediment load) (e.g., Cross and Pilger, 1978; Mirovica et al., 1989; DeCelles, 2004). The seaway covered much of western North America until ~70 Ma and extended as far east as modern-day Lake Superior.

Fig. 1.5 summarizes the key events that occurred in the western US over the last 150 Ma, as well as the age of the Farallon plate and the velocities of the Farallon and North America plates during this time (Engebretson et al., 1984). The Farallon plate lithosphere age (at the trench) was >100 Ma throughout the Sevier orogeny and the first part of the Laramide orogeny. For the entire time period, North America has moved to the west in the hotspot reference frame. At ~120 Ma, just prior to the initiation of the Western Interior Seaway, absolute westward velocity of North increased to 3.5 cm/yr and then it increased again to nearly 5 cm/yr by ~65 Ma. At the same time, the convergence rate of the Farallon and North America plates increased. At 100 Ma, the convergence rate doubled, from 5 cm/yr to 10 cm/yr.
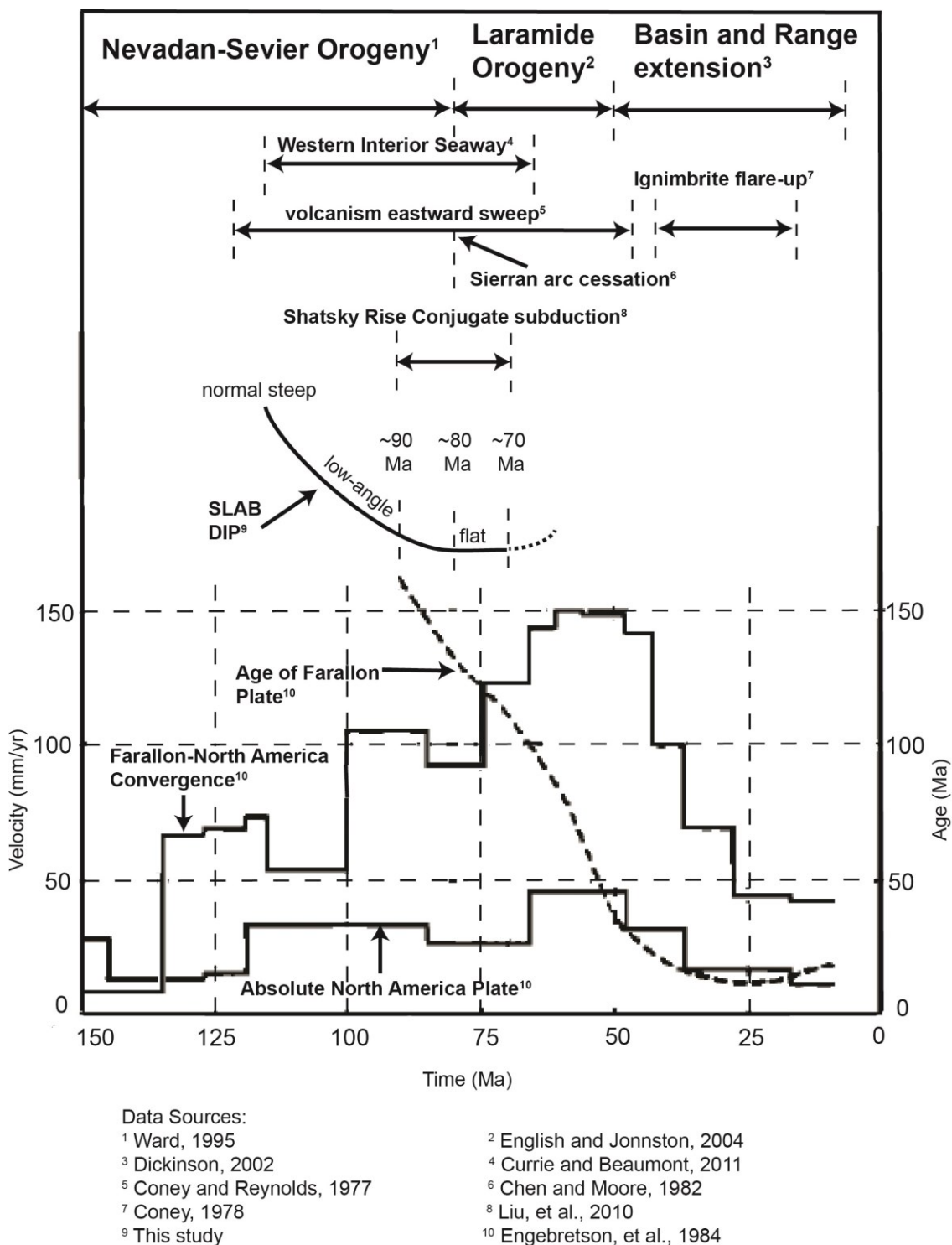
Fig. 1.5. Key geological events in the Western US over the last 150 Ma (top) and the margin-normal convergence rate of the Farallon and North America plates, absolute motion of North America, and Farallon Plate age (bottom). The variation in Farallon plate dip in the Late Cretaceous (middle) is discussed in this study.

1.3 Cause of the Laramide orogeny

Although the Laramide orogeny dominates the present-day geology of the western US, its origin is enigmatic. Various mechanisms have been proposed, including deformation associated with terrane accretion and a period of westward-directed subduction in the North America interior (e.g., Maxson and Tikoff, 1996; English and Johnston, 2004 and reference therein; Sigloch and Mihalynuk, 2013). However, most of these models can only explain one or two aspects of the geological record. The most widely accepted model is that the Laramide orogeny and contemporaneous events are the result of the Farallon plate geometry changing from a steep (normal) trajectory during the Sevier orogeny to a flat/subhorizontal geometry by the start of the Laramide orogeny (e.g., Coney and Reynolds, 1977; Dickinson and Snyder, 1978; Bird, 1988; Livaccari et al., 1981; DeCelles, 2004; Dickinson, 2004). Shallowing of the slab trajectory would have cooled the mantle wedge, which explains the eastward migration of the volcanic arc and the cessation of volcanism in California. As the shallowing slab came into contact with base of the continental lithosphere, the basal stress from plate convergence could have triggered deformation in the continental interior (e.g., Bird, 1988). This may have been localized in the Rocky Mountain foreland region by the presence of the strong Colorado Plateau block, as it was "pushed" to the northeast by the underlying flat slab (Saleeby et al., 2003). In addition, the Laramide deformation structures are similar to the modern-day Sierras Pampeanas block uplifts in northwest Argentina, which overlie a region where the Nazca plate flattens at 100 km depth (Kay and Abbruzzi, 1996). Furthermore, the spatial scale of the Western Interior Seaway is much larger than that of a typical foreland basin. Instead, it appears that this seaway is the result of an enhanced downward force on western North America by low-angle or flat subduction, rather than orogenic loading and plate flexure (e.g., Cross and Pilger, 1978; Mirovica et al., 1989; DeCelles, 2004). Finally, the post-Laramide ignimbrite flare-up has been interpreted to be the result of removal of a flat slab and rapid heating of the continental lithosphere (Humphreys, 1995).

If the hypothesis of Farallon flat-slab subduction is correct, it is necessary to consider the mechanism for generating a flat subduction geometry. During the proposed development of flat subduction, the Farallon plate age was >100 Ma (Fig. 1.5), and therefore this plate

should have been cool and dense. Three main factors have been proposed to explain the development of flat-slab subduction (Fig. 1.6, see Chapter 3 for more details):

(1) **The westward (trenchward) increase in North America motion**. Plate reconstructions show an increase in the convergence rate between North America and the Farallon plate and a modest increase in the westward motion of North America during the Late Cretaceous (Fig. 1.4; Engebretson et al, 1984). As a result of trenchward continental motion, the trench would move toward the oceanic plate, while the deeper oceanic plate was "anchored" in the mantle. This could cause a decrease in the angle of subduction.

 (2) **An increased slab suction force owing to the presence of thick Colorado Plateau lithosphere**. Geological observations indicate that, prior to the Laramide orogeny, the Colorado Plateau had a thicker and stronger lithosphere than the adjacent regions (e.g., Spencer, 1996). This would have acted as a partial barrier to mantle wedge flow associated with subduction, resulting in a decreased pressure in the mantle wedge corner (O'Driscoll et al., 2009). The pressure could be further decreased by a high mantle wedge viscosity. The low pressure would induce an upward force on the oceanic plate (slab suction) and may have lifted it to a flat geometry. Note that this would also create a downward force on the over-lying continent; Mitrovica et al. (1989) suggested that this is what caused the development of the Western Interior Seaway.

 (3) **Subduction of a low-density oceanic plateau**. Geological reconstructions and seismic tomography data suggest that during Farallon Plate subduction, an oceanic plateau, called the Shatsky Rise conjugate, was subducted below California and the Colorado Plateau between 90 and 70 Ma (e.g., Livaccari, et al., 1981; Liu et al., 2010; Fig. 1.5). An oceanic plateau is characterized by the thick basaltic crust generated by enhanced mantle melting, and as a result the plateau lithosphere has a lower average density than typical oceanic lithosphere (e.g., van Hunen et al., 2002b). The reduced negative buoyancy of this part of the oceanic plate may result in flat subduction.
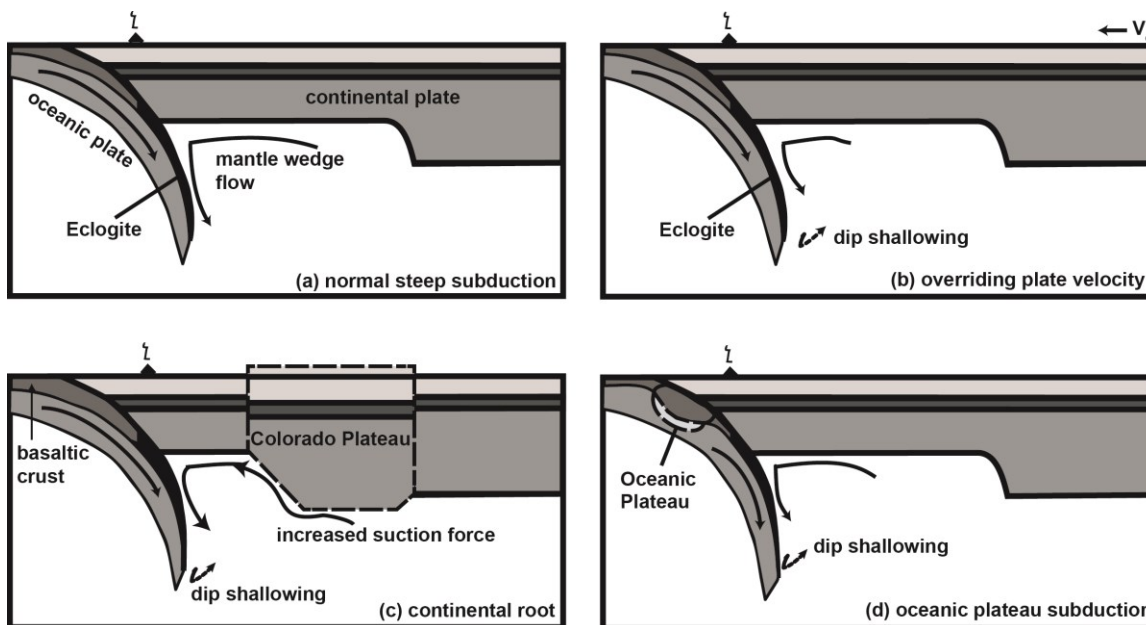
Fig. 1.6. Schematic diagrams for subduction of the Farallon plate below the western US in the Late Cretaceous: (a) normal steep subduction, (b) subduction with overriding plate trenchward motion, (c) subduction with thick Colorado Plateau lithosphere, and (d) subduction of a buoyant oceanic plateau.

1.4 Thesis objectives

In this thesis, numerical models are used to explore the subduction dynamics of the Farallon Plate before and during the first part of the Laramide orogeny (~90 Ma to ~70 Ma). The objectives are:

- To complete a systematic examination of the three mechanisms that have been proposed for generating flat-slab subduction (continental trenchward motion, high slab suction force and oceanic plateau subduction).

- To assess whether it is possible to create a flat-slab geometry for the Farallon Plate prior to the Laramide orogeny, using parameters that are consistent with western US tectonics at this time.

It should be noted that previous geodynamic modeling studies of flat-slab subduction focus on a relatively young (<50 Ma) subducting plate (e.g., van Hunen et al., 2002a,

2002b, 2004; Manea and Gurnis, 2007; Arrial and Billen, 2013). This is because flat subduction for the modern Earth occurs in areas with young plates (e.g., Lallemand et al., 2005). It is typically assumed that old oceanic plates, such as the Farallon plate (age >100 Ma), are cool and dense, and therefore they will descend steeply into the mantle. To date, there have been no detailed numerical modeling studies that address the development of the Farallon flat slab, although there have been models which use this geometry as a boundary condition for understanding the associated continental deformation (Bird, 1988) and oceanic plate dehydration (Currie and Beaumont, 2011). Therefore, this is the first study to address this important problem.

1.5 Thesis outline

This thesis is organized as follows:

- Chapter 2 reviews the numerical modeling method (the SOPALE finite element code) and presents the governing equations, model geometry and material properties, and boundary conditions of the models. The three phases of each model run are also described.

- Chapter 3 presents the numerical model results, with a detailed description of 40 models. These models investigate the effect of the individual factors (continental velocity, slab suction, oceanic plateau) on slab geometry, as well as combinations of these factors. It is demonstrated that in order to achieve a flat-slab geometry for an old oceanic plate, it is necessary for a slab break-off to occur.

- Chapter 4 discusses the model results in order to constrain the conditions needed to create flat-slab subduction. This includes a quantitative comparison of the models based on subduction dip angle and oceanic plate buoyancy to understand the relative importance of different parameters. The preferred flat-slab model for Farallon Plate subduction is presented and linked with geological observations for the western US. Limitations of the numerical models are also discussed.

- Chapter 5 gives the conclusions of this thesis and suggestions for future work.

CHAPTER 2

Numerical modeling method

2.1 Modeling approach and governing equations

The numerical models in this study address the dynamics of continental margin arc-trench systems, in which an oceanic plate (Farallon Plate) subducts beneath continental lithosphere (southwestern North American Plate). The goal of this work is to address the controls on subducting plate dynamics and specifically, to determine the conditions under which flat (subhorizontal) subduction may develop, as has been proposed for the Laramide subduction orogeny (e.g., Coney and Reynolds, 1977; Dickinson and Snyder, 1978; Bird, 1988). In this chapter, we introduce the numerical model method and the initial model setup. This section discusses the governing equations and numerical method. In section 2.2, the model geometry is presented. The material properties and model boundary conditions are given in Sections 2.3 and 2.4, respectively. Section 2.5 describes the modeling steps.

The regional, upper-mantle-scale numerical models are two-dimensional vertical cross-sections through a subduction zone. The thermal-mechanical evolution of the lithosphere-upper mantle system is calculated using the assumptions of 2D plane stain (i.e., no material deformation perpendicular to the plane of the model), incompressibility (except during metamorphic phase changes, see below) and a Reynolds number of zero. The Reynolds number is defined as the ratio of inertial forces to viscous forces in the fluid (e.g., Kundu et al., 2011). When the Reynolds number is greater than a critical Reynolds number (e.g., ~2040 for pipe flow from Kanda, 2007), the turbulent flow occurs and is dominated by inertial forces. Conversely, the laminar flow occurs at low Reynolds numbers smaller than the critical Reynolds number, where viscous forces are dominant. For the lithosphere-upper mantle system, material viscosities are high ($>10^{19}$ Pa s),

and therefore viscous forces are dominant (Reynolds number of ~0) and the system can be modeled as a creeping viscous flow (Fullsack, 1995).

Material deformation is governed by the equations of volume conservation when incompressible (mass conservation when compressible during metamorphic phase changes) and force balance:

$$\frac{\partial v_j}{\partial x_j} = 0 \qquad (2.1)$$

$$\frac{\partial \sigma_{ij}}{\partial x_i} + \rho g = 0; \quad i,j = 1,2 \qquad (2.2)$$

where $x_{i,j}$ are spatial coordinates, v_i and v_j are components of velocity, ρ is density, and g is vertical gravitational acceleration. Repeated indices indicate summation. The associated stress tensor is:

$$\sigma_{ij} = -P\delta_{ij} + \sigma'_{ij} = -P\delta_{ij} + 2\eta_{eff}\dot{\varepsilon}_{ij} \qquad (2.3)$$

where P is the dynamical pressure (mean stress), σ'_{ij} is the deviatoric stress tensor, η_{eff} is effective viscosity, δ_{ij} is the Kronecker delta (1 for i=j and 0 otherwise), and the strain rate tensor is:

$$\dot{\varepsilon}_{ij} = \frac{1}{2}\left(\frac{\partial v_i}{\partial x_j} + \frac{\partial v_j}{\partial x_i}\right) \qquad (2.4)$$

The thermal evolution is calculated by solving the energy balance equation:

$$\rho c_p \left(\frac{\partial T_K}{\partial t} + v_i \frac{\partial T_K}{\partial x_i}\right) = k \frac{\partial}{\partial x_i}\frac{\partial T_K}{\partial x_i} + A + \sigma'_{ij}\dot{\varepsilon}_{ij} + v_2 \alpha g T_K \rho \qquad (2.5)$$

where c_p is specific heat, T_K is absolute temperature in degrees Kelvin, t is time, k is thermal conductivity, A is volumetric radioactive heat production, α is thermal expansion coefficient per unit volume and v_2 is vertical velocity. The third term on the right-hand side of Equation 2.5 (product of the deviatoric stress tensor and strain rate tensor) corresponds to shear heating, assuming that dissipated mechanical energy associated with deformation is completely converted to heat. The last term on the right-hand side of Equation 2.5 is a temperature correction for adiabatic heating for vertical velocity v_2.

These equations are solved using the SOPALE finite element computer code, which computes the mechanical flow of viscous-plastic materials in the creeping flow limit and the temperature field of the system (Fullsack, 1995). Material deformation is driven by applied kinematic boundary conditions and internal buoyancy forces. The thermal field is coupled to the mechanical field through the strain heating term, the temperature-dependence of mechanical material properties (e.g., density and viscous rheology), and by the redistribution of radioactive heat-producing materials during deformation. In the calculations, a time step of 2000 years is used. This time step length is short enough to ensure model stability, but long enough so that models run in a reasonable time. For example, a model run of 30 Ma (in geological time; Ma is millions of years) requires 15,000 time steps and takes approximately 45 hours of real-time on the Westgrid Orcinus computer.

The SOPALE code has been widely applied to study the coupled thermal-mechanical behavior of the crust and upper mantle on time scales typical of subduction and orogenesis, i.e., 10^4-10^8 years (e.g., Fullsack, 1995; Beaumont et al., 2006; Currie et al., 2007; Currie and Beaumont, 2011; Krystopowicz and Currie, 2013). It has also been fully benchmarked for numerical accuracy in applications related to lithosphere dynamics (Fullsack, 1995; Pysklywec et al., 2002; Buiter et al., 2006). The SOPALE code uses the arbitrary Lagrangian-Eulerian (ALE) technique. The governing equations (Equations 2.1, 2.2 and 2.5) are solved on an Eulerian grid, which is held fixed horizontally and has an upper surface which can stretch vertically as topography develops. Material properties and their history (e.g., pressure, temperature, accumulated deformation) are tracked using a Lagrangian mesh, with additional injected Lagrangian tracer particles. The Eulerian velocity field is used to advect the Lagrangian mesh, thus allowing material to be redistributed in the model domain. In turn, the Lagrangian particles are used to update the Eulerian material properties (density, rheology, etc.) for computation of the thermal-mechanical field at the next time step. The advantage of this approach is that large amounts of distortion (deformation) can be modeled at a relatively low computational expense. Another advantage is that a stress-free upper surface can be used in the models, allowing the natural development of topography. Full details of SOPALE are given by Fullsack (1995) and Beaumont et al. (2006).

2.2 Model geometry

This study focuses on the dynamics of low-angle subduction in a situation that is analogous to southwestern United States in the time prior to the Laramide Orogeny. The model parameterization is intentionally simplified so that it contains the first-order features of this region during the timeframe of interest. We use a layers structure to construct the oceanic and continental lithospheres and impose fixed plate velocity fields at the model boundaries. The possible effects of these choices, as well as limitations of key model assumptions (e.g., the 2D nature of the models) are addressed in Chapter 4.

The model domain has a width of 2500 km and extends from the Earth's surface to a depth of 660 km (Fig. 2.1). The long axis is oriented approximately parallel to the direction of convergence between the North America and Farallon plates during the Laramide orogeny. The Eulerian mesh has 250 elements horizontally (10 km width) and 100 elements vertically, with 20 elements in the upper 60 km (3 km height), 40 elements in the middle 200 km (5 km height) and 40 elements in lower 400 km (10 km height). In the models, the oceanic plate is injected into the model domain (i.e., Eulerian grid) at its left-hand side. Therefore, the right-hand side of the Lagrangian mesh is coincident with the right boundary of the Eulerian mesh, but it extends to the left of the Eulerian grid. The Lagrangian mesh has a width of 12500 km and height of 660 km and initially, the node spacing is 3 times smaller than that of the Eulerian nodes.

The thickness of oceanic lithosphere is 90 km, including a 9 km oceanic crust. This thickness is consistent with the >100 Ma Farallon plate age prior to Laramide time (Engebretson et al., 1984). The 9 km crustal thickness accounts for a normal oceanic crustal thickness of 7 km (e.g., White et al., 1992; Cloos, 1993) and an additional 2 km of sedimentary cover, which is taken to have the same properties as the crust. This thickness ensures that the crust fills an integral number of Eulerian elements (i.e., 3 km/element). The plate boundary between the oceanic and continental plates is set at 300 km from the edge of the model domain. To aid subduction initiation, a rheologically weak zone (white seed in Fig. 2.1) is placed in the oceanic mantle lithosphere at the margin between the oceanic and continental plates.

The continental plate is divided into four horizontally-adjacent regions which are analogous to the structure of southwestern United States: (1) Southern California region (SC), which is

adjacent to the plate margin with a width of 500 km (Saleeby, 2003); (2) Colorado Plateau (CP) region with 600 km width (Roy et all, 2009); (3) Rocky Mountains (RM) and (4) Great Plains (GP). RM and GP have widths of 400 km and 700 km respectively (Erslev, 2005).

The SC region comprises Phanerozoic lithosphere with a total thickness of 120 km. This is consistent with estimates of the lithosphere thickness in this region, based on isotopic and geological data of lithosphere structure for the Sevier-Laramide orogeny (Livaccari and Perry, 1993). The 120 km thick lithospheric mantle consists of 24 km upper-mid crust, 12 km lower crust and 84 km mantle lithosphere (Mooney and Weaver, 1989; Zandt et al., 1995). The layering (i.e., two-layer crust) is designed to approximate the typical continental crust, with a refractory, intermediate granulite lower crust overlain by an upper-mid crust dominated by quartz-rich sedimentary and metasedimentary rocks with high pore fluid pressure (e.g., Beaumont et al., 2006).

The Colorado Plateau region is distinct from the regions on either side. Whereas these adjacent areas were deformed during the Sevier-Laramide orogeny, the Colorado Plateau remained relatively undeformed (e.g., Bird, 1979; Morgan and Swanberg, 1985; Spencer, 1996). It has been suggested that this is due to a greater lithosphere thickness and hence cooler, stronger lithosphere at the Colorado Plateau (e.g., Spencer, 1996; Humphreys, 2009). The greater lithosphere thickness is supported by thermobarometry observations of mantle xenoliths which show a ~>200 km thick lithosphere before Laramide modification (e.g., Grand and Helmberger, 1984; Smith and Griffin, 2005; Li et al., 2008). In addition, the Colorado plateau has a thicker crust than adjacent regions, with seismic studies indicating a crust more than 40 km thick (e.g.,Wolf and Cipar, 1993; Wilson et al., 2005). In the models, the CP lithosphere has a total thickness of 240 km thick. This is consistent with the xenolith-based estimates of lithosphere thickness, and with a recent study on the effects of deep continental roots on mantle flow in this area (O'Driscoll et al., 2009). The upper-mid crust is 30 km thick and the lower crust is 15 km thick, giving a total crustal thickness of 45 km (e.g., Wolfe and Cipar, 1993; Parsons et al., 1996; Spencer, 1996; Griffin et al., 2004). The deep continental root may promote continental compression and mantle-wedge suction (O'Driscoll et al., 2009). The effects of thick CP lithosphere on the dynamics of the subducting slab will be tested in our models.

The last two continental domains are RM and GP. The RM domain represents the area which underwent shortening during the Laramide orogeny, while the GP remained relatively undeformed (Erslev et al., 1993). In the models in this study, these regions have the same lithosphere structure and properties; they are separated in the models so that future studies can use this model geometry to investigate Laramide deformation. RM and GP have a 36 km thick crust (24 km upper-mid crust; 12 km lower crust), as in the SC area. A total lithosphere thickness of 200 km is used (164 km mantle lithosphere), under the assumption that these areas are part of the Archean-Proterozoic core of North America (e.g., Griffin et al., 2004). As these regions are >1000 km from the subduction zone, their lithosphere thickness has little effect on mantle wedge pressures or slab dynamics. However, future work should assess how variations in lithosphere thickness affect the susceptibility of the RM and GP to subduction-related deformation.
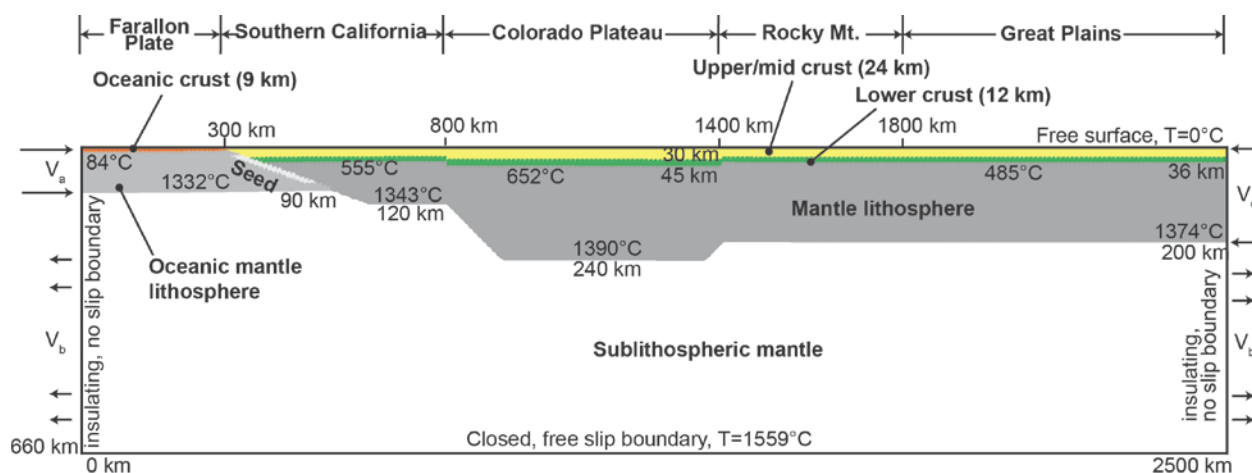
Fig. 2.1 Initial model geometry and the thermal-mechanical boundary conditions. V_a and V_c are influx velocities for the oceanic plate and continental plate respectively. These are balanced by a uniform outflux velocity (V_b) for the sublithospheric mantle in order to maintain mass balance in the model domain. SC, CP, RM and GP denote the South California, Colorado Plateau, Rocky Mountains and Great Plains regions of the continental plate.

2.3 Model material properties

2.3.1 Mechanical properties

In the finite element models, all materials have a viscous-plastic rheology. Frictional-plastic deformation is modelled with a pressure-dependent Drucker-Prager yield criterion:

$$(J_2')^{1/2} = P \sin \varphi_{eff} + C_0 \cos \varphi_{eff} \qquad (2.6)$$

where J_2' is the second invariant of the deviatoric stress tensor ($J_2' = \frac{1}{2}\sigma_{ij}'\sigma_{ij}'$), P is the dynamic pressure (mean stress), C_0 is the cohesion and the effective internal angle of friction, φ_{eff}, is defined to include the effects of pore fluid pressure through the relation $P \sin \varphi_{eff} = P(1 - \lambda) \sin \varphi$, where λ is the pore fluid pressure ratio ($\lambda = P_f/P$, where P_f is the pore fluid pressure) and φ is the dry coefficient of friction (e.g., Huismans and Beaumont, 2003). For hydrostatic fluid pressures, φ_{eff} is approximately 15°, based on Coulomb wedge and crustal modeling (e.g., Dahlen, 1984; Beaumont et al., 1996; Pysklywec and Beaumont, 2004). Frictional-plastic deformation is modeled by defining an effective viscosity which places the state of stress on yield (Fullsack, 1995; Willett, 1999; Beaumont et al., 2006). Strain softening is included by decreasing the value of φ_{eff} linearly from 15° to 2° (Table 2.1) as the accumulated strain increases from 0.5 to 1.5, following values used in previous studies (e.g., Beaumont et al., 2006; Huismans and Beaumont, 2003; Warren et al., 2008).

Where the deviatoric stress is less than the frictional-plastic yield stress, the flow is viscous with an effective viscosity (η_{eff}) given by:

$$\eta_{eff} = f(B^*)\dot{I}_2'^{(1-n)/2n} exp\left(\frac{Q+PV^*}{nRT_K}\right) \qquad (2.7)$$

where f is a scaling factor, R is the gas constant (8.3145 J mol^{-1} K^{-1}), and B*, n, Q and V* are the pre-exponential viscosity parameter, stress exponent, activation energy and activation volume, respectively, based on laboratory experiments. Note that the B* is derived by converting the pre-

exponential factor from uniaxial laboratory conditions (A*) to the 2D, plain-strain conditions in the models (e.g., Ranalli, 1987):

$$B^* = 2^{(1-n)/n}3^{-(n+1)/2n}A^{*-1/n} \quad (2.8)$$

The viscous rheologies used in the numerical models are based on a reference set of well-constrained laboratory experimental results. We then use the scaling factor (f) to linearly scale the effective viscosity up/down relative to the reference rheology value, as a means of approximating variations in strength owing to minor changes in composition or water content, or uncertainties in the rheological parameters. This approach allows reasonable variations in material strength, while reducing the complexity of the model input. Our model rheology parameters are given in Table 2.1 and are the same as those used in previous studies (e.g., Huismans and Beaumont, 2003; Beaumont et al., 2006; Warren et al., 2008; Currie and Beaumont, 2011; Krystopowicz and Currie, 2013). The upper-mid continental crust uses a wet quartzite rheology (WQ, Gleason and Tullis, 1995) with f=5, assuming that the shallow crust is drier and less silicic than WQ. The oceanic crust and continental lower crust have a viscous rheology based on dry Maryland diabase (DMD, Mackwell et al., 1998) with f=0.1, to approximate a composition that is somewhat more hydrated than dry diabase. All mantle materials have a wet olivine rheology (Karato and Wu, 1993), with f=1 for the sublithospheric mantle and f=10 for the continental and oceanic mantle lithosphere. It is assumed that the sublithospheric mantle is fertile and hydrated, whereas the mantle lithosphere has undergone dehydration and melt depletion during formation. Experimental data shows that dry olivine is 5-10 times more viscous that wet olivine (Hirth and Kohlstedt, 2003).

Table 2.1. Material properties used in initial models.

	Continental plate								
	Upper-mid Crust			**Lower Crust**			**Lithospheric mantle**		
	SC	**CP**	**RM &GP**	**SC**	**CP**	**RM& GP**	**SC**	**CP**	**RM& GP**
Plastic rheology									
C_o (MPa)	20	20	20	0	0	0	0	0	0
φ_{eff}	15-2°	15-2°	15-2°	15-2°	15-2°	15-2°	15-2°	15-2°	15-2°
Viscous rheology									
f	5	5	5	0.1	0.1	0.1	10	10	10
$A^*(Pa^{-n}s^{-1})$	1.10×10^{-28}	1.10×10^{-28}	1.10×10^{-28}	5.05×10^{-28}	5.05×10^{-28}	5.05×10^{-28}	3.91×10^{-15}	3.91×10^{-15}	3.91×10^{-15}
$B^*(Pa^{-n}s^{-1})$	2.92×10^{6}	2.92×10^{6}	2.92×10^{6}	1.91×10^{5}	1.91×10^{5}	1.91×10^{5}	1.92×10^{4}	1.92×10^{4}	1.92×10^{4}
n	4.0	4.0	4.0	4.7	4.7	4.7	3.0	3.0	3.0
$Q(kJ\,mol^{-1})$	223	223	223	485	485	485	430	430	430
$V^*(cm^{3}\,mol^{-1})$	0	0	0	0	0	0	10	10	10
Thermal parameters [1]									
$k(W\,m^{-1}K^{-1})$ [2]	2.25	2.25	2.25	2.25	2.25	2.25	2.25	5.57	3.89
$A(\mu W\,m^{-3})$	1.2	0.9	0.9	0.4	0.2	0.2	0	0	0
$c_p(J\,kg^{-1}K^{-1})$	750	750	750	750	750	750	1250	1250	1250
$Q_s(mW\,m^{-2})$	54.7	51.1	45.1						
Density									
$\rho_o(kg\,m^{-3})$	2800	2800	2800	2900	2900	2900	3250	3250	3250
$T_o(°C)$	200	200	200	500	500	500	1340	1340	1340
Eclogite $\rho_o(kg\,m^{-3})$	-	-	-	-	-	-			
Eclogite $T_o(°C)$	-	-	-	-	-	-			
$\alpha(K^{-1})$	3.0×10^{-5}	3.0×10^{-5}	3.0×10^{-5}	3.0×10^{-5}	3.0×10^{-5}	3.0×10^{-5}	3.0×10^{-5}	3.0×10^{-5}	3.0×10^{-5}

[1] k, A, c_p and Q_s are thermal conductivity, radioactive heat production, specific heat and surface heat flow, respectively
[2] Thermal conductivity at temperature below 1340°C; at high temperatures, k increases linearly from 2.25 W $m^{-1}K^{-1}$ to 52.75 $Wm^{-1}K^{-1}$ at 1380°C

Table 2.1. Continued.

	Oceanic plate		Sublithospheric mantle
	Crust	Lithospheric mantle	
Plastic rheology			
C_o (MPa)	0	0	0
φ_{eff}	15-2°	15-2°	15-2°
Viscous rheology			
f	0.1	10	1
$A^*(Pa^{-n}s^{-1})$	5.05×10^{-28}	3.91×10^{-15}	3.91×10^{-15}
$B^*(Pa^{-n}s^{-1})$	1.91×10^{5}	1.92×10^{4}	1.92×10^{4}
n	4.7	3.0	3.0
$Q(kJ\,mol^{-1})$	485	430	430
$V^*(cm^3\,mol^{-1})$	0	10	10
Thermal parameters [1]			
$k(W\,m^{-1}K^{-1})$[2]	2.25	1.37	52.75
$A(\mu W\,m^{-3})$	0	0	0
$c_p(J\,kg^{-1}K^{-1})$	750	1250	1250
$Q_s(mW\,m^{-2})$	21.1		
Density			
$\rho_o(kg\,m^{-3})$	2950	3250	3250
$T_o(°C)$	0	1340	1340
Eclogite $\rho_o(kg\,m^{-3})$	3350		
Eclogite $T_o(°C)$	500		
$\alpha(K^{-1})$	3.0×10^{-5}	3.0×10^{-5}	3.0×10^{-5}

[1] k, A, c_p and Q_s are thermal conductivity, radioactive heat production, specific heat and surface heat flow, respectively
[2] Thermal conductivity at temperature below 1340°C; at high temperatures, k increases linearly from 2.25 W m^{-1}K^{-1} to 52.75 Wm^{-1}K^{-1} at 1380°C

2.3.2 Thermal properties

The thermal parameters for each material are given in Table 2.1 and are all within the range expected for crustal and mantle materials (e.g., Jaupart and Mareschal, 2003; Currie, 2004 and references therein). Radiogenic heat production is 0.9 $\mu W\,m^{-3}$ in the upper-mid continental crust and 0.2 $\mu W\,m^{-3}$ in the lower continental crust, except in the Southern California (SC) region

where values of 1.2 µW m^{-3} and 0.4 µW m^{-3} are used for upper-mid and lower crust, respectively. The higher values are mostly used to help generate a thinner and therefore hotter lithosphere in SC. There is no radiogenic heat production in the oceanic crust or mantle.

All materials have a thermal conductivity of 2.25 W m^{-1} K^{-1} at temperatures below 1340°C within lithospheric mantle, except the Colorado Plateau mantle lithosphere (5.57 Wm^{-1}K^{-1}) and Rocky Mountains & Great Plains mantle lithosphere (3.89 Wm^{-1}K^{-1}). The higher conductivity for these regions is used to decrease the vertical thermal gradient within the mantle lithosphere in Phase I (more details in Section 2.5) so that the temperature at the base of the lithosphere is equal to the mantle adiabat at this depth. This ensures that the thermal structure is consistent with the mechanical structure. For all materials, the thermal conductivity linearly increases from the given values to 52.75 W m^{-1} K^{-1} between 1340°C and 1380°C. The high conductivity is therefore primarily limited to the sublithospheric mantle below 240 km depth. This artificial conductivity reflects a scaling of the true thermal conductivity by the Nusselt number of upper mantle convection (Pysklywec and Beaumont, 2004; Currie and Beaumont, 2011), and it provides a way to mimic the thermal effects of upper mantle convection without the need to explicitly model convective motions. The main purpose of this is to maintain a nearly constant temperature at the base of the lithosphere that is compatible with a 1296°C mantle adiabat and an adiabatic gradient of 0.4°C/km in the sublithospheric mantle, as expected for a well-stirred mantle.

2.3.3 Material densities

All materials have a temperature-dependent density:

$$\rho(T) = \rho_0[1 - \alpha(T - T_0)] \qquad (2.9)$$

where ρ_0 is the reference density at temperature T_0 (°C) and α is the volumetric thermal expansion coefficient. The oceanic crust is slightly (5-10 kg m^{-3}) denser than continental lower crust at the same temperature. The upper-mid continental crust has a reference density of 2800 kg m^{-3} to reflect that it has a more granitic (silica-rich) composition than the mafic materials that make up the lower crust and oceanic crust. The reference density of the mantle (3250 kg m^{-3}) is consistent with the density of fertile upper mantle (Poudjom Djomani et al., 2001).

In most models, a metamorphic phase change to eclogite is included for oceanic crust. One of the key characteristics of the eclogite phase transition is the appearance of garnet, and as a result eclogite rocks have a high density than their protolith. Eclogite forms when mafic rocks (i.e., basalt or gabbro) are subjected to high pressures and temperatures. Fig. 2.2 shows the stability field of eclogite used in our models, based on Hacker et al. (2003). Under equilibrium conditions, mafic crust transforms to eclogite as it enters the eclogite stability field (generally at a depth of ~50 km). However, there are geological observations that demonstrate the crust remain metastable (e.g., Austrheim, 1991; Austrheim et al., 1997; van Hunen et al., 2004). In other words, the crust may not transform to eclogite, even when it is within the eclogite stability field. The process of eclogitization is not solely constrained by pressure-temperature conditions, but also appears to be related to the presence of hydrous fluids (Leech, 2001). When fluids are present, the reaction can proceed rapidly, but if the crust is relatively dry, the reaction is kinetically delayed, leading to metastability. Variations in fluid distribution within the crust may also lead to heterogeneous eclogitization, whereby part of the crust may transform to eclogite and other parts remain metastable (e.g., Austrheim et al., 1997). The density of eclogitized rocks depends on their initial composition and the extent of eclogitization. Field and experimental data suggest that eclogitized oceanic crust may be 50-300 kg m^{-3} denser than mantle (e.g., Bousquet et al., 1997; Jull and Kelemen, 2001).

In the models, the pressure and temperature of oceanic crust are tracked and compared with the eclogite stability field. We consider two end-member scenarios: (1) full metastability, where no phase change occurs and the oceanic crust remains ~400 kg m^{-3} less dense than mantle (at the same temperature), and (2) immediate eclogitization as the crust enters the eclogite stability field, resulting in an increase in density of ~15%, such that the eclogitized oceanic crust density is ~20 kg m^{-3} greater than that of the mantle (at the same temperature). Higher densities models have been tested, but the results are not shown here because the higher-density crust material increases the negative buoyancy of the oceanic plate and hence reduces the tendency for flat-slab subduction to develop. The phase change is implemented following the approach of Warren et al. (2008) where Eulerian elements that experience densification undergo a minor volume decrease at the time of eclogitization to ensure mass conservation.
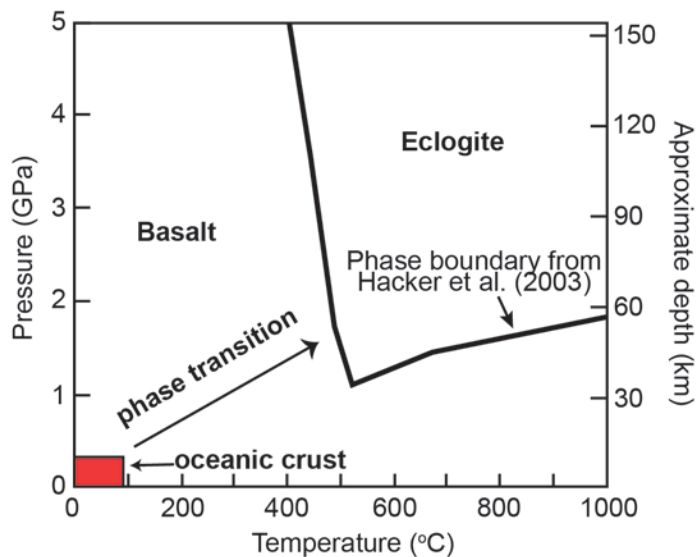
Fig. 2.2 Pressure-temperature diagram showing the stability fields for basalt and eclogite (Hacker et al., 2003). The red box shows the pressure-temperature conditions of the oceanic crust at the start of the models. During subduction, its pressure and temperature increase (arrow), and as it enters the eclogite stability field, the phase change occurs.

2.4 Boundary conditions

2.4.1 Mechanical boundary conditions

The mechanical boundary conditions applied during the model runs are shown in Fig. 2.1. The top boundary is a stress-free surface, which allows topography to develop. The bottom boundary is a closed, free-slip boundary. Velocities are imposed on the full thickness of lithosphere at each of the side boundaries, in order to drive plate convergence between the oceanic and continental plates. Prior to Laramide time (~100-80 Ma), the convergence velocity of the Farallon Plate relative to North America was 10 cm/yr, and the absolute plate motion of North America relative to the Atlantic hotspots was 3-4 cm/yr (Engebretson et al., 1984; Fig. 1.5). Plate velocities did vary over time, with an increase in Farallon-North America to ~15 cm/yr during the Laramide orogeny and a modest speed-up in North America Plate motion to ~5 cm/yr. As our study addresses whether it is possible to generate flat-slab subduction prior to the Laramide, the models use pre-Laramide convergence velocity of 10 cm/yr, and for simplicity, this is kept constant throughout the model run. As part of the model tests, we have examined continental plate velocities of V_c=0, 3 and 4 cm/yr; the corresponding oceanic plate velocities are V_a=10, 7

and 6 cm/yr to maintain a 10 cm/yr convergence rate. The models are run in the continental reference frame by adding velocity V_c to all vertical boundaries. That is to say, the continental plate has a velocity of 0 cm/yr, the oceanic plate enters the model domain at a velocity of V_a+V_c, and the side boundaries of the sublithospheric mantle have a velocity of V_c toward the right (Fig. 2.3).

In addition to the plate velocities, it is necessary to add a small outflux velocity, V_b, to the side boundaries of the sublithospheric mantle, in order to maintain a constant mass in the model domain. There is no material flux through the base of the model. Given the influx velocity of the oceanic plate, the outflux velocity is given by:

$$h_0(v_a + v_c) = (h_1 + h_2)v_b \qquad (2.10)$$

where h_0 is the thickness of oceanic plate (90 km in our model), V_a+V_c is the plate convergence rate (10 cm/yr), and h_1 and h_2 are length of the outflow region on the left and right boundaries, respectively. The top of the outflow region is taken to be 10 km below the base of the lithosphere on each side of the model. In this transition region, the velocity has a linear transition from the plate velocity to V_b. Finally, the lithostatic pressure at the base of the model at Eulerian column 240 (x=2400 km) is monitored throughout the model run. If the pressure increases/decreases, the outflow velocities are increased/decreased to keep the pressure constant, and therefore maintain an approximately constant mass within the model domain. Fig. 2.3 shows the velocity boundary conditions described here.
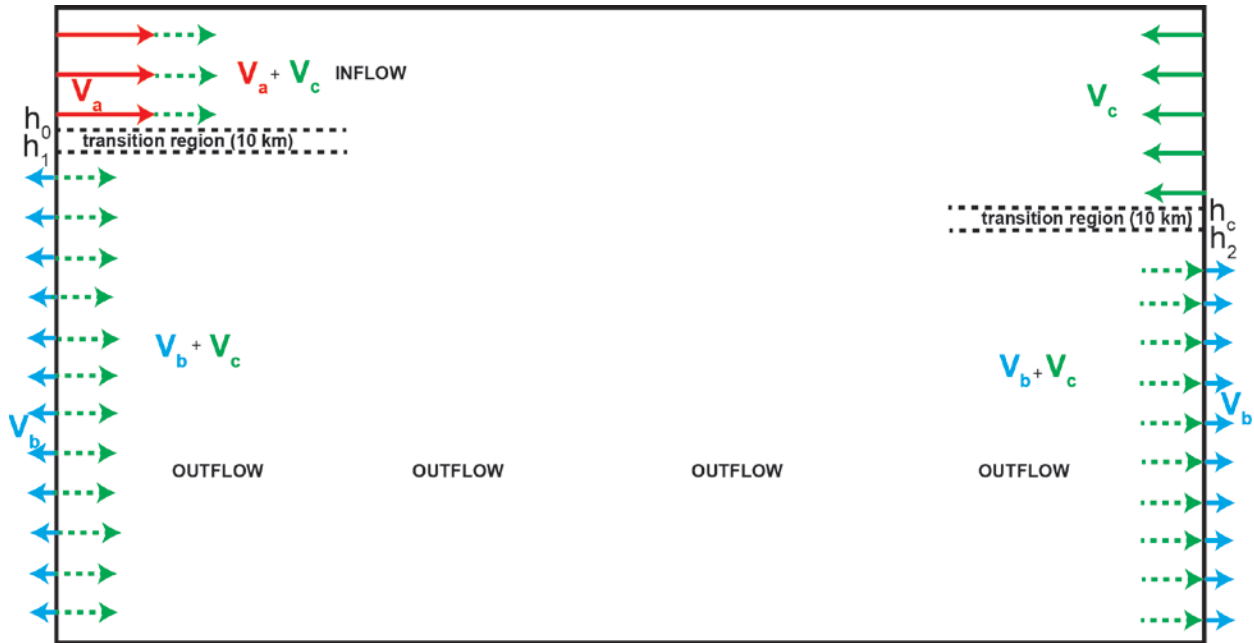
Fig. 2.3 Model velocity boundary conditions; h_0 and h_c are the base of inflow velocity at the oceanic and continental plates respectively; h_1 and h_2 are the point at which the full outflow velocity begins. The dash horizontal lines indicate a smooth velocity transition zone between the influx and outflux velocities with 10 km thick. A velocity of V_c is added to all boundaries (dashed green arrows) so that models are run in the continental reference frame.

2.4.2 Thermal boundary conditions

The thermal boundary conditions are as follows: (1) the top boundary has a fixed temperature of 0°C, (2) the bottom boundary has a fixed temperature of 1559°C; this is consistent with estimates of the temperature at the base of the mantle transition zone (e.g., Katsura and Ito, 1989). (3) the side boundaries of the sublithospheric mantle have a horizontal heat flux of 0 mW/m^2 (i.e., insulating boundaries), (4) the oceanic lithosphere side boundary has a prescribed oceanic geotherm where the temperature linearly increases from 0°C at the surface to 1332°C at the base of the lithosphere (90 km depth); this approximates the geotherm for an old (>100 Ma) oceanic plate (e.g., Stein and Stein, 1992) and is consistent with the age of the Farallon plate prior to the Laramide orogeny (Fig. 1.5), and (5) the continental lithosphere side boundary has a prescribed continental geotherm. To calculate the continental geotherm, the one-dimensional, steady-state, conductive heat equation with the boundary conditions of surface heat flow (Q_s) and surface temperature (T_0) is used (e.g., Chapman, 1986):

$$T(z) = T_0 + \frac{Q_s}{k(z)}z - \frac{A_T(z)}{2k(z)}z^2 \qquad (2.11)$$

where z is the depth, T_0 is the surface temperature (0°C), Qs is the surface heat flow, k(z) is the thermal conductivity at depth z, and A_T is the radiogenic heat production at depth z.

At the Great Plains boundary, a surface heat flow of 45.1 mW/m^2 is assumed, which is similar to the average heat flow in Archean- Proterozoic provinces of North America (Jaupart and Mareschal, 2003). To calculate the geotherm, the Earth is divided into layers of thickness Δz (taken to be the height of the Eulerian elements). For each layer, the temperature (T_t) and heat flow (Q_t) at the top of each layer are used to calculate the temperature (T_b) and heat flow (Q_b) at the bottom of the layer:

$$T_b = T_t + \frac{Q_t}{k_t}\Delta z - \frac{A_l}{2k_l}(\Delta z)^2 \qquad (2.12)$$

$$Q_b = Q_t - A_l \Delta z \qquad (2.13)$$

where A_l and k_l are the heat production and thermal conductivity in the layer, respectively. Equations 2.12 and 2.13 are solved using the layered structure of the Great Plain lithosphere, and the GP surface heat flow (45.1 mW/m^2) and surface temperature (0°C) as the top boundary condition. This calculation gives the conductive geotherm. The base of the lithosphere is defined as the intersection of this geotherm with a mantle adiabat that has a potential (zero pressure) temperature of 1296°C and an adiabatic gradient of 0.4°C/km. For the given thermal parameters, the intersection occurs at a depth of 200 km, and therefore the geotherm is consistent with the mechanical material distribution (Fig. 2.1).

2.5 Model phases

The numerical models are carried out in three phases. In Phase I, the 2D thermal structure of the model domain is calculated using the thermal boundary conditions and material properties. For this phase, we vary thermal conductivities for mantle layer in oceanic and continental plate (Table 2.1) to make sure the base of the mantle lithosphere was at the adiabatic temperature. The model then undergoes isostatic adjustment, in which materials can move vertically but there is no

horizontal velocity. The oceanic plate and each region of the continental plate have distinct layer densities and thicknesses, so they must come into isostatic equilibrium. The main effect of this is that the dense oceanic plate sinks by ~4 km relative to the continent. The Colorado Plateau region has a thicker crust and therefore its elevation is ~0.5 km higher than SC and 0.8 km higher than RM/GP. Fig. 2.4a shows the full model domain at the end of Phase I (start of Phase II). Note the variation in thermal structure within the continental plate, owing to the variations in layer thicknesses and thermal properties.
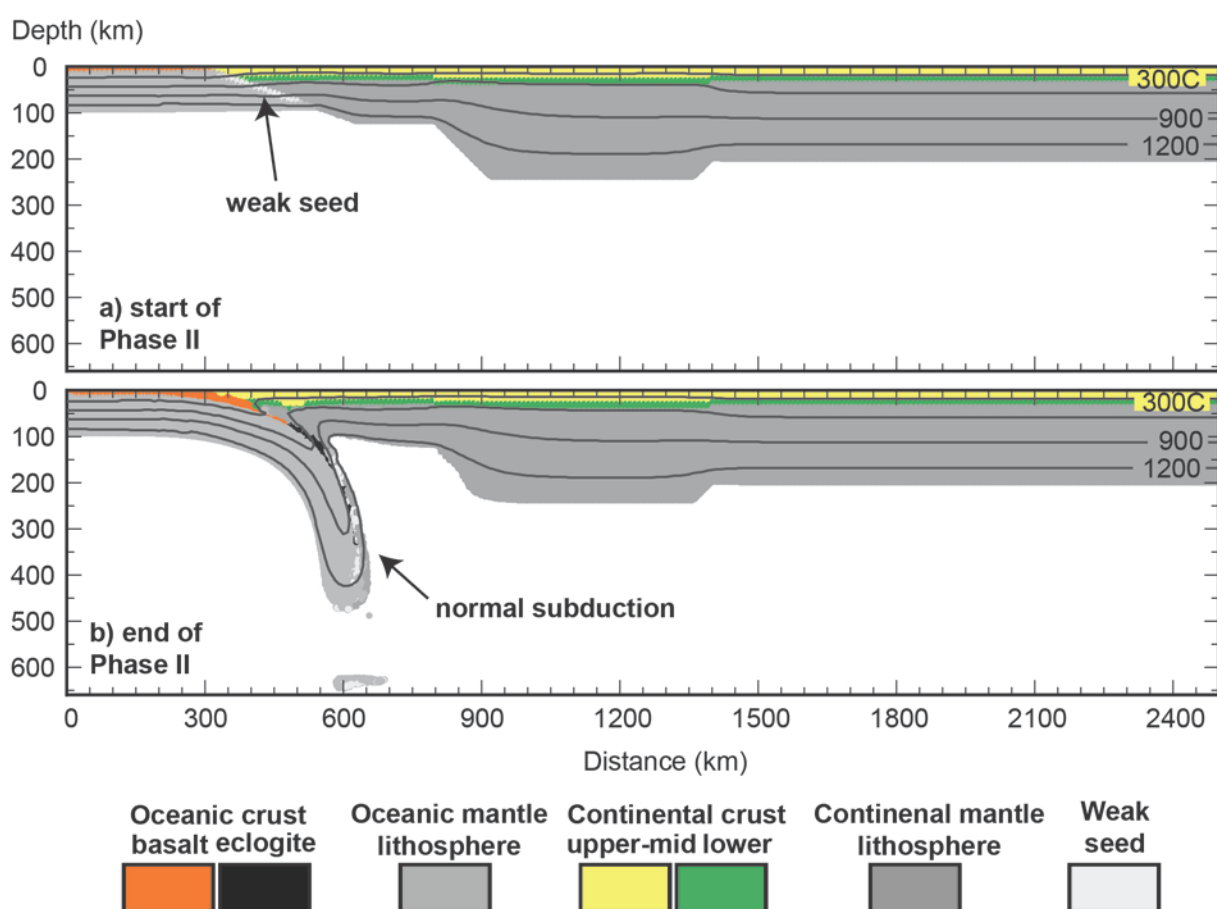
Fig. 2.4 An example of the initial phases of a model run. a) The start of Phase II, after the initial 2D thermal calculations and isostatic adjustment (Phase I). At this point, plate convergence is imposed to initiate subduction. b) The end of Phase II, where a normal steep-angle subduction zone has formed. The Colorado Plate is the area of thicker lithosphere a distances of 800-1400 km.

In Phase II of the models, subduction initiation occurs and a subduction zone is formed. For this, plate convergence is imposed using a boundary velocity of 5 cm/yr for the oceanic plate; the continental velocity is 0 cm/yr. The presence of the weak seed between the oceanic and continental lithosphere (Fig. 2.1) helps to localize deformation and form the subduction thrust fault. As shown in Fig. 2.4b, this material is subducted to the deep model domain with the oceanic plate and has no effect on subsequent model evolution. Phase II is run to a plate convergence of ~500 km (10 Ma). At this point, a subduction zone has developed, and the geometry of the subducting plate is similar to that of a typical 'steep dip' subduction zones (~> 45°) (e.g., Turcotte and Schubert, 2002).

The numerical model experiments conducted in this study start from the end of Phase II and form Phase III of the model run. In Phase III, we investigate how the different factors discussed in Chapter 1 may affect the dynamics of the subducting oceanic plate, and specifically, how the oceanic plate may transition from a steep dip angle to shallow/flat subduction. All model times are reported in Ma-emt, i.e., million years of elapsed model time (emt). A time of 0 Ma-emt corresponds to the start of Phase III (end of Phase II), with the steep-dip geometry shown in Fig. 2.4b. This corresponds to the inferred Farallon plate geometry at 100-90 Ma in geological time, which is 10-20 Ma before the Sierra Nevada arc shut down (e.g., Chen and Moore, 1982) and 20-30 Ma before the start of the Laramide orogeny (Fig. 1.5). We therefore run Phase III of the models for 20-40 Ma to study the slab dynamics. The results of the numerical experiments are presented in the next chapter.

CHAPTER 3

Numerical model results

3.1 Introduction

The dominant driving force for subduction is the negative buoyancy of the dense oceanic plate (Wortel et al., 1991), which should produce a relatively steep subduction zone. However, low-angle/flat subduction does not fit in these normal subduction dynamics and additional mechanisms are needed in order to allow the oceanic plate to bend into the mantle to underthrust the upper plate and then unbend in order to have a low-angle or flat trajectory. As outlined in Chapter 1, three mechanisms are: trenchward motion of the overlying plate, an enhanced slab suction force, and subduction of a buoyant oceanic plateau or aseismic ridge (Fig. 3.1). These three factors have been discussed as being important for Farallon plate subduction during the Laramide orogeny (e.g., Dickinson and Snyder, 1978; Livaccari, et al., 1981; Bird, 1988;), but to date there have been no quantitative geodynamic modeling studies that specifically address the plate dynamics for this region. Instead geodynamic studies have either focused on generic models (e.g., van Hunen 2002b; Manea and Gurnis, 2007; Arrial and Billen, 2013) or on models for modern-day flat subduction in South America (e.g., van Hunen 2004, Manea et al., 2012).

Regardless of the mechanism for creating low-angle/flat subduction, there are several constraints on its timing for the southwestern US. (1) Prior to ~100 Ma, there was typical arc volcanism in the Sierra Nevada arc region, which ceased at ~80 Ma (e.g., Chen and Moore, 1982; Dumitru et al., 1991) and was accompanied by an eastward migration in magmatism (Coney and Reynolds, 1977). (2) Laramide-style deformation in the interior of the North America Plate, >1000 km from the plate margin, that initiated in the Late Cretaceous (80-75 Ma) (e.g., Dickenson and Snyder, 1978; English and Johnston, 2004). (3) The formation Western Interior Seaway in the Late

Cretaceous from broad subsidence of western North America, up to 1500 km inboard of the trench (e.g., Cross and Pilger, 1978; Mitrovica et al., 1989; Smith et al., 1994; Currie and Beaumont, 2011). Together, these observations are consistent with 'normal' steep-angle subduction in the Early Cretaceous, followed by a shallowing of the slab in the Late Cretaceous (starting at ~100 Ma) to a flat trajectory by 80-70 Ma. Thus, slab flattening is inferred to have occurred over a time period of 10-30 Ma.
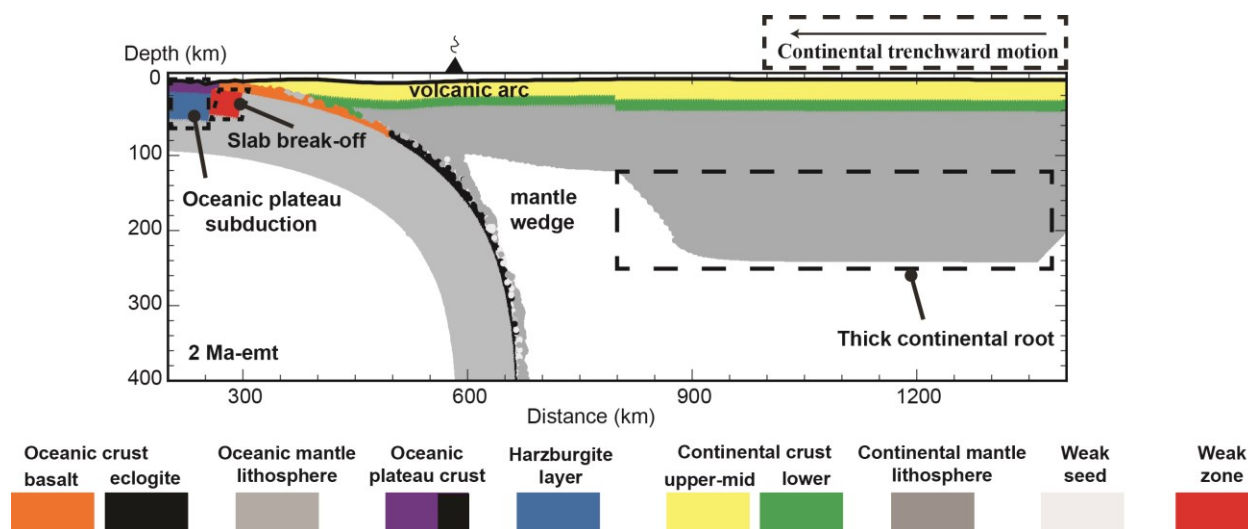
Fig. 3.1. The factors tested in the numerical models to assess the development of a flat-slab subduction: continental trenchward motion, oceanic plateau subduction, thick continental root (i.e., Colorado Plateau) and slab break-off. This plot is at 2 Ma-emt, where emt is the elapsed model time since the start of Phase III.

In this chapter, we present a series of numerical model experiments that systematically investigate each of the proposed mechanisms for generating low-angle/flat subduction. As discussed in Chapter 2, the model experiments start with a well-developed steep-angle subduction zone, (i.e., end of Phase II), and the dynamics of the slab during each experiment (Phase III of the models) are monitored. The model parameter tests are given in Tables 3.1 and 3.2. More than 70 models have been tested during this research, but only a subset will be presented in detail here. To quantitatively describe and compare the models, we measure two different dip angles for the top of the oceanic plate: α_s, shallow dip, which is the average dip from the trench (~5 km depth) to 100 km depth, and α_d, the deep dip between 100 and 200 km

depth. In some models, we also track the approximate location of the volcanic arc. Arc volcanism arises from partial melting of the mantle wedge, where melting is induced by a reduction in the mantle solidus by water released from the oceanic plate (Schmidt and Poli, 1998). Geochemical observations and experimental data suggest that most arc volcanism requires temperatures greater than 1200°C in the mantle wedge (e.g., Schmidt and Poli, 1998). Therefore, the most trenchward position of the 1200°C isotherm in the mantle wedge is taken as a proxy for the lateral position of the volcanic arc front in the models.

The individual model experiments are described below. Sections 3.2, 3.3 and 3.4 examine the effects of continental plate velocity, slab suction and an oceanic plateau, respectively. In Section 3.5, combinations of these factors are investigated. These models demonstrate that slab breakoff (i.e. detachment of the deep part of the subducted oceanic plate) may be important in producing flat subduction. Therefore, in Section 3.6, we look at slab breakoff in more detail. Section 3.7 provides a summary of the model experiments. As a reminder, the model times reported below are in Ma-emt (million years of elapsed model time), where 0 Ma-emt corresponds to the start of Phase III (the start of the given model experiment).

Table 3.1. List of numerical models to test continental motion, slab suction and an oceanic plateau.

Model group		Cont. Velocity[1] V_c (cm/yr)	Slab suction force Thick litho. C.P.[2]	Slab suction force Mantle viscosity[3] Low/High	Oceanic crust Eclogite	Oceanic crust Strength[4] DMD*f	HL[2] $\Delta\rho$[5] (km/m^3)	HL[2] Strength[4] WO*f	Width (km)	Location (km)[6]	Figure #
GROUP A: test V_c and mantle viscosity. No C.P. or oceanic plateau.											
A1	a	0		Low							3.2a-c
	b	3		Low							
	c	4		Low							3.2d-f
A2	a	0		High							
	b	3		High							
	c	4		High							
GROUP B: include C.P.; test V_c and mantle viscosity. There is no oceanic plateau.											
B1	a	0	Yes	Low							3.3
	b	3	Yes	Low							
	c	4	Yes	Low							3.9
B2	a	0	Yes	High							3.5
	b	3	Yes	High							
	c	4	Yes	High							
GROUP C: include oceanic plateau; test V_c and oceanic plateau properties. There is no C.P.											
C1	a	0		Low	Yes	0.1	0	10	400	-500	3.6a-c
	b	3		Low	Yes	0.1	0	10	400	-500	
	c	4		Low	Yes	0.1	0	10	400	-500	3.11a-c
C2	a	0		Low	--	0.1	0	10	400	-500	3.6d-f
	b	3		Low	--	0.1	0	10	400	-500	
	c	4		Low	--	0.1	0	10	400	-500	3.11d-f
C3	a	0		Low	Yes	0.1	-50	10	400	-500	3.7a-c
	b	0		Low	--	0.1	-50	10	400	-500	3.7d-f
	c	3		Low	--	0.1	-50	10	400	-500	
	d	4		Low	Yes	0.1	-50	10	400	-500	3.12a-c
	e	4		Low	--	0.1	-50	10	400	-500	3.12d-f
C4	a	0		Low	Yes	0.1	-100	10	400	-500	3.8a-c
	b	0		Low	--	0.1	-100	10	400	-500	3.8d-f
	c	3		Low	--	0.1	-100	10	400	-500	
	d	4		Low	Yes	0.1	-100	10	400	-500	3.13a-d
	e	4		Low	--	0.1	-100	10	400	-500	3.13e-h
GROUP D: include C.P. and oceanic plateau (no eclogitization); test V_c and low-density harzburgite layer											
D1	a	0	Yes	Low	--	0.1	0	10	400	-500	3.15a
	b	3	Yes	Low	--	0.1	0	10	400	-500	
	c	4	Yes	Low	--	0.1	0	10	400	-500	3.16d-f

Group											
	a	0	Yes	Low	--	0.1	-50	10	400	-500	3.15b
D2	b	3	Yes	Low	--	0.1	-50	10	400	-500	
	c	4	Yes	Low	--	0.1	-50	10	400	-500	3.17d-f
	a	0	Yes	Low	--	0.1	-100	10	400	-500	3.15c
	b	3	Yes	Low	--	0.1	-100	10	400	-500	
D3	c	4	Yes	Low	--	0.1	-100	10	400	-500	3.18d-f

GROUP E: include C.P. and oceanic plateau (no eclogitization); test V_c and low-density harzburgite layer

Group											
	a	3	Yes	Low	Yes	0.1	0	10	400	-500	
E1	b	4	Yes	Low	Yes	0.1	0	10	400	-500	3.16a-c
E2	a	3	Yes	Low	Yes	0.1	-50	10	400	-500	
	b	4	Yes	Low	Yes	0.1	-50	10	400	-500	3.17a-c
	a	3	Yes	Low	Yes	0.1	-100	10	400	-500	
E3	b	4	Yes	Low	Yes	0.1	-100	10	400	-500	3.18a-c

GROUP F: include C.P. and oceanic plateau; test oceanic plateau properties (eclogitization, rheology, location and width)

Group											
	a	4	Yes	Low	--	0.1	0	10	200	-500	3.19a-c
F1	b	4	Yes	Low	--	0.1	0	10	800	-500	3.19d-f
	a	4	Yes	Low	--	0.1	0	10	400	-1100	3.20a-d
F2	b	4	Yes	Low	Yes	0.1	0	10	400	-1100	
	c	4	Yes	Low	--	0.1	0	10	400	-200	3.20e-h
	a	4	Yes	Low	--	1	0	10	400	-500	
F3	b	4	Yes	Low	--	0.1	0	100	400	-500	
	c	4	Yes	Low	--	1	0	100	400	-500	

[1] Cont. Velocity, V_c is the trenchward velocity of the continental plate

[2] HL is the harzburgite layer; C.P. is the Colorado Plateau (region of 240 km thick lithosphere)

[3] Low mantle viscosity uses a wet olivine (WO) flow law; high mantle viscosity is an order of magnitude larger (WO×10)

[4] Strength varied with a linear scaling (f) of the base dry Maryland diabase (DMD) and wet olivine (WO) rheologies

[5] $\Delta\rho$ is the density difference between the harzburgite layer and mantle at the same temperature

[6] initial position of the landward edge of the oceanic plateau relative to the trench prior to subduction (negative is seaward)

Table 3.2. Additional numerical model experiments to examine the effect of variations in oceanic plate characteristics. All models contain a Colorado Plateau and continental velocity V_c=4 cm/yr.

Model group	Weak zone strength[1], WO*f	Oceanic plate			Oceanic plateau		Figure #
		Crustal eclogite	Mantle lith. strength[1], WO*f	HL[2], Δρ (km/m³)	Crustal eclogite	HL[2], Δρ (km/m³)	
GROUP G: test variation in oceanic plate mantle lithosphere strength. No oceanic plateau							
G a		--	5	--			
b		--	2	--			
c		--	1	--			3.22a-c
GROUP H: test oceanic crust eclogitization and harzburgite layer for oceanic plate. No oceanic plateau							
H[3] a		Yes	10	18, -100			3.14a-c
b		--	10	18, -100			3.14d-f
GROUP I: test weak zone strength and crustal eclogitization in the oceanic plate. No oceanic plateau							
I a	1	Yes	10	--			3.22d-f
b	1	--	10	--			
c	0.1	Yes	10	--			
d	0.01	Yes	10	--			
GROUP J: test weak zone strength and oceanic plate properties. Oceanic plateau has 9 km thick crust but has a HL[2].							
J a	1	Yes	10	--	Yes	-100	
b	1	--	10	--	--	-100	
c	0.1	Yes	1	--	Yes	-100	
GROUP K: test weak zone with oceanic plateau (variations in eclogitization and harzburgite layer density)							
K a	1	Yes	10	--	--	--	3.23
b	1	--	10	--	--	--	
c	1	Yes	10	--	Yes	-100	3.24a-c
d	1	Yes	10	--	--	-100	3.24d-f

[1] Strength varied with a linear scaling of the base wet olivine rheology (WO) by factor f, preferred model is K-d

[2] HL is the harzburgite layer; Δρ is the density difference between the harzburgite layer and mantle at the same temperature

[3] The harzburgite layer is underlying the oceanic plate crust with same width and double thickness (18 km) in model group H

3.2 Effect of continental plate velocity

3.2.1 Proposed mechanism

In a continental arc-trench system, the subduction zone is located at the continental margin and the continent forms the over-riding plate. Oceanic plates older than 10 Ma are denser than the mantle owing to the cooler temperatures, and they tend to sink (Cloos, 1993). This should cause trench retreat, where the position of the trench moves oceanward relative to the deep mantle. However, trench retreat requires that the mantle below the oceanic plate is displaced. In a subduction zone with a wide (along-strike) oceanic plate that extends to the deep upper mantle, the oceanic plate acts as a keel that resists lateral motion. This provides a slab anchor force that holds the subduction zone in place (in the absence of large-scale mantle convection) (Lallemand et al., 2005; Schellart, 2008). Lateral movement of the trench is therefore primarily controlled by upper plate motion. Indeed, global subduction studies show that the absolute trench motion is well-correlated with the absolute motion of the upper plate (Cross and Pilger, 1978; Lallemand et al., 2005; Schellart, 2008). If the continental plate moves toward the trench (advances), it over-rides the oceanic plate, which is anchored in the mantle. The trench will move seaward with the continental plate, while the deep oceanic plate has little lateral motion. As a result, the slab dip angle will decrease.

Plate reconstructions show that plate convergence and subduction started along the western margin of North America during the Jurassic (e.g., Coney, 1978; Engebretson et al., 1984). From the Late Cretaceous to Middle Eocene, there was an increase in both the Farallon-North America convergence velocity and westward motion of the North America plate (Fig. 1.5). At this time, the subduction zone was found almost the entire length of western North America (>10,000 km). Schellart et al. (2010) argue that the large width of the subduction zone created an oceanic plate that resisted retreat. As North America moved west, it over-rode the subduction zone and creating low-angle subduction. In this section, we assess whether enhanced westward motion of North America prior to the Laramide orogeny could have triggered flat subduction. Note that our plane-strain models assume a 2D geometry, which is the equivalent of having an infinitely wide subduction zone.

3.2.2 Model results

The models start at the end of Phase II, with a well-developed steep-angle subduction zone (Fig. 2.4). At this point, the convergence rate of the oceanic plate relative to the continental plate (V_a+V_c) is increased to 10 cm/yr, consistent with the inferred North America-Farallon convergence rate at 100-70 Ma (Engbretson et al., 1984; Fig. 1.5). We have tested three different continental velocities (V_c): 0, 3 and 4 cm/yr; the corresponding oceanic plate velocities (V_a) are 10, 7 and 6 cm/yr. For simplicity, all velocities are held constant during the model run.

Fig. 3.2 shows the evolution of models with V_c=0 cm/yr and V_c=4 cm/yr. The model with V_c=3 cm/yr is not shown as the slab geometry is intermediate between these two models. In the model with a stationary continental plate (V_c=0 cm/yr), the trajectory of the oceanic plate remains fairly steep for over 20 Ma-emt, with a shallow dip of α_s = 22° and a deep dip of α_d = 50.6° (Fig. 3.2a-b). During the model run, interactions between the subducting slab and the closed bottom boundary of the model domain cause the slab to fold on itself at the bottom boundary. This produces changes in dip of 10-20° in the shallower part of the slab on time scales of <5 Ma (e.g., the shallower dip angle at ~200 km depth in Fig. 3.2c). This model also shows significant erosion of continental crust by the subducting plate. The eroded crust is carried into the mantle by the oceanic plate, where it detaches and upwells as small plumes, owing to its low density relative to the surrounding mantle (e.g., Currie et al., 2007). This material accumulates in the vicinity of the volcanic arc.

If a continental plate velocity of V_c=4 cm/yr is applied, the trajectory of the subducting plate gradually becomes shallower during the model run (Fig. 3.2d-f). In this model, the dip angle of the shallow part of the plate (α_s) is similar to that in the model with the stationary continent (Fig. 3.2a-c), but the deep dip angle (α_d) decreases to an angle of α_d = 28° at 30 Ma-emt (Fig. 3.2f). With the decrease in dip angle, the volcanic arc is predicted to move ~200 km landward over 30 Ma-emt. The progressive shallowing and landward arc migration is a consequence of the fact that continental plate has over-ridden the oceanic plate which is 'anchored' in the deep upper mantle. The same amount of continental crust has been eroded and subducted in this model. However, the subducted crust carried laterally below the continental plate (>1500 km inboard), and therefore the continental plumes are not visible in the region that is plotted in Fig. 3.2.
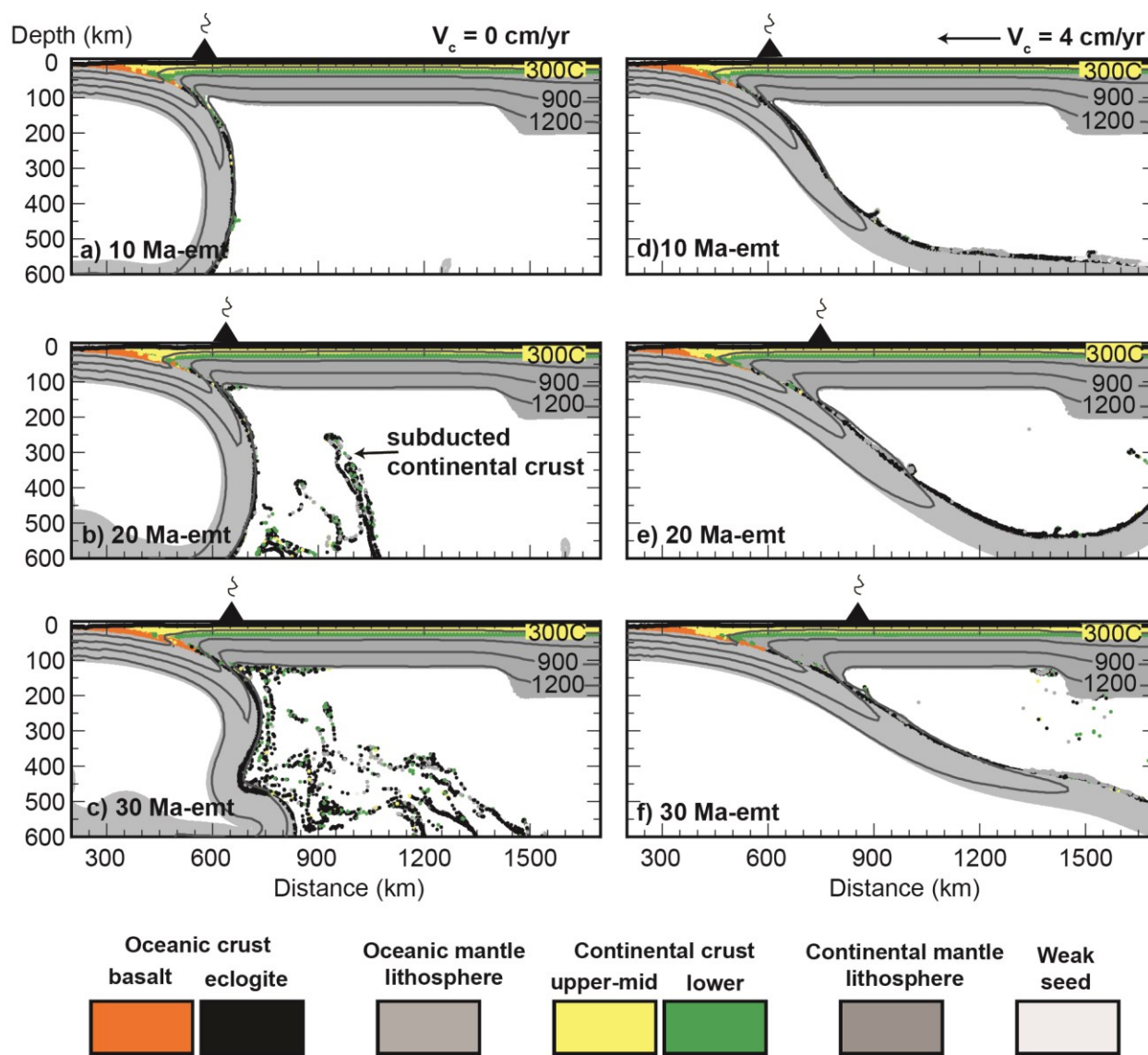
Fig. 3.2. Numerical model results for variations in continental plate velocity: Model A1-a (left column) with $V_c = 0$ cm/yr at a) 10 Ma-emt, b) 20 Ma-emt, c) 30 Ma-emt; and Model A1-c (right column) with $V_c = 4$ cm/yr, d) 10 Ma-emt, e) 20 Ma-emt, f) 30 Ma-emt. Note that the basaltic oceanic crust undergoes the metamorphic phase change to higher density eclogite at a depth of ~70 km.

These models show that the velocity of the continental plate has a significant effect on the trajectory of the subducting plate. Trenchward motion of the continent produces a decrease in the subduction dip angle, with a faster rate of shallowing as the continental velocity increases. In these models, the subduction zone evolves from a steep-angle geometry ($\alpha_d > 45°$) to low-angle

geometry (α_d between 15° and 45°). None of the models show the development of flat (subhorizontal) subduction (α_d <15°).

3.3 Effect of increased slab suction force

3.3.1 Proposed mechanism

Enhanced slab suction, or low hydrodynamic pressure, has been proposed as a possible cause for low-angle or flat subduction (Stevenson and Turner, 1977; van Hunen et al., 2004; O'Driscoll et al., 2009). As the oceanic plate subducts into the mantle, the overlying mantle material is entrained and carried downward with the subducting plate (e.g., Stevenson and Turner, 1977). This creates a negative dynamic pressure in the mantle wedge corner. As a result, mantle material from the backarc is 'pulled' into the wedge corner. This sets up the mantle wedge corner flow pattern, which replenishes the mantle wedge with hot material from the backarc and is fundamental for magma generation at the volcanic arc (e.g., Stevenson and Turner, 1977). The low pressure also acts on the oceanic and continental plates, producing an upward force on the oceanic plate (slab suction) and downward force on the continental plate.

The magnitude of the (negative) dynamic pressure in the wedge corner is proportional to the mantle wedge viscosity and subduction rate and inversely proportional to the slab dip angle (Turcotte and Schubert, 2002). Manea and Gurnis (2007) demonstrated that the mantle wedge viscosity has the strongest control on subduction dynamics, and they argued that steep subduction requires a relatively low (<10^{20} Pa s) mantle wedge viscosity. At higher viscosities, the slab suction force may lift the oceanic plate and create low-angle subduction. In addition, O'Driscoll et al. (2009) showed that the presence of anomalously thick continental lithosphere affects the dynamic pressure in the mantle wedge corner. A region of thick lithosphere in the backarc will restrict the amount of material that can flow into the wedge corner, and therefore there will be an enhanced negative dynamic pressure and a larger slab suction force. In this section, we examine the effect of both thick continental lithosphere and variations in mantle viscosity on the trajectory of the subducting plate. In these experiments, the continental plate has a velocity of 0 cm/yr.

3.3.2 Model results

We first examine how thick backarc lithosphere may influence slab dynamics. This is motivated by the observation that the region of proposed flat slab subduction for western North America coincides with the subduction path of the Farallon plate beneath the Colorado Plateau (e.g., Saleeby et al., 2003; Liu et al., 2010). Prior to the Laramide orogeny, the Colorado Plateau lithosphere had a greater thickness than the Southern California lithosphere further west (e.g., O'Driscoll et al., 2009; see discussion in Chapter 2). To test the effect of this, a "Colorado Plateau" is introduced to the continental plate. This region contains both thicker crust and mantle lithosphere and has a total lithosphere thickness of 240 km, twice that of the adjacent Southern California lithosphere (Fig. 2.1).

Fig. 3.3a shows this model just after the start of Phase III. As subduction proceeds, the dip angle of the slab decreases slightly, especially at depths > 100 km. At 14 Ma-emt, the deep dip angle is $\alpha_d = 50.6°$ (Fig. 3.3b), whereas this angle is $\alpha_d = 55°$ in the model without thick Colorado Plateau lithosphere (Fig. 3.2). The size of the mantle wedge below Southern California progressively shrinks as the subducting slab trajectory shallows and the slab moves toward the Colorado Plateau (Fig. 3.3c). The position of the volcanic arc is predicted to shift ~100 km landward during the model run. Note that the lower part of the Colorado Plateau lithosphere is weak enough to be entrained by subduction-induced mantle flow and carried below the Southern California block.

The only difference between this model and the previous model in Fig. 3.2 is the presence of the Colorado Plateau. O'Driscoll et al. (2009) showed that a continental root (i.e., Colorado Plateau) will cause the mantle wedge pressure to be 30-40 MPa lower than for a case with no thick root. This lower pressure is what induces the suction force on the subducting plate and the small decrease in subduction angle over time. However, this is not sufficient to overcome the negative buoyancy of the slab and create flat subduction within 30 Ma-emt (Fig. 3.3).
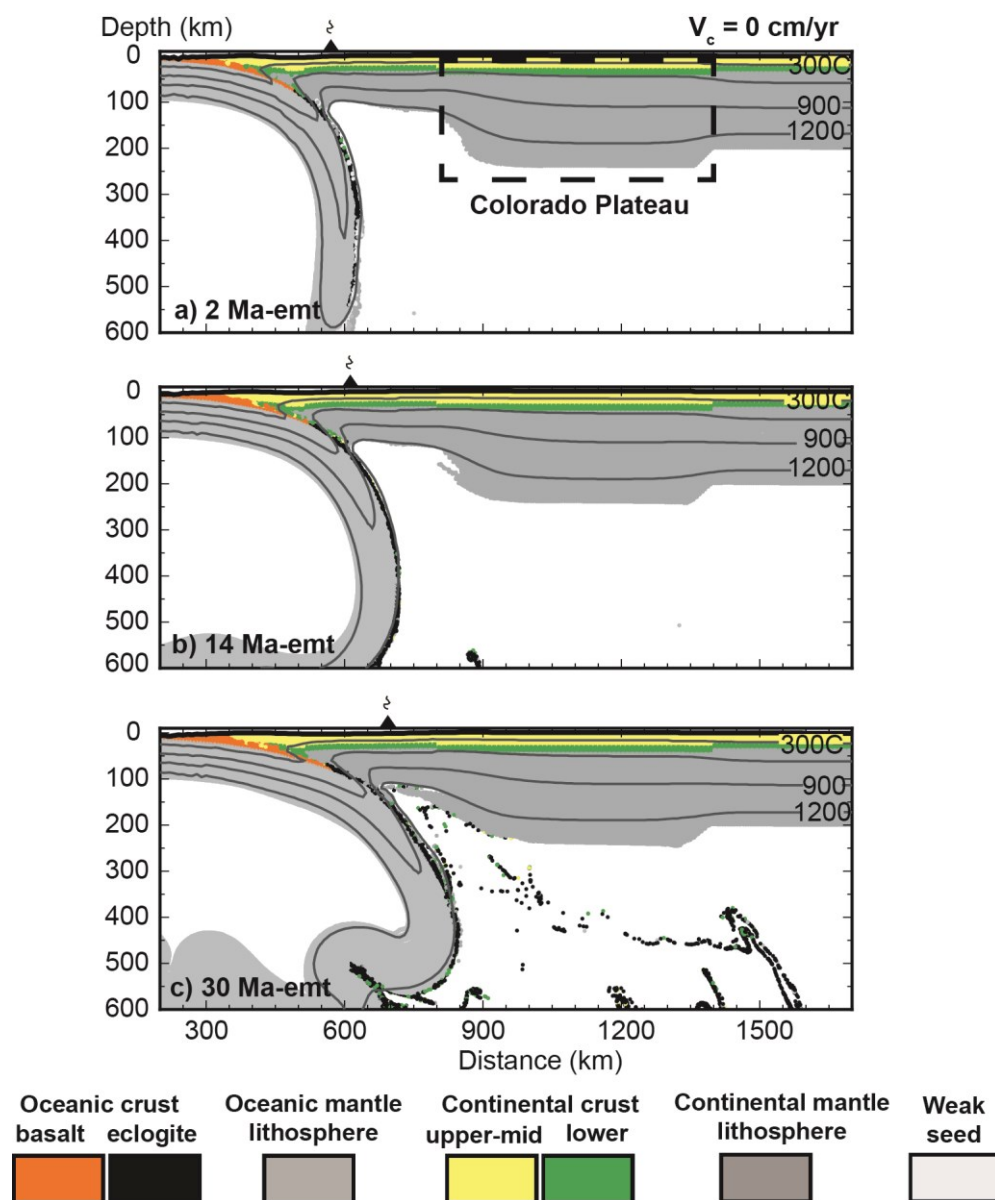
Fig. 3.3. Evolution of Model B1-a with a thick Colorado Plateau lithosphere: a) 2 Ma-emt, b) 14 Ma-emt and c) 30 Ma-emt. The black dashed rectangle in (a) indicates the lithosphere root of the Colorado Plateau.

The slab suction force is proportional to the viscosity of the mantle wedge (Turcotte and Schubert, 2002). In the model with the Colorado Plateau, the viscosity is less than 5×10^{19} Pa s (Fig. 3.4), which results in a relatively low slab suction force (Manea and Gurnis, 2007). Fig. 3.5 shows a model in which the viscosity of the sublithospheric mantle is 10 times larger (i.e., its rheology is wet olivine with f=10). The higher viscosity produces an enhanced shallowing of the

subduction angle. At 14 Ma-emt, the deep dip angle of the slab (α_d) is approximately 10° less than that in the model with a lower viscosity mantle (Fig. 3.3). However, flat subduction is not generated. The increased mantle viscosity results in a stronger shear zone along the top of the subducting plate. As the slab shallows, the length of the shear zone increases and its temperature decreases. This increases the strength of the shear zone, making it more difficult for subduction to occur. Near the end of the model run, the strength of the shear zone exceeds the strength of the oceanic plate, and subduction stops as the oceanic plate fails.
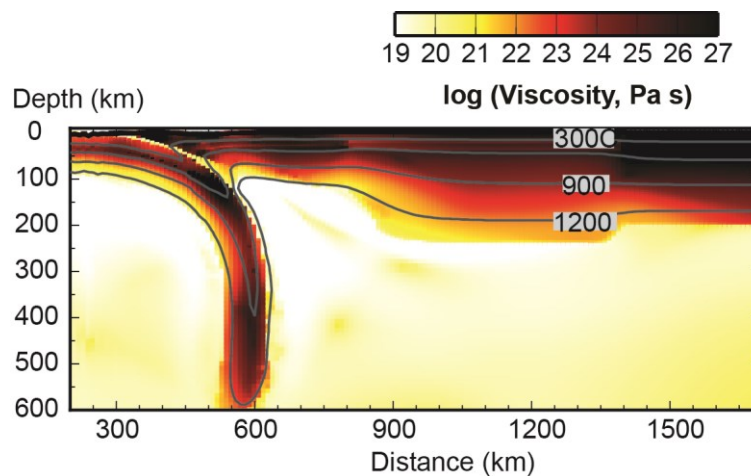
Fig. 3.4. The viscosity structure of the model with a thick Colorado Plateau at 2 Ma-emt (Fig. 3.3a).

An even higher viscosity would enhance slab suction and could generate a shallower slab trajectory. Additional model tests with a constant mantle viscosity (not shown here) demonstrate that a mantle viscosity of $>10^{21}$ Pa s is needed to develop a low-angle slab. However, if the mantle viscosity is increased, subduction is hindered and the oceanic plate breaks outboard of the trench (i.e., similar to Fig. 3.5c). Subduction models of Manea and Gurnis (2007) that extend into the lower mantle show that flat slab subduction may develop for upper mantle viscosities of 10^{21} Pa s or greater. In contrast, post-glacial rebound and post-seismic deformation studies show that the viscosity of the mantle above a subducting plate is 10^{18}-10^{19} Pa s on geological time scales, due to hydration of the mantle wedge by volatiles released from the subducting lithosphere (e.g., Craig and McKenzie, 1986; Karato and Wu, 1993; Dixon et al., 2004). In

addition, constraints on the mantle wedge properties from gravity, heat flow, seismic velocities and attenuation are consistent with a relatively low viscosity (e.g., Roth et al., 2000; Billen and Gurnis, 2001; Abers et al., 2006; Currie and Hyndman, 2006; Wada et al., 2011). The inferred viscosities are 1-3 order of magnitude less than what numerical models require for the development of flat subduction.
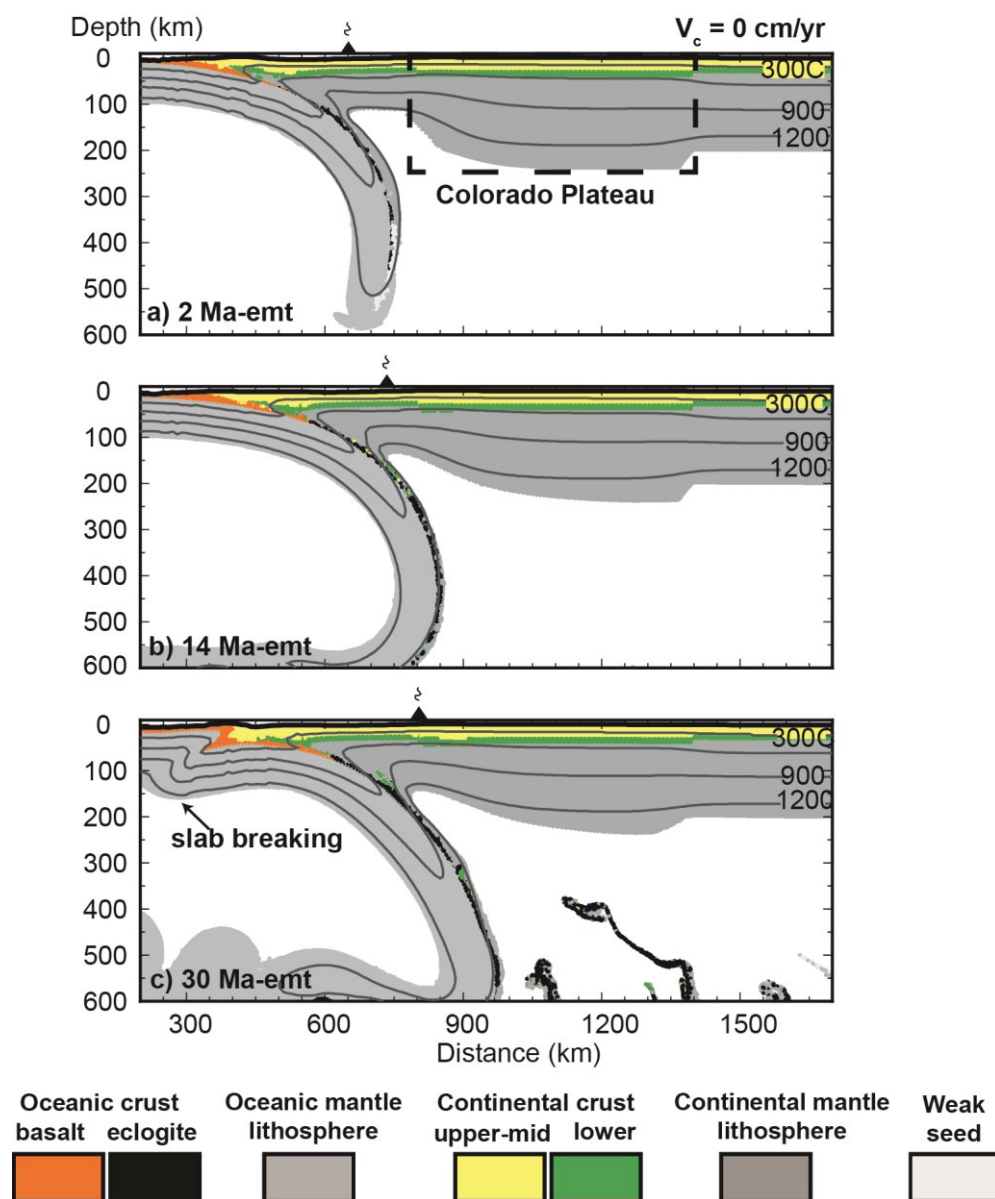
Fig. 3.5. Evolution of Model B2-a with the thick Colorado Plateau lithosphere and a mantle viscosity that is 10 times greater than the reference viscosity at: a) 2 Ma-emt, b) 14 Ma-emt and c) 30 Ma-emt. The black dashed

rectangle indicates the Colorado Plateau lithosphere root. Prior to 30 Ma-emt, subduction stops and the slab starts to break at the trench.

In summary, the models in this section demonstrate that a thick continental root (i.e., Colorado Plateau) will increase the slab suction force and promote low-angle (but not flat) subduction, even for a low viscosity mantle wedge. The slab suction can be further increased with a higher viscosity. However, for reasonable mantle wedge viscosities, the slab suction force is insufficient to create flat subduction.

3.4 Effect of an oceanic plateau

3.4.1 Proposed mechanism

Oceanic plate subduction is primarily driven by the negative buoyancy of the oceanic plate that arises from its cool temperature relative to the surrounding mantle (e.g., Cloos, 1993). In general, oceanic plates have a thin (6-7 km) basaltic crust. However, there are many examples of places where thicker crust has been created through enhanced mid-oceanic ridge magmatism and mantle plume activity (e.g., Ito and Clift, 1998; Skinner and Clayton, 2010). A region with anomalously thick crust is called an oceanic plateau or aseismic ridge. As oceanic crust has a lower density than the mantle, the thick crust will decrease the negative buoyancy of the oceanic plate. In addition, thick crust is generated by enhanced partial melting of the mantle, which may leave a melt-depleted layer in the shallow mantle (e.g., Turcotte and Schubert, 2002). This layer has a harzburgite composition and a lower density than undepleted mantle. The presence of thick oceanic crust, with or without a harzburgite layer, reduces the average density of the oceanic plate, retarding its tendency to sink and possibly promoting slab flattening (e.g., Oxburgh and Parmentier, 1977; van Hunen et al., 2002; van Hunen et al., 2004; Arrial and Billen, 2013).

Earlier researchers predicted that an oceanic plateau with crust thinner than ~17 km would subduct, whereas subduction would not occur if the crust is thicker than 30 km (e.g., Cloos, 1993). However, geophysical observations do not support this (e.g., Mann and Taira, 2004). For instance, the Ontong Java Plateau with 30-40 km thick crust has been subducted to the deep upper mantle (Phinney et al., 2004). The main control on oceanic plate subduction is the total

buoyancy of the slab. If the total buoyancy is negative, the slab will tend to subduct into the asthenosphere with little resistance. The total buoyancy depends on the composition of subducting plate (e.g., normal oceanic crust or a thick oceanic plateau), metamorphic phase transitions within the plate, and the age of subducting plate (Arrial and Billen, 2013). Cloos (1993) showed that even with a thick oceanic plateau, the total buoyancy of the oceanic plate will be negative for oceanic plate ages greater than 100 Ma. Therefore, there is still much debate about the effect of an oceanic plateau on subduction dynamics.

In the case of the Laramide orogeny, plate reconstructions show that an oceanic plateau may have subducted below southwestern North America in the Late Cretaceous (Henderson et al., 1984; Tarduno et al., 1985; Liu et al., 2010). This is the conjugate of the Shatsky Rise oceanic plateau, which is a region of thick crust that is presently located offshore Japan. The inferred timing and location of the subduction of the Shatsky conjugate coincides the proposed onset of flat subduction and the location of Laramide orogeny, and therefore these events may be linked (e.g., Saleeby et al., 2003; Liu et al., 2010).

Here, we test the effect of a buoyant oceanic plateau on subduction dynamics, for the case where the continental plate is stationary (V_c=0cm/yr) and there is no thick Colorado Plateau in the continental plate. The oceanic plateau has a width of 400 km, which is consistent with other numerical models of plateau subduction (e.g., van Hunen et al., 2004; Arrial and Billen, 2013). The plateau is initially located 500 km from the trench, such that it enters the trench at the start of Phase III of the models (e.g., Fig. 3.1). The oceanic crust in the plateau has a thickness of 18 km, which is twice that of the normal oceanic crust in the models, and its material properties (density, rheology, etc.) are the same as normal oceanic crust. Several different models are run to test the effects of an eclogite phase change for plateau crust and a low-density harzburgite mantle layer.

3.4.2 Model results

In the first two models, the oceanic plateau does not include a harzburgite layer. Fig. 3.6a shows the model geometry at 2 Ma-emt, just after the oceanic plateau has started to subduct. During subduction, the basaltic crust of the oceanic plateau transforms to eclogite at the same pressure-

temperature conditions as used for the adjacent oceanic crust (Fig. 3.6 b-c). The eclogitized crust has approximately the same density of mantle (at the same temperature). As a result, the oceanic plateau loses its buoyancy at a depth of ~70 km, and the oceanic plate dip angle follows a generally steep trajectory into the mantle, similar to that seen in the reference model with normal-thickness oceanic crust (Fig. 3.2 a-c).

The second model tests the effect of basalt metastability for the oceanic plateau (Fig. 3.6d-f). Experimental data shows that the eclogite phase change may be delayed if conditions are relatively dry (Austrheim, 1991; Hacker, 1996; Leech, 2001; van Hunen et al., 2004 and references therein) and the oceanic crust remains as basalt. We examine the end-member case where there is no eclogite phase change for the plateau, i.e., complete metastability. The assumption is that as the oceanic plateau formed, the extensive mantle melting resulted in dehydration of the underlying mantle, and therefore there is insufficient water in the plateau mantle lithosphere to trigger the eclogite phase change during subduction. The initial subduction of the oceanic plateau (Fig. 3.6d) is identical to that in the previous models. However, as the plateau reaches greater depth, the upper part of the crust starts to detach from the descending oceanic lithosphere, owing to the low density of this material (~400 kg m^{-3} less dense than the mantle at the same temperature). The detached crust accumulates in the mantle wedge corner (Fig. 3.6e) and then migrates laterally and perturbs the continental mantle lithosphere (Fig. 3.6f). Only a thin layer of metastable crust remains attached to the oceanic plate and it is subducted to depth. This has little effect on the trajectory of the remaining oceanic plate, and the subducting plate maintains a relatively steep dip. The oceanic plate curls under itself at the bottom of the model domain. At this point, the oceanic plateau crust starts to buoyantly upwell, causing some crust to detach and float to the base of the oceanic plate. If the oceanic crust is stronger (e.g., the crust material is DMD*1), it does not detach from upper part of slab. However, this increases the strength of the subduction interface (shear zone), which causes subduction to stop and the slab to break near the trench.
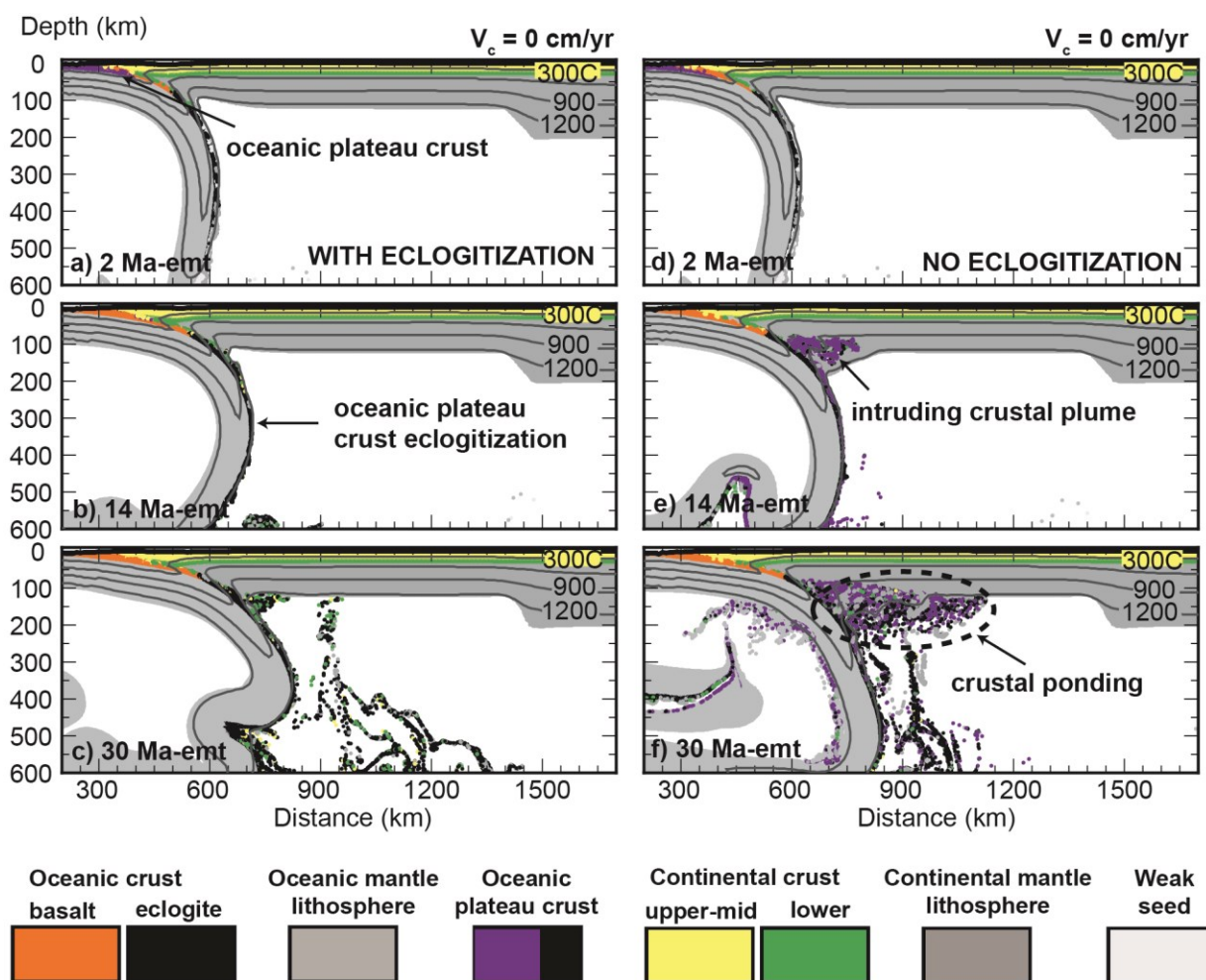
Fig. 3.6. Numerical models for oceanic plateau subduction with crustal eclogitization (Model C1-a; left column) and with no eclogitization (Model C2-a; right column) at: a & d) 2 Ma-emt, b & e) 14 Ma-emt and c & f) 30 Ma-emt respectively. These models have no continental velocity or Colorado Plateau.

In order to produce thickened basaltic crust, at least 20% partial melting of undepleted upper mantle must occur, and melt extraction should leave a depleted, low-density, harzburgite residuum (Turcotte and Schubert, 2002). The thickness of the harzburgite layer is proportional to the thickness of the overlying oceanic crust, and its density depends on the extent of melting and depletion during basalt extraction (Oxburgh and Parmentier, 1977; Turcotte and Schubert, 2002). In the next models, a 36-km thick harzburgite layer is placed immediately below the oceanic plateau crust. This thickness is twice that of the oceanic plateau crust. We test harzburgite layers with densities that are 50 and 100 kg m^{-3} less than that of mantle (at the same temperature). This

thickness and density structure is within the range expected for harzburgite formation through relatively large amounts of partial melting (e.g., van Hunen et al. 2002b and references therein).

Fig. 3.7 shows two models that have a harzburgite layer with a density contrast relative to the mantle ($\Delta\rho$) of -50 kg m^{-3}, one with plateau crust eclogitization (left column) and one without eclogitization (right column). In both models, the oceanic plateau has entered the subduction zone by 2 Ma-emt (Fig. 3.7a, d). In the model with eclogitization, the oceanic plateau causes a slight decrease (<3°) in the deep dip of the oceanic plate. The plateau crust transforms to higher density eclogite at a depth of ~70 km, which increases the negative buoyancy of the oceanic plate. By 14 Ma-emt, the plateau region has been subducted to >500 km depth, where it curls under the steeply-dipping slab (Fig. 3.7b). At this point, the buoyant harzburgite layer starts to upwell beneath the oceanic side of the subduction zone (Fig. 3.7c). Some material accumulates below the oceanic lithosphere and some is removed through the open side boundary of the model. However, this has little effect on the geometry of the subduction zone, which maintains a relatively steep angle. This model exhibits erosion and subduction of continental crust, which ponds in the mantle wedge corner.

The model with no eclogite phase change (Fig. 3.7d-f) also shows a relatively steep slab trajectory during plateau subduction, with only a modest decrease in slab dip relative to the model without an oceanic plateau. As seen previously, part of the low-density basaltic crust detaches from the oceanic plate and accumulates in the shallow sublithospheric mantle. The remaining plateau region is subducted to the bottom of the model domain and curls under the shallower oceanic plate, where there is some bending and uplift of this part of the slab, owing to its buoyancy. Overall, a harzburgite layer with $\Delta\rho$= -50 kg m^{-3} does not significantly affect the subduction trajectory at depths <200 km.
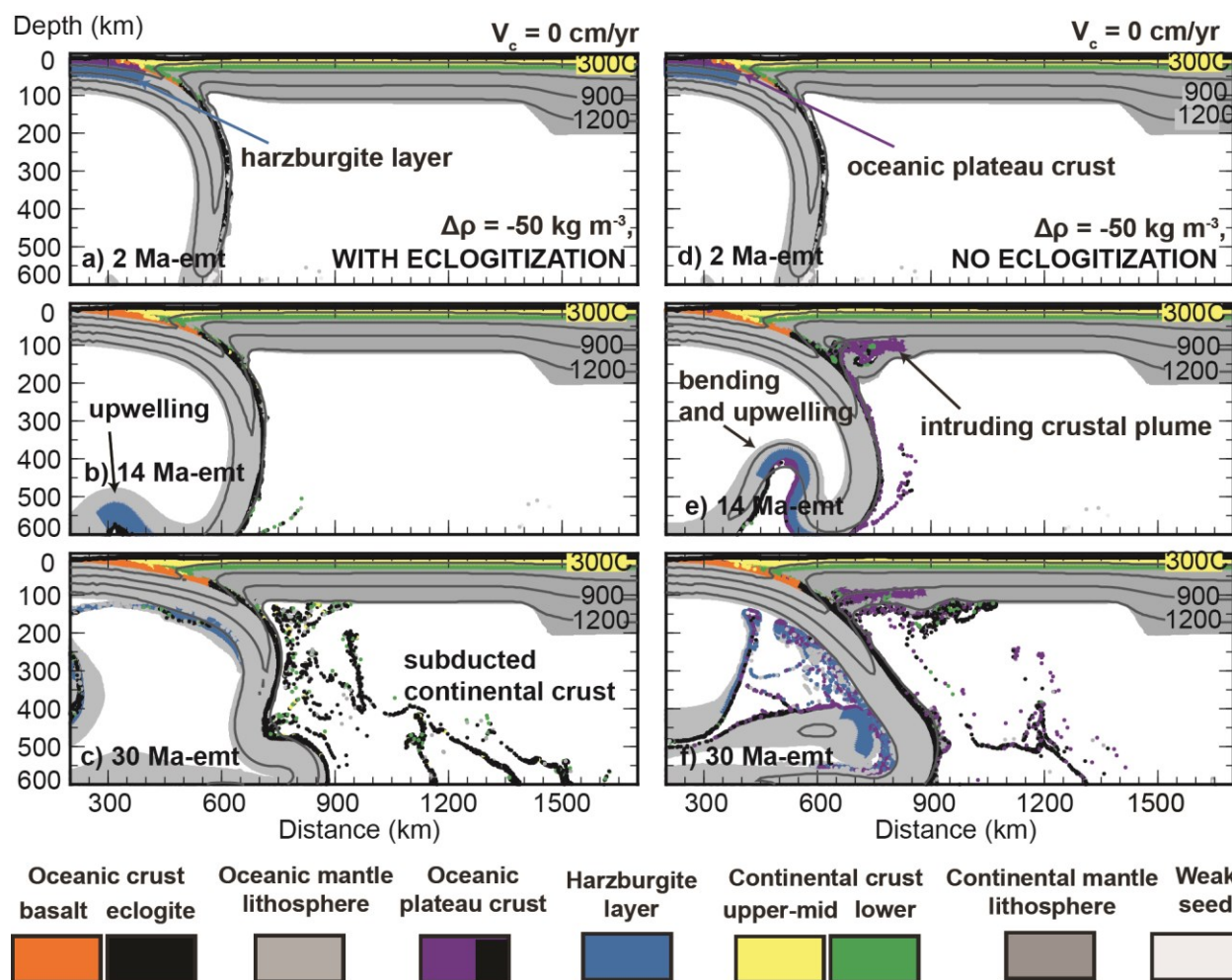
Fig. 3.7. Models of subduction of an oceanic plateau with a low-density harzburgite layer ($\Delta\rho$ = -50 kg m^{-3} relative to the mantle). The left column shows Model C3-a, with eclogitization of the oceanic crust, at: a) 2 Ma-emt, b) 14 Ma-emt and c) 30 Ma-emt. The right column shows Model C3-b, with no plateau crust eclogitization, at: d) 2 Ma-emt, e) 14 Ma-emt and f) 30 Ma-emt. These models have no continental velocity or Colorado Plateau.

Fig. 3.8 shows two models that have a harzburgite layer (HL) with $\Delta\rho$= -100 kg m^{-3} and either plateau crust eclogitization (left column) or metastability (right column). In both models, the slab dip is slightly less than that observed in the previous models with HL $\Delta\rho$= -50 kg m^{-3} (Fig. 3.7), with a decrease in α_d of up to 5° during plateau subduction. In addition, with a basaltic plateau (and HL $\Delta\rho$= -100 kg m^{-3}), the α_d is ~13° less than in the model with no oceanic plateau (Fig. 3.2, left column). With eclogitization, the slab descends relatively steeply to the base of the model (Fig. 3.8a-c). The low-density harzburgite layer starts to upwell below the oceanic plate, causing

a complex geometry in the mantle on the oceanic side of the subduction zone. If plateau crust does not eclogitize, the buoyant crust detaches from the oceanic plate and ponds in the shallow mantle (Fig. 3.8d-f). In addition, as the plateau reaches the bottom of the model, the low-density harzburgite starts to upwell, causing the slab to break (Fig. 3.8e). The remaining slab is then deflected horizontally along the bottom boundary of the model (Fig. 3.8f), rather than folding on itself.
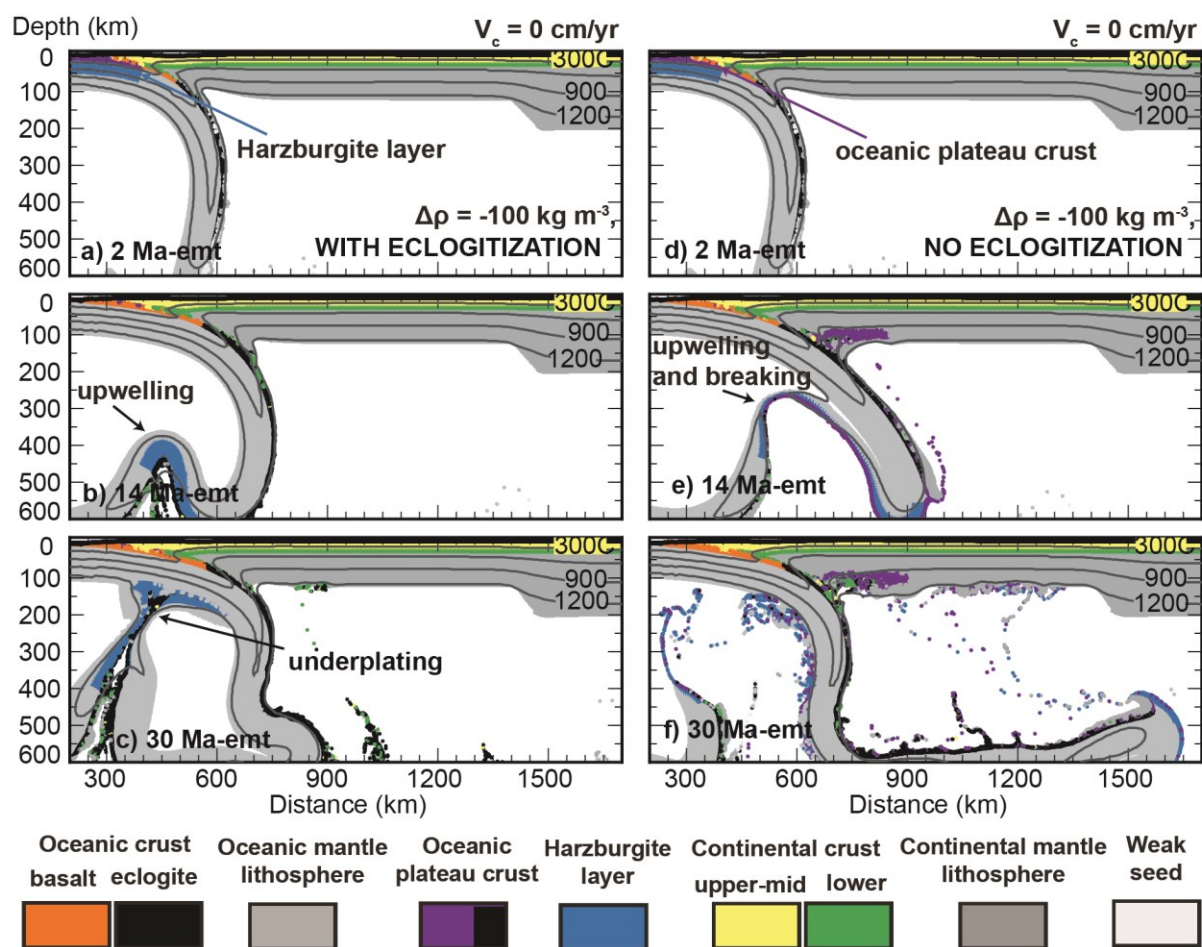
Fig. 3.8. Models of subduction of an oceanic plateau with a low-density harzburgite layer ($\Delta\rho$ = -100 kg m^{-3} relative to the mantle). The left column shows Model C4-a, with eclogitization of the oceanic crust, at: a) 2 Ma-emt, b) 14 Ma-emt and c) 30 Ma-emt. The right column shows Model C4-b, with no plateau crust eclogitization, at: d) 2 Ma-emt, e) 14 Ma-emt and f) 30 Ma-emt. These models have no continental velocity or Colorado Plateau.

The preceding six models demonstrate that a buoyant oceanic plateau causes a visible decrease (∼2°-13°) in the deep dip angle of the slab as the plateau is subducted. In all cases, a full metamorphic phase change of oceanic plateau basalt to eclogite (with a density similar to that of mantle) results in a decrease in buoyancy of the slab and the subduction trajectory remains fairly steep during plateau subduction. If the oceanic crust remains metastable, some of the crust detaches from the oceanic plate at 100-150 km depth. As noted above, detachment can be inhibited if the crust has a stronger rheology, but this then leads to the oceanic plate breaking near the trench. The presence of a low-density harzburgite layer produces a slight shallowing of the subduction trajectory, but this is not sufficient to generate flat subduction at shallow depths (<200 km).

3.5 The influence of multiple factors on the slab dip angle

The results from Sections 3.2-3.4 show that each individual factor (enhanced continental velocity; increased slab suction due to the Colorado Plateau root; subduction of a low-density oceanic plateau) can decrease in the dip angle of the subducted oceanic plate. However, none of the models shows a transition to flat (subhorizontal) subduction. As discussed above, it appears that all three factors may have occurred in the southwestern United States prior to the Laramide orogeny. Therefore in this section, we present models that consider combinations of the three factors in order to explore whether multiple factors can create flat subduction.

3.5.1 Continental velocity and Colorado Plateau

First, the combination of a trenchward continental velocity (V_c=4 cm/yr) and a 240 km thick Colorado Plateau is examined (Fig. 3.9). In this model, as the oceanic plate subducts, its dip angle becomes shallower over time. By 30 Ma-emt, the oceanic plate is in contact with the thickened lithosphere of the Colorado Plateau (Fig. 3.9c). At this time, some shortening is observed at the left side of the Colorado Plateau. This is likely because as the slab shallows, the temperature along the subduction interface (shear zone) decreases, which leads to an increase in the strength of the shear zone and greater coupling between the oceanic and continental plates.

This is sufficient for some of the plate convergence to be partitioned into compressive deformation in the overlying continent.

During the 30 Ma model run, the slab trajectory shallows, and the model predicts a landward migration of the volcanic arc by >400 km. However, there is no indication of further unbending of the slab to create flat subduction beneath the continent. This model can be compared to the model with only a high continental velocity (Fig. 3.2d-f) and the model with only a Colorado Plateau (Fig. 3.3). At 14 Ma-emt, the model with both factors has a deep slab dip of $\alpha_d=39°$, whereas the dip is $\alpha_d=41.2°$ with only a high V_c and $\alpha_d=50.6°$ with only a Colorado Plateau. From this, we infer that slab shallowing is primarily controlled by the high V_c, but the presence of the thick Colorado Plateau lithosphere enhances the rate of shallowing.
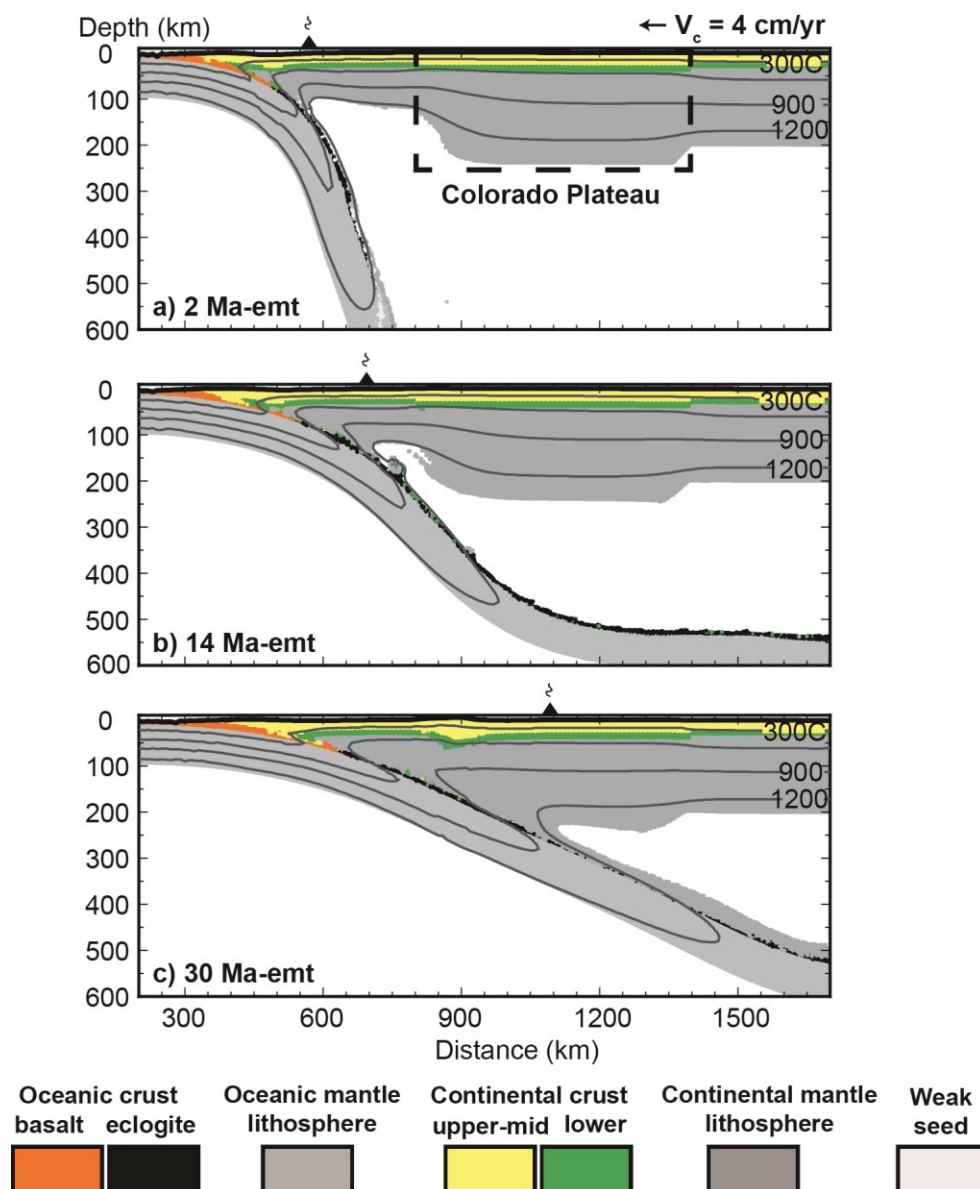
Fig. 3.9. Evolution of Model B1-c with thick Colorado Plateau lithosphere and V_c = 4 cm/yr at: a) 2 Ma-emt, b) 14 Ma-emt and c) 30 Ma-emt.

As discussed in Section 3.3, slab shallowing may also be enhanced with a high mantle wedge viscosity. To illustrate the effect of mantle viscosity on slab dynamics, we have rerun the previous model (Model B1-c with Colorado Plateau and V_c=4 cm/yr) with different viscosities in the sublithospheric mantle. The original model uses a wet olivine rheology, which is both temperature and strain-rate dependent. For simplicity, we have replaced this with a constant

sublithospheric mantle viscosity (η_{SLM}). For $\eta_{SLM} = 10^{19}$ Pa s (Fig. 3.10a), the slab dip shallows over time, with a geometry is similar to that in the model with the wet olivine at 14 Ma-emt (Fig. 3.9b). This reflects the fact that the effective viscosity of the sublithospheric mantle in the original model is close to 10^{19} Pa s (see, for example, Fig. 3.4). At higher values of η_{SLM}, the slab suction force increases, resulting in more rapid slab shallowing. For $\eta_{SLM} = 10^{21}$ Pa s (Fig. 3.10b), the slab shallows and collides with the Colorado Plateau lithosphere by 14 Ma-emt. This causes entrainment of the deep lithosphere root by the subducting plate, as well as compressive deformation and shortening in the overlying continent. Note that the slab still has an inclined geometry. For $\eta_{SLM} = 10^{22}$ Pa s (Fig. 3.10c), a sub-horizontal slab does appear by 14 Ma-emt, but the slab itself shows significant internal deformation. In the initial stages of this model, the slab trajectory shallows. However, with the high mantle viscosity, it is difficult for the slab to penetrate into the deep part of the upper mantle, and the slab is emplaced below the continental lithosphere. With continued plate convergence, the slab breaks and deforms. In the latter part of the model run, subduction ceases and plate convergence causes shortening in the continental crust. Therefore, the flat slab in this model appears to be primarily due to the fact that the high mantle viscosity prevents deep subduction, as opposed to lifting of the slab by the suction force. Given that observational data suggest upper mantle viscosities of ~10^{21} Pa s, with even lower viscosities in a subduction zone mantle wedge (10^{18}-10^{19} Pa s) (see Section 3.3.1), we do not consider this to be a reasonable model of flat subduction.
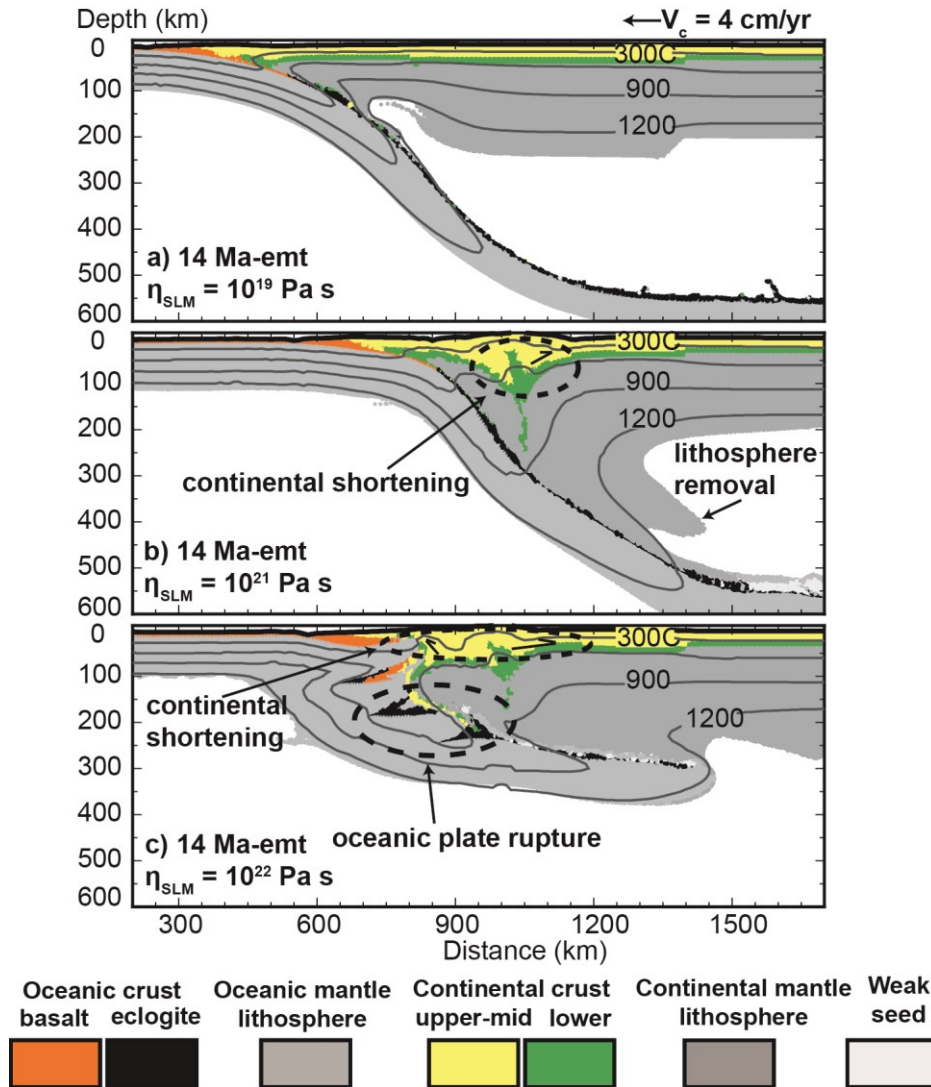
Fig. 3.10. Models with V_c = 4cm/yr and a thick Colorado Plateau at 14 Ma-emt. Models use a constant viscosity for the sublithospheric mantle (η_{SLM}): a) 10^{19} Pa s, b) 10^{21} Pa s and c) 10^{22} Pa s respectively.

3.5.2 Continental velocity and oceanic plateau

In this set of models, we consider the effect of oceanic plateau subduction with a continental velocity of V_c=4 cm/yr; there is no Colorado Plateau in the continental plate. Fig. 3.11 shows models with 18-km thick crust but no harzburgite layer in the oceanic plateau. If the plateau undergoes eclogitization during subduction (Fig. 3.11a-c), the model evolution is similar to that seen in the model with no oceanic plateau (Fig. 3.2d-f). At 14 Ma-emt, the slab has a deep dip

angle of α_d=38.7°, which is slightly less than the model with no plateau. If the oceanic plateau crust remains metastable, the slab dip angle is even shallower, α_d=36.5° at 14 Ma-emt (Fig. 3.11e). Some of the low-density crust detaches from the oceanic plate and ponds in the shallow mantle. This material perturbs the continental lithosphere causing parts of the lower continental lithosphere to undergo gravitational destabilization because it is cool and dense (Fig. 3.11f). A thin layer of plateau crust remains intact on the oceanic plate and is subducted into the deeper mantle (Fig. 3.11e). The buoyancy of this material causes uplift of the slab and a transient flat region at ~400 km depth. However, at depths <200 km, the slab maintains an inclined trajectory, with a slab dip that is slightly shallower than in the model with eclogitization.
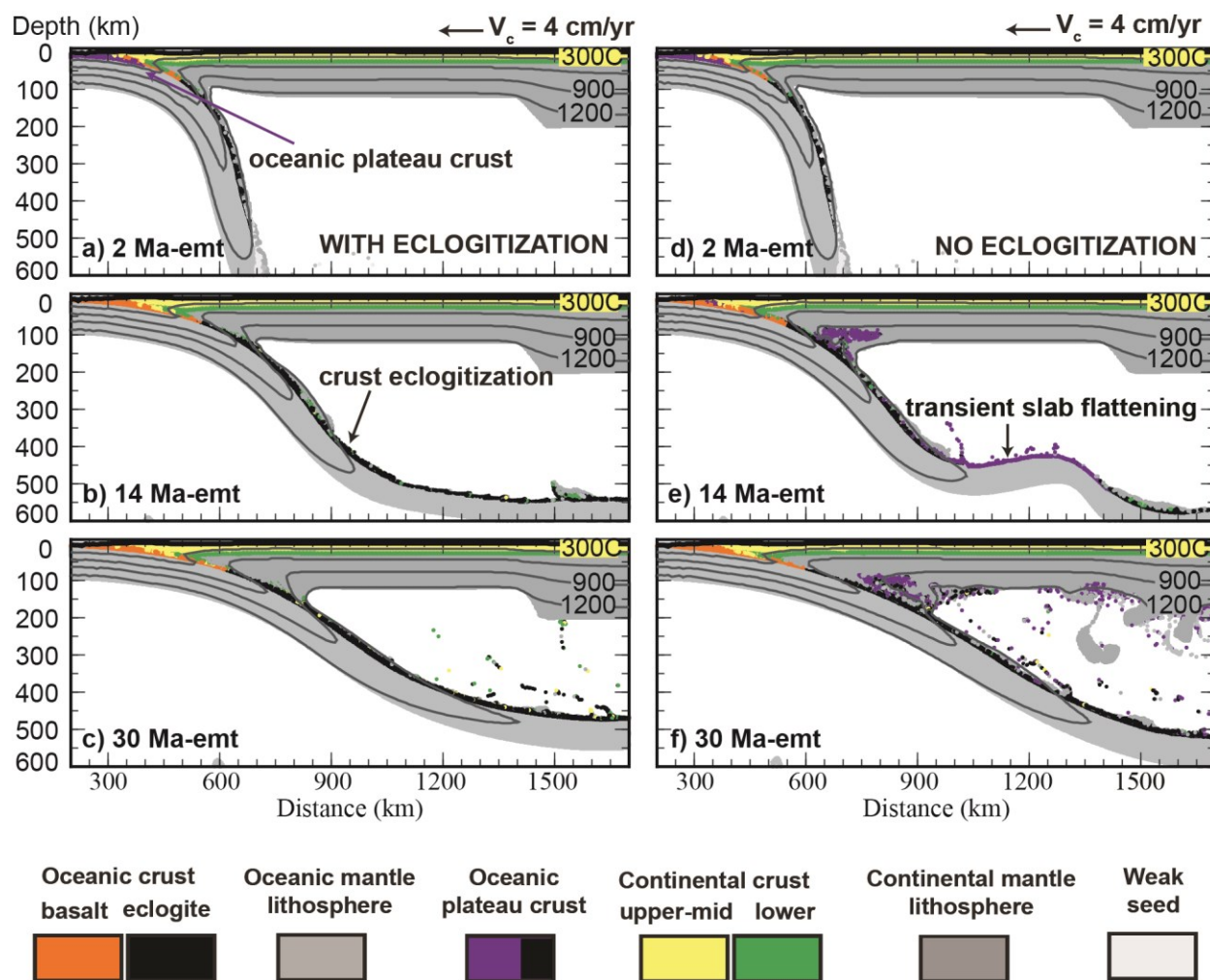
Fig. 3.11. Evolution of models with oceanic plateau subduction and V_c = 4 cm/yr. The left column shows Model C1-c that has crustal eclogitization at: a) 2 Ma-emt, b) 14 Ma-emt and c) 30 Ma-emt. The right column shows Model C2-c with no crustal eclogitization at: d) 2 Ma-emt, e) 14 Ma-emt and f) 30 Ma-emt.

In the next models, a low-density 36-km-thick harzburgite layer is added to the oceanic plateau. Fig. 3.12 shows two models where the harzburgite density is 50 kg m^{-3} less than that of mantle. If the oceanic crust undergoes eclogitization (Fig. 3.12, left column), the oceanic plateau has little effect on subduction dynamics and the slab geometry is only slight shallower than in the model with no plateau (Fig. 3.2d-f). This shows that it is the trenchward velocity of the continental plate that has the largest effect on slab geometry. As the harzburgite layer is subducted to ~400 km depth, its buoyancy causes the slab to bend upward, creating a transient flat slab in the deep upper mantle. There is little effect on the slab dip at <200 km depth.

The right column of Fig. 3.12 shows a model in which the oceanic plateau crust remains metastable. During subduction, the upper part of the plateau crust buoyantly detaches and accumulates in the shallow mantle (Fig. 3.12e). With the trenchward continental velocity, the plateau is subducted laterally under the continent. The slab breaks at a depth of ~400 km (~1000 km landward of the trench). The break-off is caused by the competing effects of the positively buoyant oceanic plateau and the negatively buoyant slab material landward of the plateau (hereafter called the frontal slab). The plateau region resists subduction and starts to upwell, while the frontal slab sinks. After the break-off, the new slab tip has an upward curvature, but this does not affect the geometry of the shallower subduction zone. With continued subduction, some of the harzburgite layer floats up to the top of the sublithospheric mantle but the oceanic plate maintains an inclined geometry (Fig. 3.12f). In the comparable model with no continental velocity (Fig. 3.7d-f), the slab curls under itself at the base of the model and the harzburgite layer is pushed to the oceanward side of the subduction zone where it upwells.
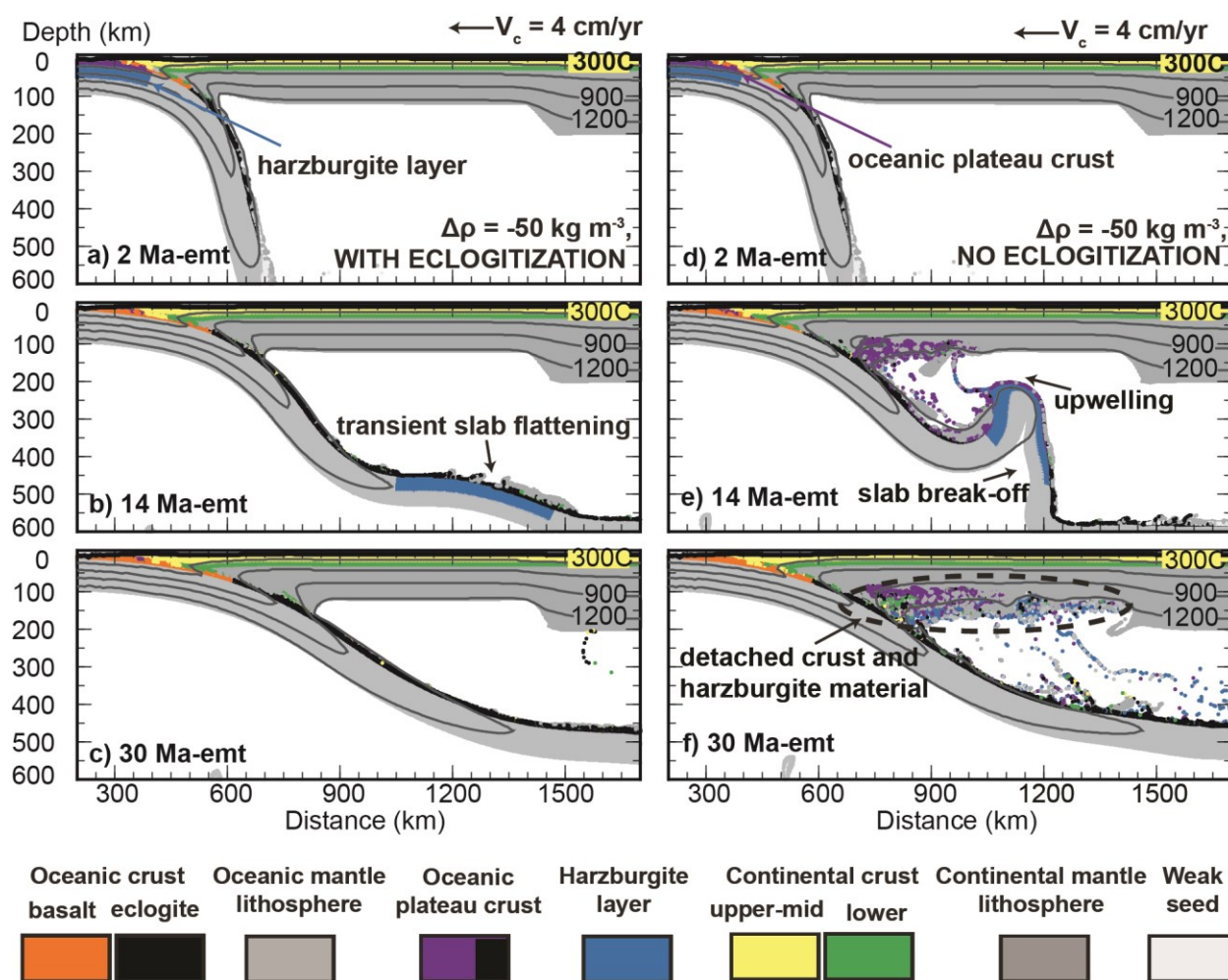
Fig. 3.12. Evolution of models with V_c = 4 cm/yr and an oceanic plateau with a low-density harzburgite layer ($\Delta\rho$ = -50 kg m^{-3} relative to the mantle). The left column shows Model C3-d that has crustal eclogitization at: a) 2 Ma-emt, b) 14 Ma-emt and c) 30 Ma-emt. The right column shows Model C3-e with no crustal eclogitization at: d) 2 Ma-emt, e) 14 Ma-emt and f) 30 Ma-emt.

The next models include a harzburgite layer with a density contrast of $\Delta\rho$ = -100 kg m^{-3} relative to the mantle. If the oceanic plateau crust undergoes eclogitization (Fig. 3.13, left column), the subduction zone exhibits a moderate decrease in subduction trajectory over time; this appears to be primarily due to the continental plate motion. The plateau harzburgite layer is subducted below the continent and starts to upwell owing to its low density. This causes the slab to break and the harzburgite layer to be emplaced at the base of the continent. However, this does not result in a significant decrease in subduction dip angle at depths less than 200 km.

In contrast, flat subduction is generated in the model in which there is no eclogitization of the oceanic plateau crust (Fig. 3.13, right column). This model exhibits a relatively steep subduction angle at 2 Ma-emt (Fig. 3.13e). The slab then undergoes a break-off at 10 Ma-emt (Fig. 3.13f), and at 14 Ma-emt, the slab transits to flat (subhorizontal) subduction (Fig. 3.13g). The onset of flat subduction is the result of several events: 1) trenchward motion of the continent causes a decrease in slab dip angle; 2) a further reduction in dip angle is induced as the low-density oceanic plateau crust and harzburgite layer are subducted into the mantle; and 3) the slab break-off at a depth of ~150 km, near the landward end of the oceanic plateau. Owing to (1) and (2), the plateau is emplaced below the continent, instead of curling under the subduction zone (as seen in models with V_c=0 cm/yr). Following the slab break-off, the negatively buoyant frontal slab detaches and sinks to the bottom of the model domain. The oceanic plateau remains attached to the subducting plate, its buoyancy is sufficient to cause flat subduction at a depth of ~100 km. This depth appears to be controlled by the thickness of the strong continental lithosphere. The subhorizontal slab perturbs the deeper (weaker) part of the continental lithosphere, causing this material to delaminate. Later in the model evolution, the oceanic breaks at the trench and subduction below the continent stops (Fig. 3.13h). This is because the strength of the subduction interface (shear zone) has exceeded the strength of the oceanic plate.
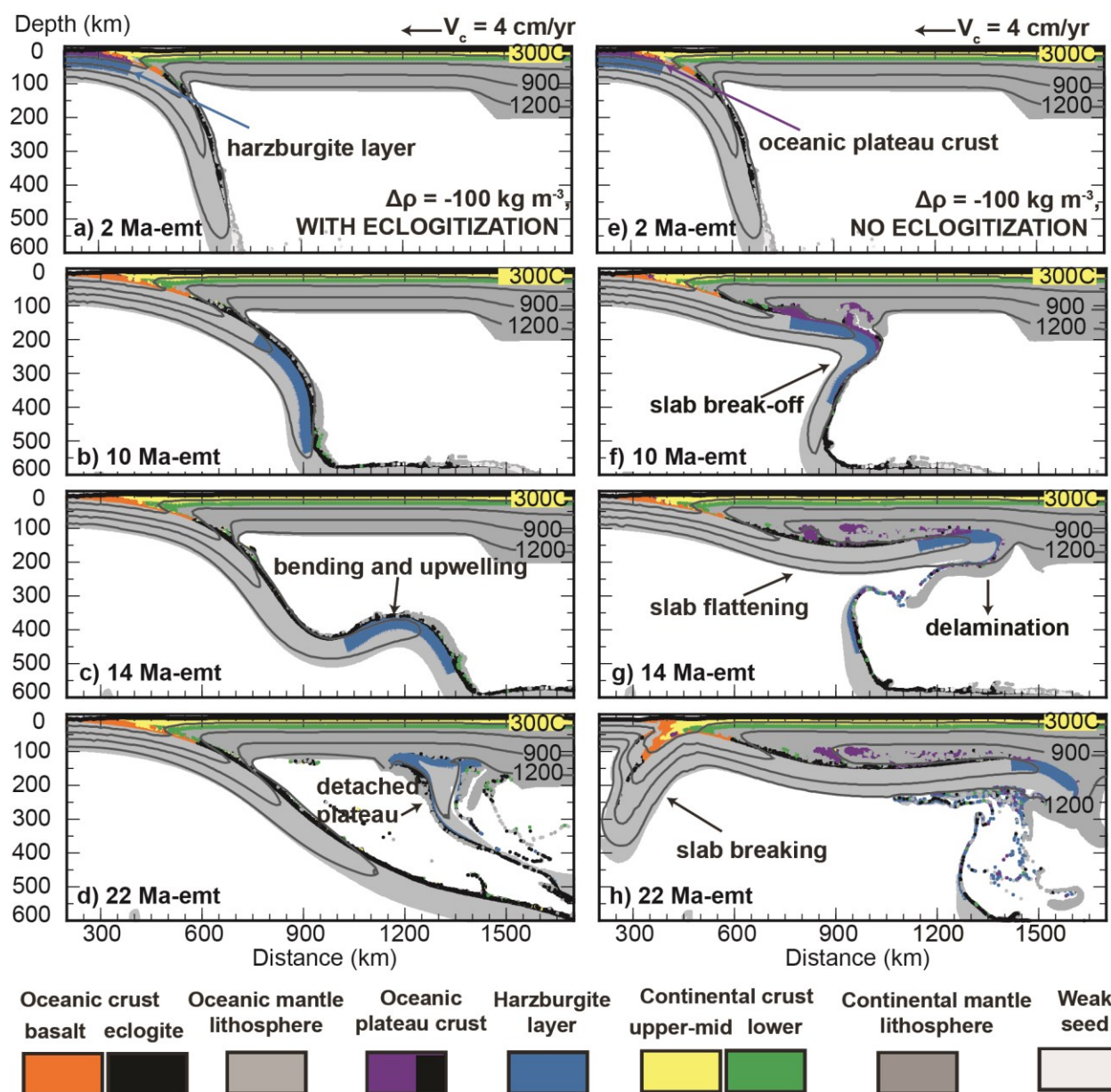
Fig. 3.13. Evolution of models with V_c = 4 cm/yr and an oceanic plateau with a low-density harzburgite layer ($\Delta\rho$ = -100 kg m^{-3} relative to the mantle). The left column shows Model C4-d that has crustal eclogitization at: a) 2 Ma-emt, b) 10 Ma-emt, c) 14 Ma-emt and d) 22 Ma-emt. The right column shows Model C4-e with no crustal eclogitization at: e) 2 Ma-emt, f) 10 Ma-emt, g) 14 Ma-emt and h) 22 Ma-emt.

The previous models show that the presence of a low-density harzburgite layer has a strong effect on subduction dynamics for a subduction zone with an advancing upper plate. This brings up the question of whether flat subduction could be generated for a case with V_c=4 cm/yr and an

oceanic plate that has normal thickness oceanic crust and a low-density harzburgite layer. A harzburgite layer is generated through >20% partial melting of the mantle, and these conditions may be met during the generation of normal-thickness oceanic crust at a mid-ocean ridge, although the harzburgite layer would be thinner and less depleted (Oxburgh and Parmentier, 1977; Turcotte and Schubert, 2002). We test an extreme case of an 18-km thick harzburgite layer with $\Delta\rho$ = -100 kg m^{-3}; this lies below normal thickness oceanic crust (Model Group H, Table 3.2). The results are shown in Fig. 3.14 for a model that includes oceanic crust eclogitization (left column) and a model with no eclogitization (right column). At the start of Phase III of the models, the slab dip is less than in the previous models, because of the low-density harzburgite. In both models, the trenchward velocity of the oceanic plate (V_c=4 cm/yr) causes the subducting plate dip to further decrease over time. However, the low-density harzburgite layer is not sufficient to create sub-horizontal subduction in either case. Close to the trench (depth <200 km), both slab geometries are similar to the geometry observed in the model with no harzburgite layer (Fig. 3.2d-f). In the model with no eclogitization (Fig. 3.14, right column), the oceanic crust buoyantly separates from the oceanic plate and it accumulates below the continental lithosphere. In addition, after reaching the bottom of the model domain, the slab undergoes bending and upwelling (Fig. 3.14d), which causes some slab material to detach and underplate the continent (Fig. 3.14e). This produces substantial compositional heterogeneity under the continent (Fig. 3.14f), but the geometry of subducting slab is not significantly affected. On the basis of these models, we conclude that subduction of a continuous low density layer is not able to create subhorizontal subduction in the shallow mantle. Instead, it appears that a perturbation to the slab density structure, such as the presence of an oceanic plateau, is needed to induce flattening.
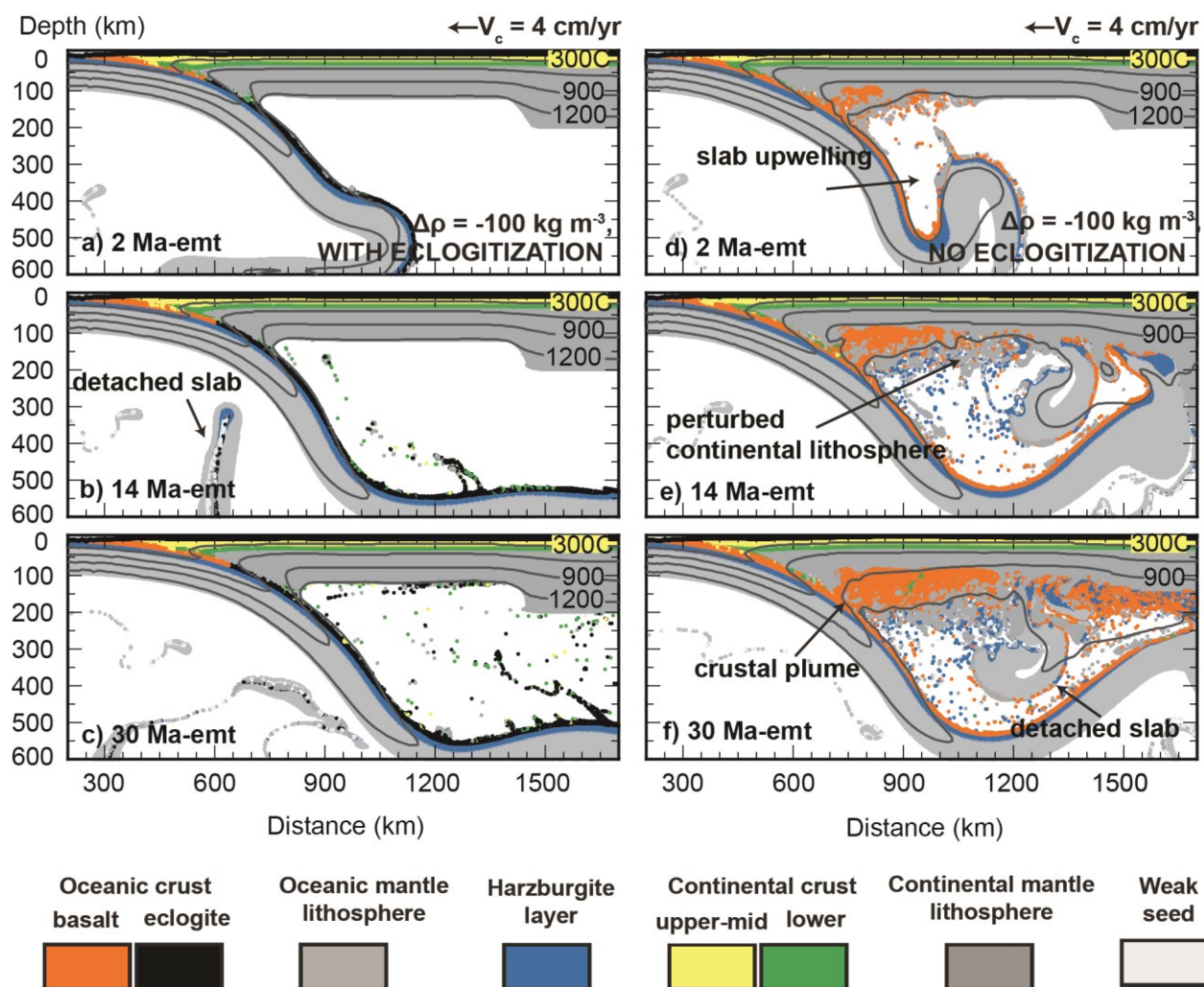
Fig. 3.14. Evolution of models with a continental velocity of $V_c = 4$ cm/yr and a normal-thickness oceanic crust and a harzburgite layer ($\Delta\rho = -100$ kg m^{-3} relative to the mantle). The left column shows Model H-a with oceanic crust eclogitization at: a) 2 Ma-emt, b) 14 Ma-emt and c) 30 Ma-emt. The right column shows Model H-b with no eclogitization at: d) 2 Ma-emt, e) 14 Ma-emt and f) 30 Ma-emt.

3.5.3 Colorado Plateau and oceanic plateau

In this section, the combination of thick Colorado Plateau lithosphere and a buoyant oceanic plateau is tested. In these models, the continent is stationary (V_c=0 cm/yr) and the oceanic plateau crust does not undergo eclogitization. Three different models are presented: one with no oceanic plateau harzburgite layer (Fig. 3.15a), one with a harzburgite layer with $\Delta\rho = 50$ kg m^{-3} (Fig. 3.15b), and one with a harzburgite layer with $\Delta\rho = 100$ kg m^{-3} (Fig. 3.15c). In all cases, the

subduction trajectory remains relatively steep through the model evolution, with a slightly (<12°) lower dip at 100-200 km depth as the harzburgite layer density decreases. With the steep trajectory, the slab curls under itself as it encounters the bottom of the model domain. At this point, the models, especially those with a buoyant harzburgite layer, exhibit upwelling of this material on the oceanic side of the subduction zone, but do not induce flat subduction.
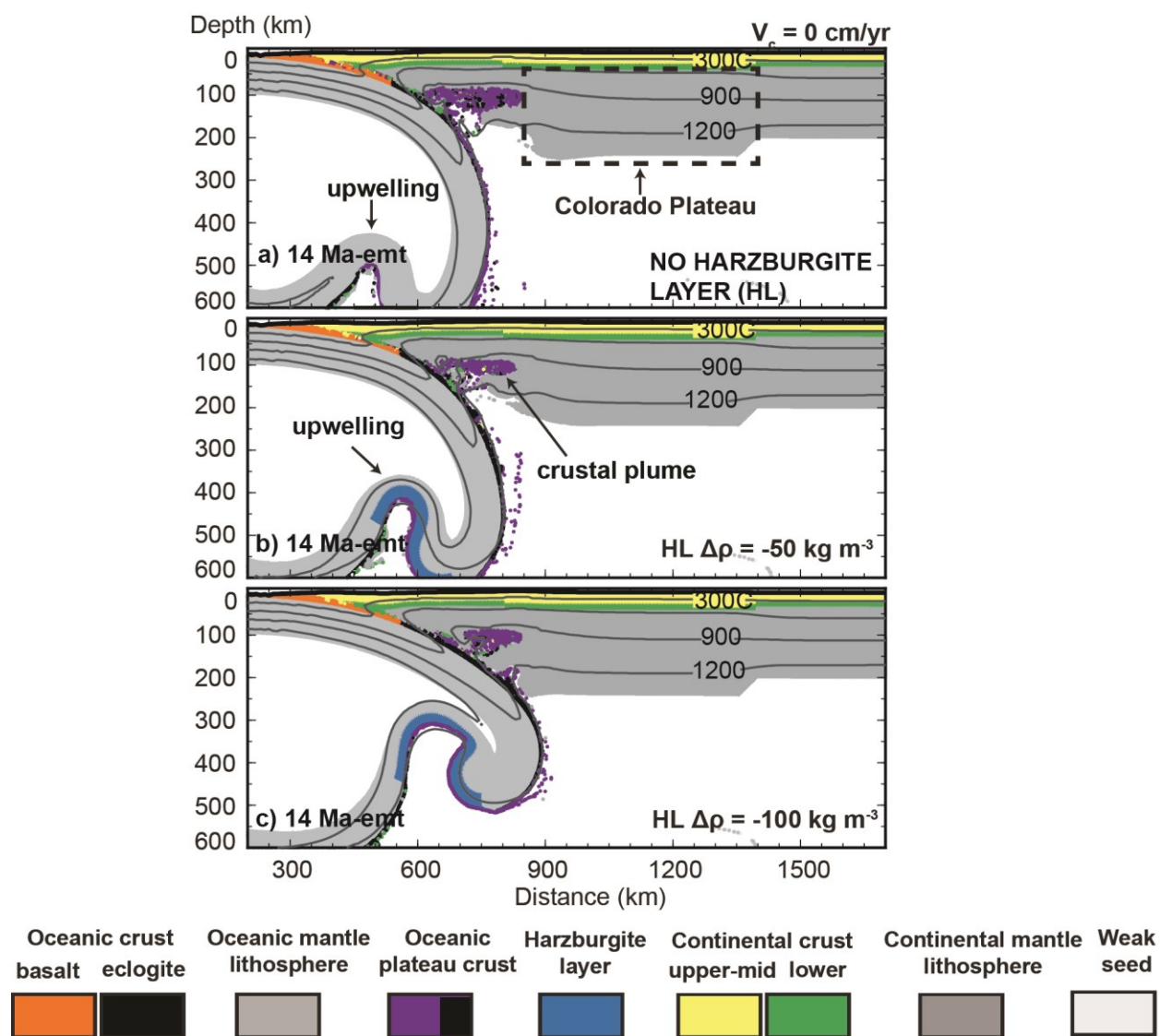
Fig. 3.15. Numerical models with a Colorado Plateau and oceanic plateau at 14 Ma-emt: a) Model D1-a with no harzburgite layer; b) Model D2-a with a harzburgite layer with $\Delta\rho = -50$ kg m^{-3} and c) Model D3-a with a harzburgite layer with $\Delta\rho = -100$ kg m^{-3}. The oceanic plateau crust does not undergo eclogitization and the continental plate is stationary.

3.5.4 Continental velocity, Colorado Plateau and oceanic plateau

We now combine all three factors: a continental plate velocity (V_c=4 cm/yr), a 240 km thick Colorado Plateau block in the continental plate, and a buoyant oceanic plateau. Fig. 3.16 shows models that do not include a harzburgite layer in the oceanic plateau, for a case with oceanic plateau crust eclogitization (left column) and a case with no eclogitization (right column). In both models, the slab trajectory shallows over time and pinches out the mantle wedge corner below the Southern California. It is predicted that the volcanic arc would migrate landward by >500 km. The rate of slab shallowing is slightly faster than observed in models with only a continental plate velocity (Fig. 3.2d-f) or with a continental plate velocity and Colorado Plateau (Fig. 3.9). This suggests that the oceanic plateau enhances the development of low-angle subduction. If the oceanic plateau crust undergoes eclogitization, the slab maintains an inclined trajectory throughout the model run (Fig. 3.16a-c). As the slab encounters the edge of the thick Colorado Plateau lithosphere, some plate convergence is partitioned into continental shortening at the edge of the Colorado Plateau (Fig. 3.16c). If there is no eclogite phase change, an inclined trajectory is also observed during plateau subduction (Fig. 3.16d). As the plateau enters the mantle, some oceanic plateau crust detaches and is emplaced within or below the continental lithosphere. The remaining plateau crust is subducted into the deeper mantle and its buoyancy causes uplift and flattening of the oceanic plate at ~400 km depth (Fig. 3.16e), but this does not cause shallowing of the updip part of the slab.
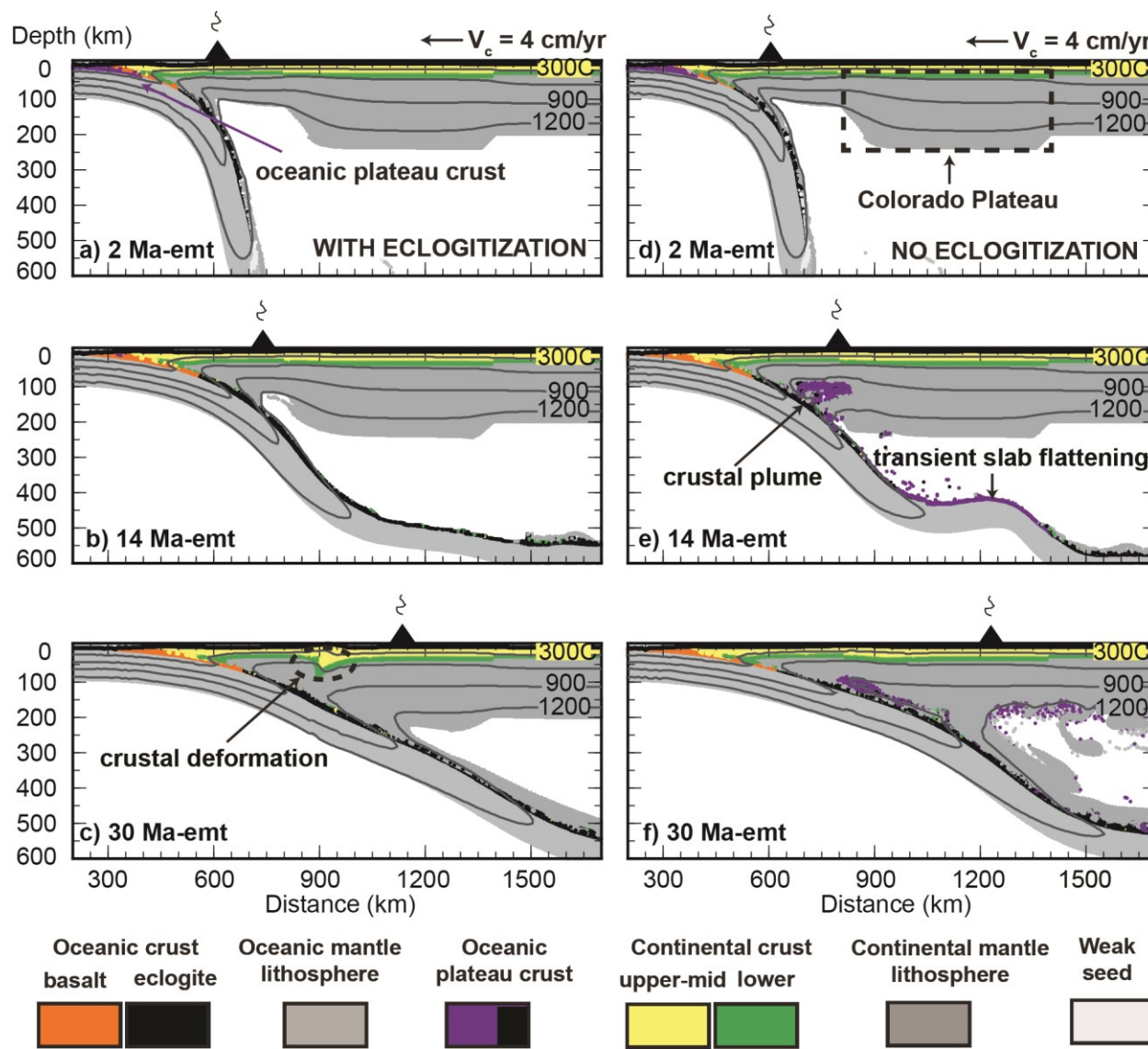
Fig. 3.16. Evolution of models that combine continental plate velocity ($V_c = 4$ cm/yr), thick Colorado Plateau lithosphere and subduction of an oceanic plateau with no harzburgite layer. The left column shows a model with oceanic plateau crust eclogitization (Model E1-b) and the right column shows a model with no eclogitization (Model D1-c) in oceanic plateau: a & d) 2 Ma-emt, b & e) 14 Ma and c & f) 30 Ma-emt.

The next models include an oceanic plateau with a low-density harzburgite layer that has a density contrast (relative to the mantle) of -50 kg m^{-3} (Fig. 3.17) and -100 kg m^{-3} (Fig. 3.18). The overall model evolution is similar to that observed in the comparable models with V_c=4 cm/yr and an oceanic plateau but no Colorado Plateau (Fig. 3.12 and 3.13, respectively). In the new models, the slab trajectory shallows over time and the presence of the Colorado Plateau appears

to cause a slight increase in the rate of shallowing. The models in which the oceanic plateau crust undergoes eclogitization do not develop flat subduction at shallow depths (Fig. 3.17a-c; Fig. 3.18a-c), although there is some uplift of the oceanic plate by the low-density harzburgite layer in the deep upper mantle (>300 km depth); the effect is largest for the lower density harzburgite layer (Fig. 3.18b). After the plateau has been subducted to >300 km depth, the subducting plate contacts the edge of the Colorado Plateau lithosphere. This produces enhanced coupling along the subduction interface (shear zone), which induces deformation of the overlying continent (Fig. 3.17c and 3.18c).

The models in which there is no oceanic plateau crust eclogitization show a decrease in the angle of subduction and buoyant detachment of the upper part of the plateau crust in the mantle. The remaining plateau is subducted below the continental lithosphere. With a harzburgite layer with $\Delta\rho = -50$ kg m^{-3}, the slab undergoes break-off at ~400 km depth and the plateau upwells and intrudes the base of the Colorado Plateau lithosphere (Fig. 3.17e). The oceanic plateau then moves landward by continued plate convergence, and the deep part of the slab exhibits a flat region at a depth of 400 km, but the shallower slab does not flatten (Fig. 3.17f). With $\Delta\rho = -100$ kg m^{-3}, the oceanic plateau is sufficiently buoyant to cause an enhanced slab shallowing as the plateau is subducted (Fig. 3.18e). The slab undergoes breakoff at a depth of 200-300 km, and the slab attains a sub-horizontal geometry at a depth of 200 km. With continued plate convergence, the slab displaces the lower continental mantle lithosphere, causing it to delaminate. The coupling along the subducting interface increases as the sub-horizontal slab moves landward, and the subduction zone eventually fails as the slab breaks at the trench (Fig. 3.18f).

This last model is another example of the successful development of flat subduction at the base of the continental lithosphere. The difference between this model (Fig. 3.18, left column) and the previous flat slab model (Fig. 3.13, left column) is that this one contains a thick Colorado Plateau lithosphere. This lithosphere is cool and strong, which causes the slab to be deflected along the deep part of the lithosphere, producing a flat slab that is ~100 km deeper than that in the model with no Colorado Plateau.
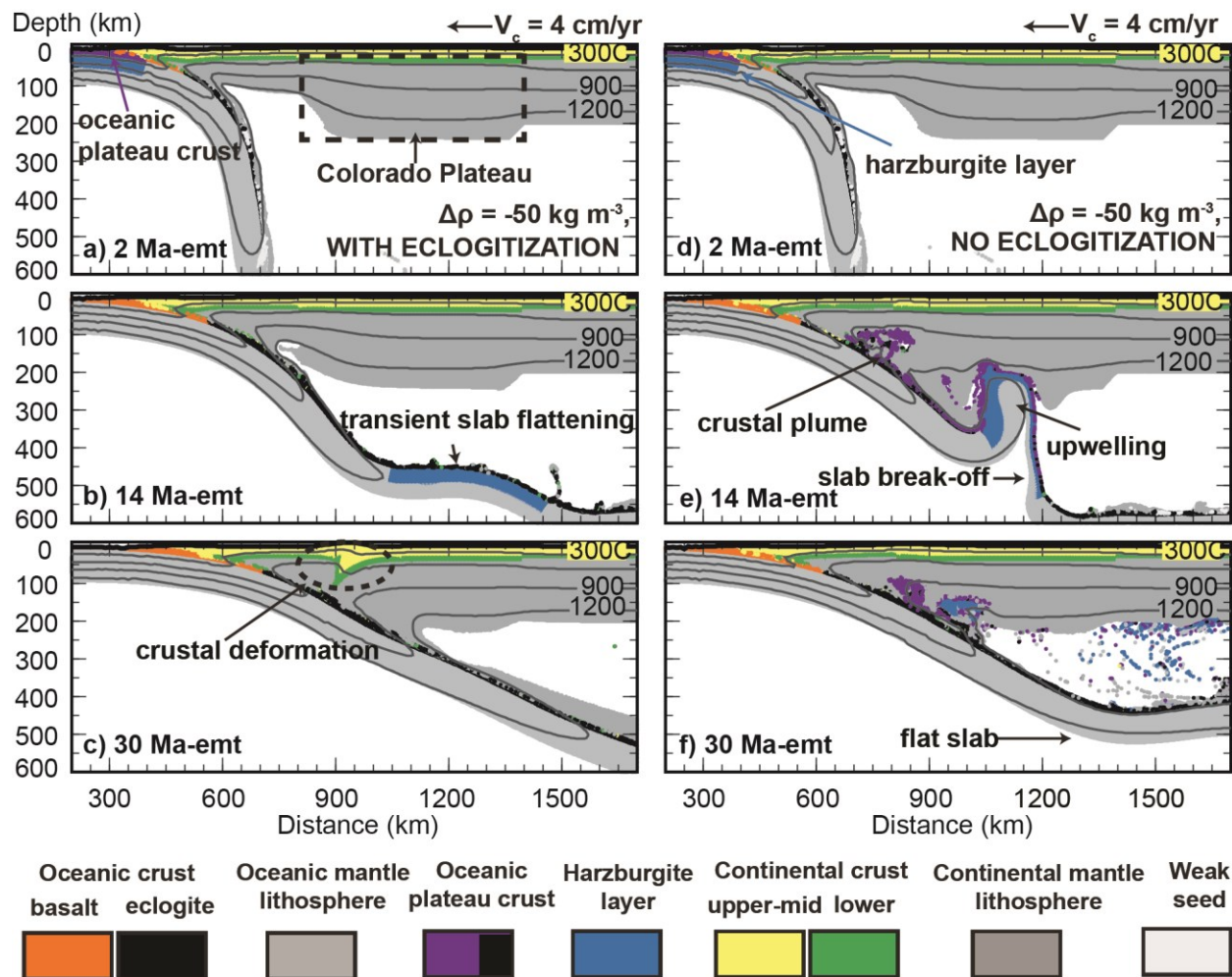
Fig. 3.17. Evolution of models that combine continental plate velocity (V_c = 4 cm/yr), the presence of thick Colorado Plateau lithosphere and subduction of an oceanic plateau with harzburgite layer ($\Delta\rho$ = -50 kg m^{-3} relative to the mantle). The left column shows a models with oceanic plateau crust eclogitization (Model E2-b) and the right column shows a model with no eclogitization (Model D2-c) in oceanic plateau: a & d) 2 Ma-emt, b & e) 14 Ma and c & f) 30 Ma-emt.
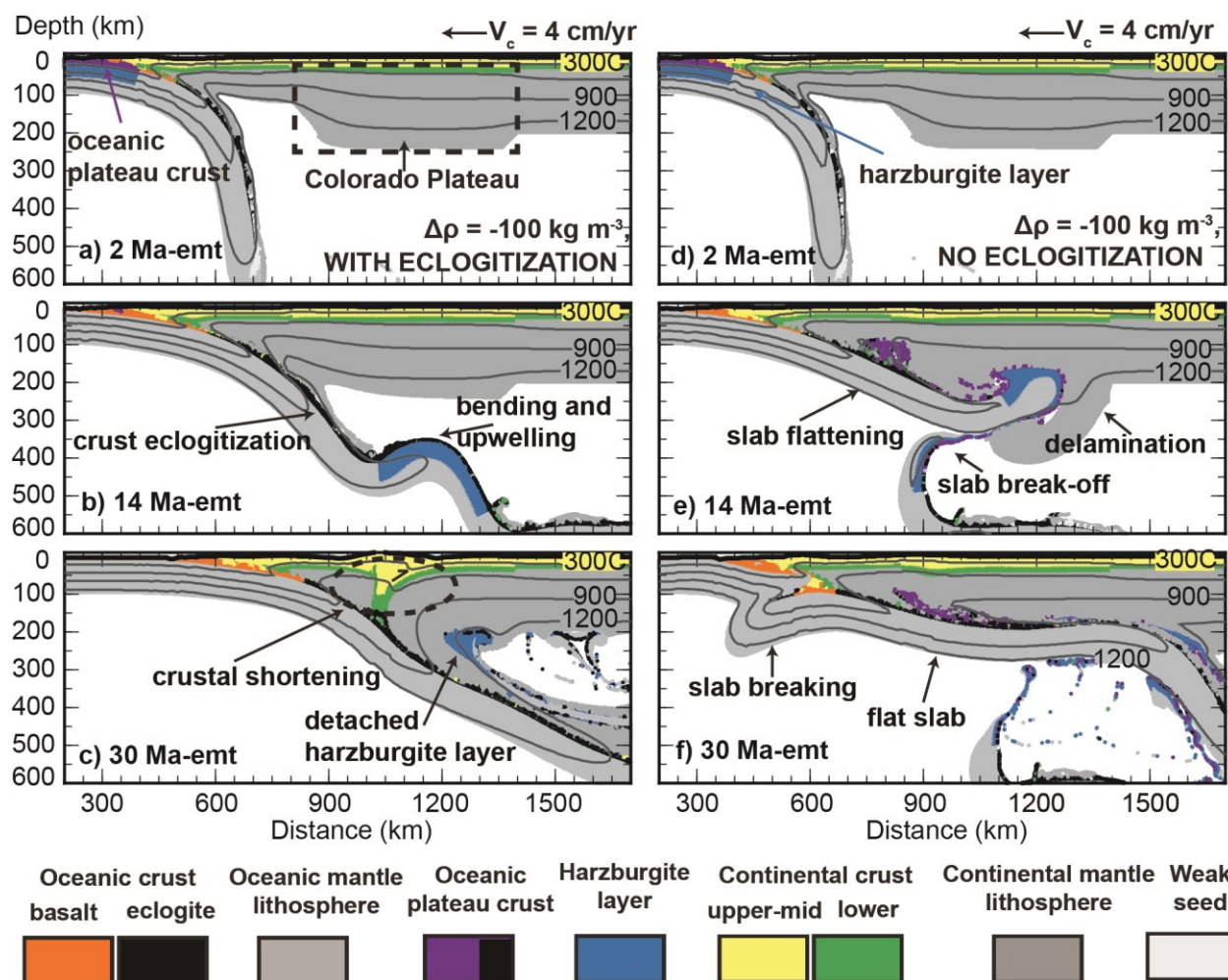
Fig. 3.18. Evolution of models that combine continental plate velocity (V_c = 4 cm/yr), the presence of thick Colorado Plateau lithosphere and subduction of an oceanic plateau with harzburgite layer ($\Delta\rho$ = -100 kg m^{-3} relative to the mantle). The left column shows a models with oceanic plateau crust eclogitization (Model E3-b) and the right column shows a model with no eclogitization (Model D3-c) in oceanic plateau: a & d) 2 Ma-emt, b & e) 14 Ma and c & f) 30 Ma-emt.

On the basis of all the models presented so far, we find that the continental plate velocity is a primary control on the dip angle of the subduction zone. In order to develop a low-angle subduction zone, a rapid trenchward velocity of the continental plate is needed. The dip angle can be further decreased by the slab suction force created by a thick lithosphere in the continental backarc, but this effect is minor. In order for low-angle subduction to develop into flat (subhorizontal) subduction, anomalously buoyant material must be subducted. In our models,

this corresponds to an oceanic plateau that has thickened oceanic crust. During subduction, the thickened oceanic crust must remain less dense than mantle (i.e., it can not undergo extensive eclogitization) and there must be a low-density harzburgite layer within the plateau mantle lithosphere. The depth of the flat slab depends on the density structure of the oceanic plate. In our two successful models of flat subduction at a depth of 100-200 km (Fig. 3.13, left column and Fig. 3.18 left column), the oceanic plateau includes metastable crust and a low-density harzburgite layer ($\Delta\rho$ = -100 kg m^{-3} relative to mantle). In addition, the oceanic plate experiences a slab break-off. This removes the dense frontal slab, and the remaining oceanic plateau is buoyant enough to deflect the low-angle slab to a sub-horizontal trajectory near the base of the continental lithosphere.

3.5.5 Variations in plateau width and location

The above models show that a buoyant oceanic plateau is the key to creating flat subduction. These models have a plateau with a width of 400 km and located at the trench at the time that the continental plate started to move trenchward. However, for Cretaceous western North America, neither the geometry nor timing of subduction of the Shatsky Ridge conjugate are well-constrained. In this section, we examine variations in the width and location of the oceanic plateau. For these models, the continental plate has a velocity of V_c=4 cm/yr and contains a thick Colorado Plateau lithosphere. The oceanic plateau has 18 km thick metastable crust (i.e., there is no eclogite phase change) but no harzburgite layer. As we show, it is possible to generate flat subduction with only buoyant crust by changing the plateau location and width. The presence of a harzburgite layer would further enhance flat subduction in these cases, and we do not believe it would significantly affect the models that do not flatten.

The first two models look at variations in plateau width. The original 400 km width is based on the plateau width suggested by van Hunen et al. (2004) and is similar to the proposed width of the Shatsky conjugate for western North America (e.g., Liu et al., 2010). Recent generic models of oceanic plateau subduction show that the plateau width can affect subduction dynamics (Arrial and Billen, 2013). We test plateau widths of 200 km and 800 km, which are each a factor of 2 different from our original models (Fig. 3.19). In both cases, we observe that the subduction

dip angle decreases slightly as the plateau is subducted and some oceanic plateau crust detaches and ponds in the mantle wedge corner. With the narrower plateau (Fig. 3.19, left column), the subduction zone maintains a relatively steep trajectory throughout the model run. The slab exhibits a slight flattening by the remaining metastability plateau crust at ~450 km depth (Fig. 3.19c). With a wider plateau, the greater length of time needed for the plateau to enter the subduction zone leads to enhanced shallowing of the subduction trajectory at depths <200 km (Fig. 3.19d). At 12 Ma-emt, the slab undergoes break-off as the dense frontal slab detaches from the buoyant plateau region (Fig. 3.19e). The subduction zone simultaneously begins to break near the trench. Later, the remaining slab, which has a fairly shallow trajectory below the continent, exhibits subhorizontal geometry at a depth of ~200 km (Fig. 3.19f). The failure appears to be the result of the low-angle plateau interacting with the thick Colorado Plateau lithosphere at 150-200 km depth, which resists deformation as it is cool and strong.
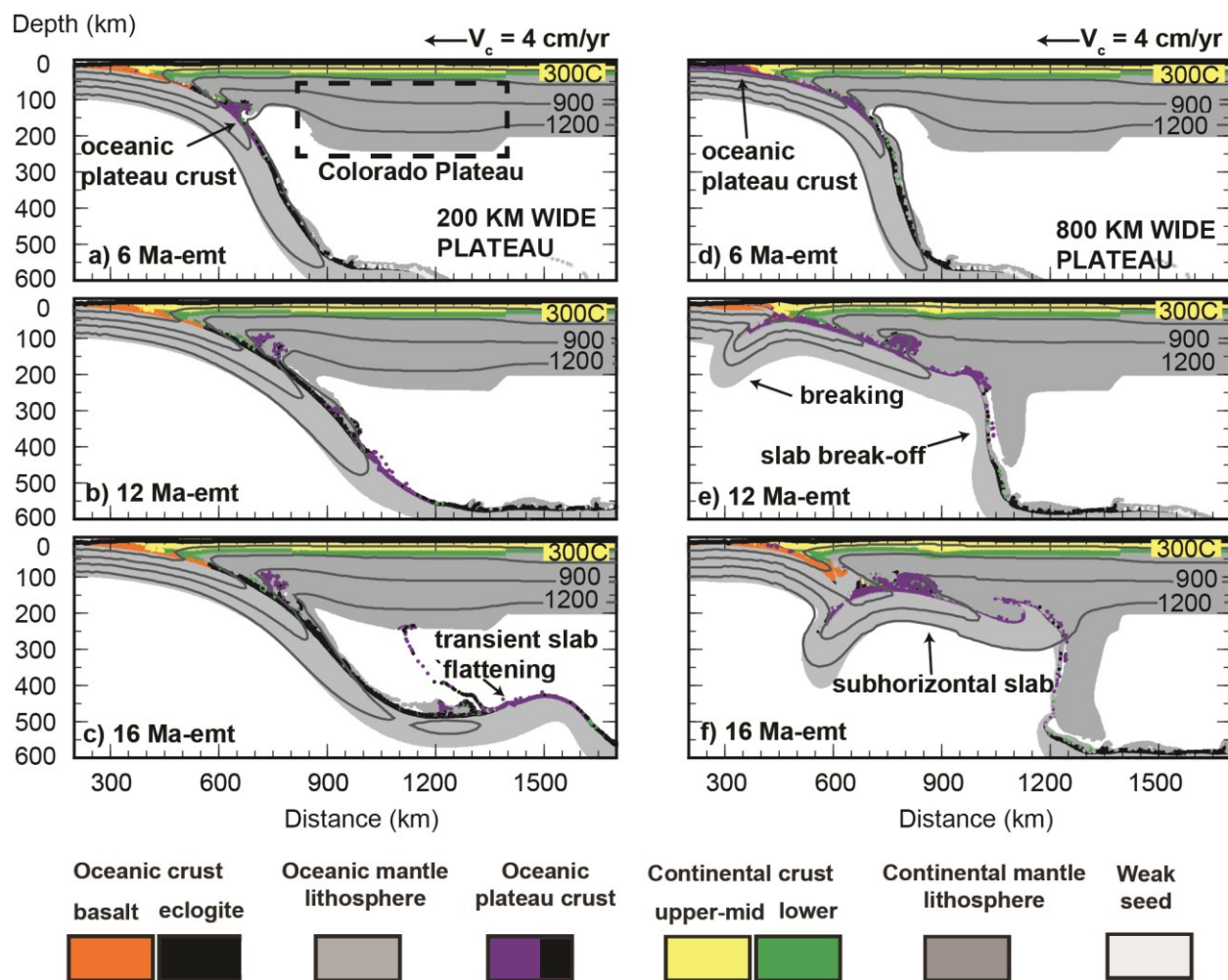
Fig. 3.19. Evolution of models with oceanic plateau widths of 200 km (Model F1-a, left column) and 800 km (Model F1-b, right column at: a & d) 6 Ma-emt, b & e) 12 Ma-emt and c & f) 16 Ma-emt. There is no eclogite phase change for oceanic plateau crust. $V_c = 4$ cm/yr.

We now vary the position of the oceanic plateau with respect to the trench, using a plateau width of 400 km. In the original models, the plateau was initially located 500 km seaward of the trench, such that it entered the trench at the start of Phase III of the models. In the new models, the location of the plateau is shifted by 300 km in landward direction (closer to trench) or 600 km in the seaward direction (further from trench). The length of the Phase II is constant in the model runs, which means that the leading edge of the oceanic plateau does not correspond with the trench at the start of Phase III. Therefore, these tests examine the effect of the relative timing of oceanic plateau subduction and onset of trenchward continental plate motion.

For the model with the plateau 300 km closer to the trench, the plateau has already started to subduct at the start of Phase III and is 1100 km inboard of the trench at 6 Ma-emt (Fig. 3.20e). The dip angle (α_d) is slightly smaller than the original model (Fig. 3.16 right column), due to shorter length of the frontal slab. As the plateau enters the trench earlier, the buoyant metastable crust enhances the shallowing of slab. But slab break-off does not occur because frontal slab is not dense enough, and thus slab does not attain flat subduction angle (Fig. 3.20, right column). Some oceanic plateau crust buoyantly detaches from the slab and perturbs the continental lithosphere (Fig. 3.20f). The remaining plateau crust is subducted into the deeper mantle and its buoyancy causes bending and upwelling of the oceanic plate at ~400 km depth.

If the plateau is shifted 600 km further from the trench, the plateau does not enter the trench until 6 Ma-emt after the continental plate velocity is imposed (Fig. 3.20a). At 16 Ma-emt, the slab undergoes a break-off and the negatively buoyant frontal slab is removed (Fig. 3.20b). The plateau has subducted to >300 km depth and there is some detachment of the buoyant plateau crust at the same time. The remaining slab then develops a flat trajectory at ~200 km depth below the continent (Fig. 3.20c). At ~30 Ma-emt, the tip of the slab is >1600 km from the trench and the subduction zone starts to fail as the oceanic plate breaks (Fig. 3.20d). It is interesting that this model develops flat subduction at a depth of ~200 km, whereas the comparable model with the plateau located at the trench at 0 Ma-emt showed only transient flat subduction (Fig. 3.16d-f). There appear to be two reasons for this. First, with the 6 Ma-emt delays in plateau subduction, the slab dip angle is decreased due to trenchward continental motion. Secondly, and more importantly, the frontal slab is 300 km longer in this model. This provides sufficient negative buoyancy for the slab to break during subduction. The combination of the decreased subduction angle and removal of the dense frontal slab make it possible for flat subduction to be induced with a buoyant thick plateau crust; a low-density harzburgite layer is not needed.

From these models, it appears that the history of subduction prior to oceanic plateau subduction is important in controlling whether flat subduction can be induced. If there is a long-lived subduction zone with a steep slab, the plateau must be much more buoyant than mantle (e.g., contain a low-density harzburgite layer and/or have a large width) to produce a transition to a flat slab. In our successful models of flat subduction in contact with the continental lithosphere, the transition to flat subduction occurred following a slab break-off which removed the dense frontal

slab. Further, the onset of continental trenchward motion should occur prior to, or be coincident with, oceanic plateau subduction in order to create flat subduction at shallow depth. In the next section, additional models provide support for these conclusions.
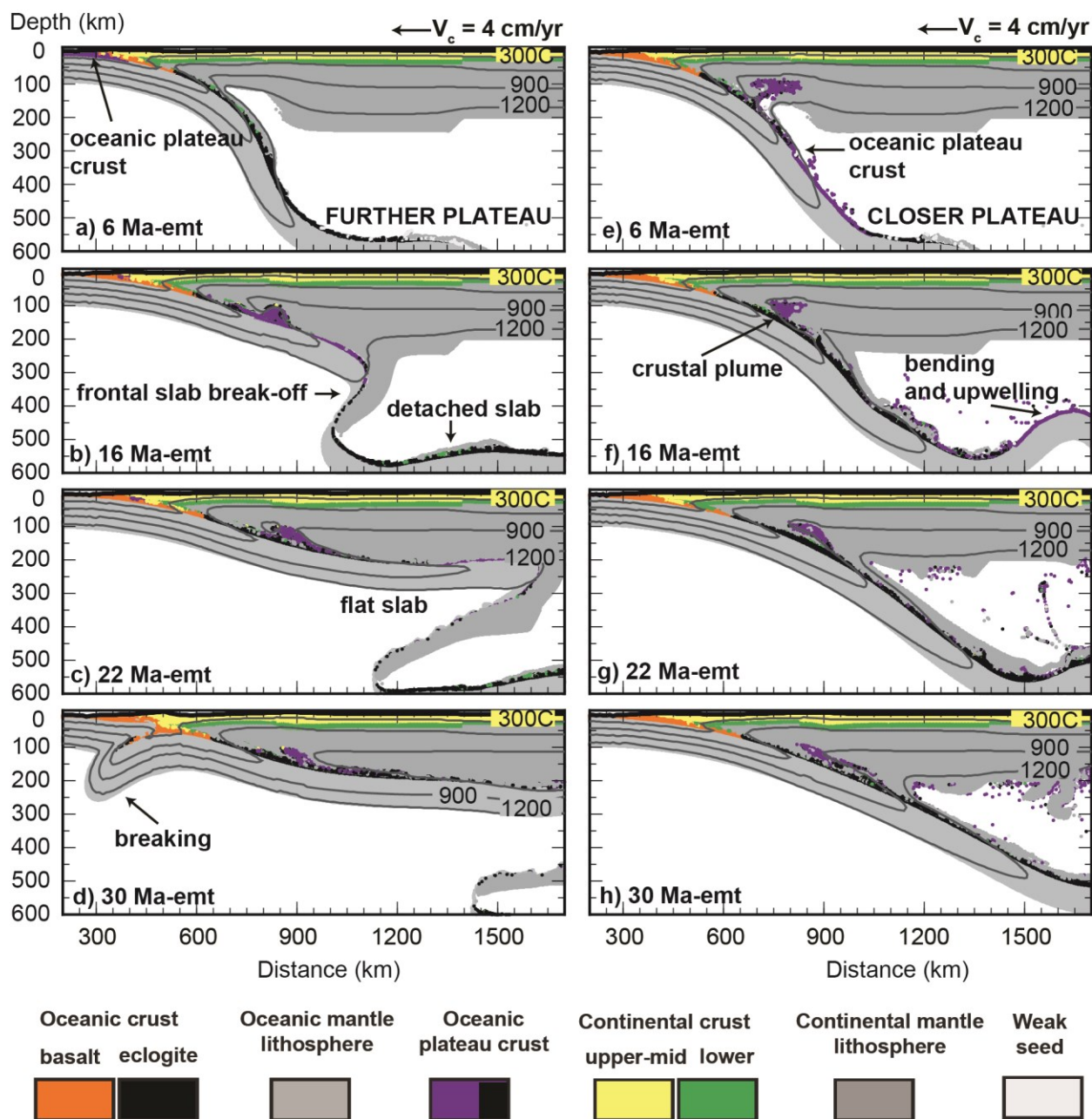
Fig. 3.20. Evolution of models with oceanic plateau 600 km further (Model F2-a, left column) and 300 km closer (Model F2-c, right column with respect to the location (500 km far away the trench) at: a & e) 6 Ma-emt, b & f) 16 Ma-emt, c & g) 22 Ma-emt, and d & h) 30 Ma. The oceanic plateau crust has no eclogitization and $V_c = 4$ cm/yr.

3.6 Effect of slab strength

Of the models presented above, a transition to flat subduction at a depth of 100-200 km was observed only in those models that exhibited a slab break-off (e.g., Fig. 3.13, 3.18, 3.19, 3.20). In this section, the strength of the oceanic plate is addressed, using models with either a weaker oceanic plate or a weak zone that forces a slab break-off.

3.6.1 Proposed mechanism

Although the slab strength does not influence the buoyancy of the slab, it does affect how easily a slab can bend or break during subduction. A weaker slab may be more readily bent upward into a subhorizontal trajectory. The strength of the oceanic plate depends primarily on its viscous rheology, which in turn depends on the thermal structure and composition. Older plates are cooler and thicker and will therefore have a higher viscosity (Equation 2.7). In our models, the oceanic mantle lithosphere has a wet olivine rheology (Karato and Wu, 1993) scaled upward by a factor of 10 to approximate strengthening due to dehydration. However, the actual rheology of mantle materials under geological conditions is poorly constrained. It is possible that oceanic mantle lithosphere may be weaker than we have assumed owing to partial hydration. In addition, the uncertainty in the rheological parameters of olivine permit strengths that are a factor of 5-10 times lower than what we have assumed (e.g., Beaumont et al., 2006).

In contrast to a bulk reduction in strength, there may be localized zones of inherited weakness in the oceanic plate that originate from processes occurring prior to subduction (e.g., localized serpentinization or damage that arises from plate flexure outboard of the trench; Gerya and Stoeckhert, 2002). After subduction, this weak zone may promote slab break-off, which reduces the negative buoyancy of the slab and may allow flat subduction (Fig. 3.21).
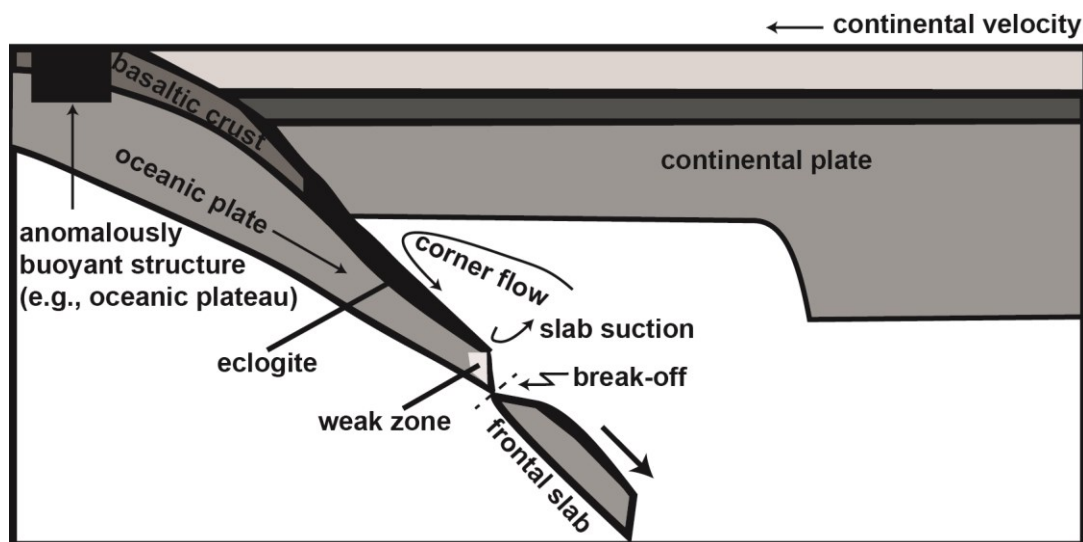
Fig. 3.21. Schematic diagram of subduction with a slab break-off. The weak zone allows the dense frontal slab to detach and sink. The remaining slab starts to shallow and may even flatten beneath the continental lithosphere, depending on its buoyancy and on additional factors, such as continental plate motion and slab suction forces.

3.6.2 Model results

We have conducted several model experiments to assess the effect of slab strength and the presence of a weak zone (Table 3.2). For all models, the continental velocity is $V_c = 4$ cm/yr and the continental plate includes thick Colorado Plateau lithosphere.

The first two models do not have an oceanic plateau, and the entire oceanic plate is comprised of normal thickness oceanic crust. In the first model, strength of the oceanic mantle lithosphere is decreased by an order of magnitude by changing the scaling factor (f) from 10 to 1 (Equation 2.7). The evolution of this model is shown in Fig. 3.21 (left column). This model exhibits a subduction zone that progressively gets shallower over time, owing to the trenchward advance of the continent. A comparison between this model and the analogous model with a strong oceanic plate (Fig. 3.9) shows that the overall evolution of the shallow part of subduction zone (<200 km depth) is fairly similar in the two models. In particular, there is no tendency for a weaker slab to develop into flat subduction. The major difference is that the weaker slab experiences stretching and necking in the deep part of the mantle. This is due to the fact that the negative buoyancy of the oceanic plate causes it to sink at a rate that is greater than the subduction rate (10 cm/yr) and

the weaker slab is not able to support this negative buoyancy. The repeated removal events mean that the coherent slab only extends to a depth of ~500 km. This model demonstrates the importance of slab strength in subduction. Because this model did not show enhanced slab shallowing, we have not pursued weak slab models further in this study. However, slab strength could be more important for subduction zones with a young, warm slab, which would be more buoyant and sink at a slower rate.

In the second model, we return to an oceanic plate that has the reference viscosity structure, but contains a weak zone in the oceanic mantle. The weak zone has a rectangular shape (40 km width and 36 km thick) and it is placed at the leading edge of the oceanic plateau (Fig. 3.1). A rheology of wet olivine (Karato and Wu, 1993) with f=1 is used in this weak block, such that it is 10 times weaker than the adjacent material. Tests show that this is sufficient to induce slab break-off. This model is shown in Fig. 3.21 (right column). The subduction zone starts with an initially steep trajectory. The presence of the weak zone induces a slab break-off at 8 Ma-emt, at a depth of ~400 km. However, this does not significantly affect the trajectory of the slab, compared to the model with no slab break-off (Fig. 3.9). The subduction angle slowly shallows over time but does not evolve into flat subduction over 30 Ma-emt. From this, we conclude that slab break-off for an oceanic plate with a standard thin-crust structure is not sufficient to create a transition to flat subduction.
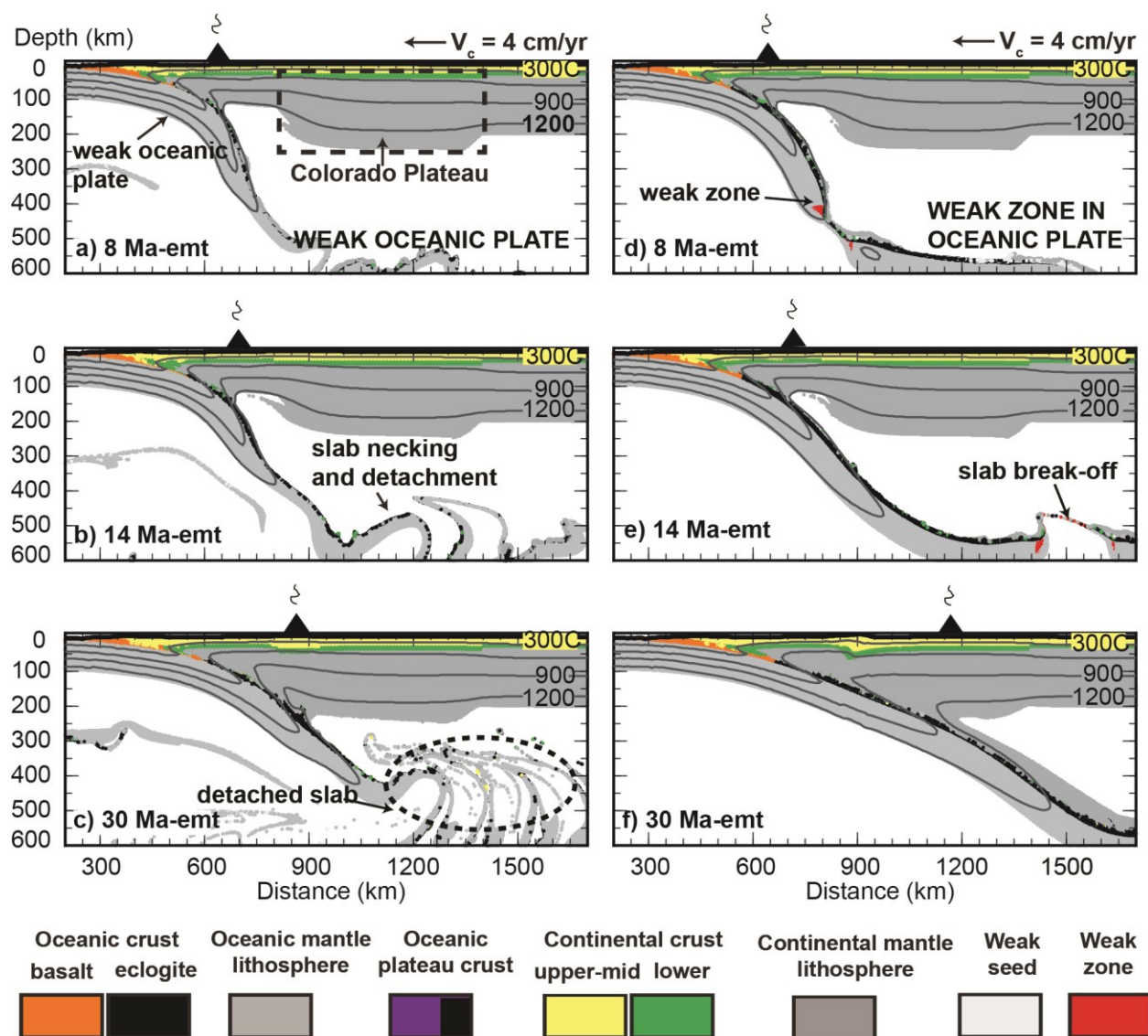
Fig. 3.22. Numerical model results for a weak oceanic mantle lithosphere (Model G-c, left column) and a weak zone in the oceanic plate (Model I-a, right column) at: a & d) 8 Ma-emt, b & e) 14 Ma-emt and c & f) 30 Ma-emt. There is no oceanic plateau and the oceanic crust undergoes eclogitization.

The next models include an oceanic plateau, as well as a weak zone which forces the frontal slab to break-off during subduction. The weak zone is placed at the landward side of the oceanic plate; this is the same location as in the previous model without an oceanic plate. The first model has only thickened oceanic crust in the plateau (no harzburgite layer) and there is no eclogitization of the plateau crust. If eclogitization occurs, the plateau becomes negatively buoyant and the model

evolves in a manner similar to that in Figure 3.16 (left column). The subduction zone initially has a steep dip (Figure 3.23a). As the plateau is subducted, some of the metastable plateau crust detaches and ponds in the mantle wedge corner (Figure 3.23b). The weak zone induces a slab break-off at ~8 Ma-emt, at a depth of ~400 km. At this time, the seaward end of the plateau is at >80 km depth. After the break-off, the plateau region flattens at a depth of ~400 km (Figure 3.23c), and then upwells (Figure 3.23d). However, this does not significantly affect the shallow part of the subduction zone (<200 km depth), where the dip angle is similar to that seen in the comparable model without slab break-off (Figure 3.16, right column).

This model should also be compared to the model in which the oceanic plateau was located 600 km further from the subduction zone (Figure 3.20, right column). That model also undergoes a slab-break-off at ~300 km depth, once the plateau had been subducted to >80 km depth (Figure 3.20b); the break-off in this case is induced by having a longer frontal slab, rather than a weak zone. It then evolves into a flat subduction zone at a depth of ~200 km (Figure 3.20c). The reason that flat subduction develops at a shallower depth in this model appears to be related to the dip of the subduction zone at the time of the slab break-off. The model in Figure 3.20 has a shallower dip, as trenchward advance of the continent started prior to plateau subduction. As a result, the slab break-off happens at a slightly shallower depth (~300 km vs. ~400 km depth). After the break-off event, the buoyant plateau is then able to "pull" the slab up to have a subhorizontal trajectory and be in direct contact with the continental lithosphere.
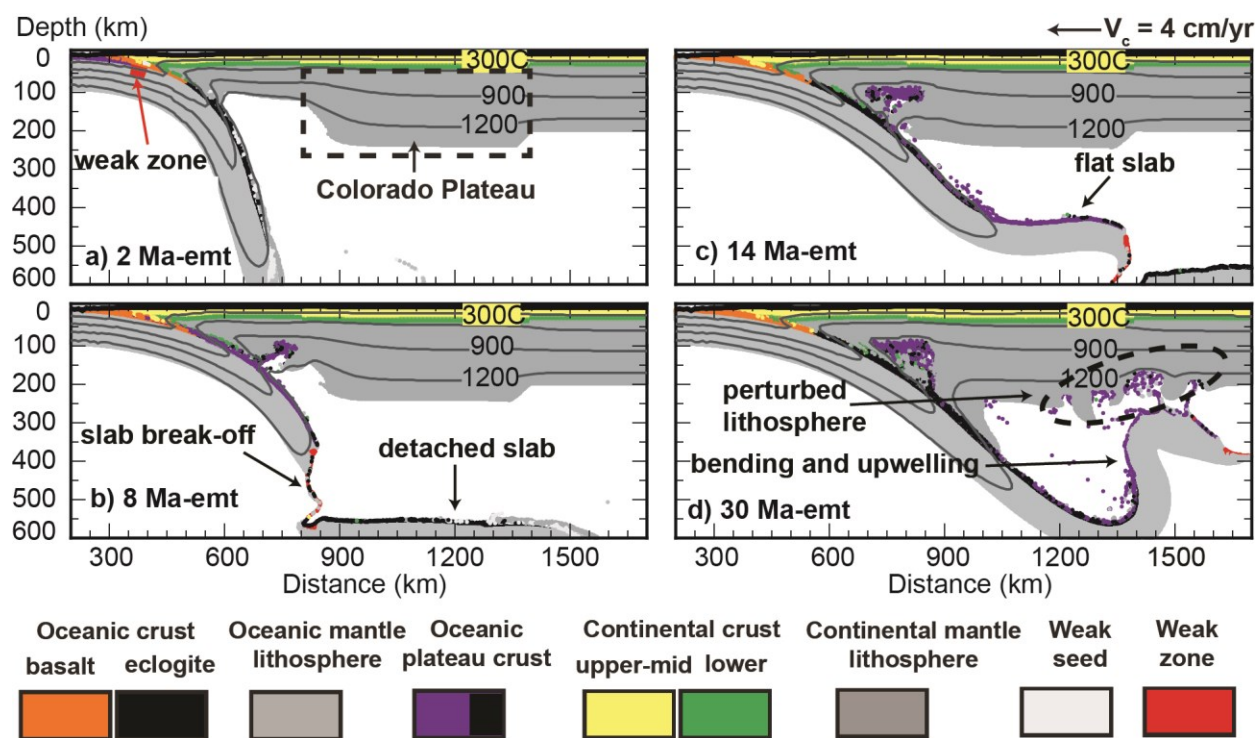
Fig. 3.23. Evolution of Model K-a that has an oceanic plateau (thick, uneclogitized crust only) and a weak zone in the mantle lithosphere adjacent to the plateau: a) 2 Ma-emt, b) 8 Ma-emt, c) 14 Ma-emt and d) 30 Ma-emt.

Figure 3.24 shows two models with a weak zone and an oceanic plateau with a harzburgite layer that is 100 kg m^{-3} less dense than mantle. The left column is a model in which the oceanic crust undergoes eclogitization and the right column is a model where the plateau crust remains metastable. In both models, the weak zone induces a slab break-off at a depth of 250-300 km. In the model with eclogitization, the shallow part of the subduction zone (<200 km depth) remains an inclined trajectory and the plateau region is subducted to ~350 km before starting to upwell owing to its low density (Figure 3.24b). This model does not evolve into flat subduction, but by the end of the model run, the enhanced coupling between the low-angle slab and overlying continent creates significant upper plate shortening (Figure 3.24c).

The model without oceanic plateau crust eclogitization evolves in a similar manner to the comparable model without a weak zone (Figure 3.18, right column). In both models, a slab break-off occurs, followed by a transition to sub-horizontal subduction at ~200 km depth and then failure of the subduction zone. The main difference is that when a breakoff is induced by a

weak zone, the slab has a longer region of flat subduction (Figure 3.24e), instead of a "hook-like" appearance (Figure 3.18e). This seems to be due to the fact that the induced break-off occurs at a shallower depth, such that the plateau does not upwell as much before coming into contact with the continental lithosphere.
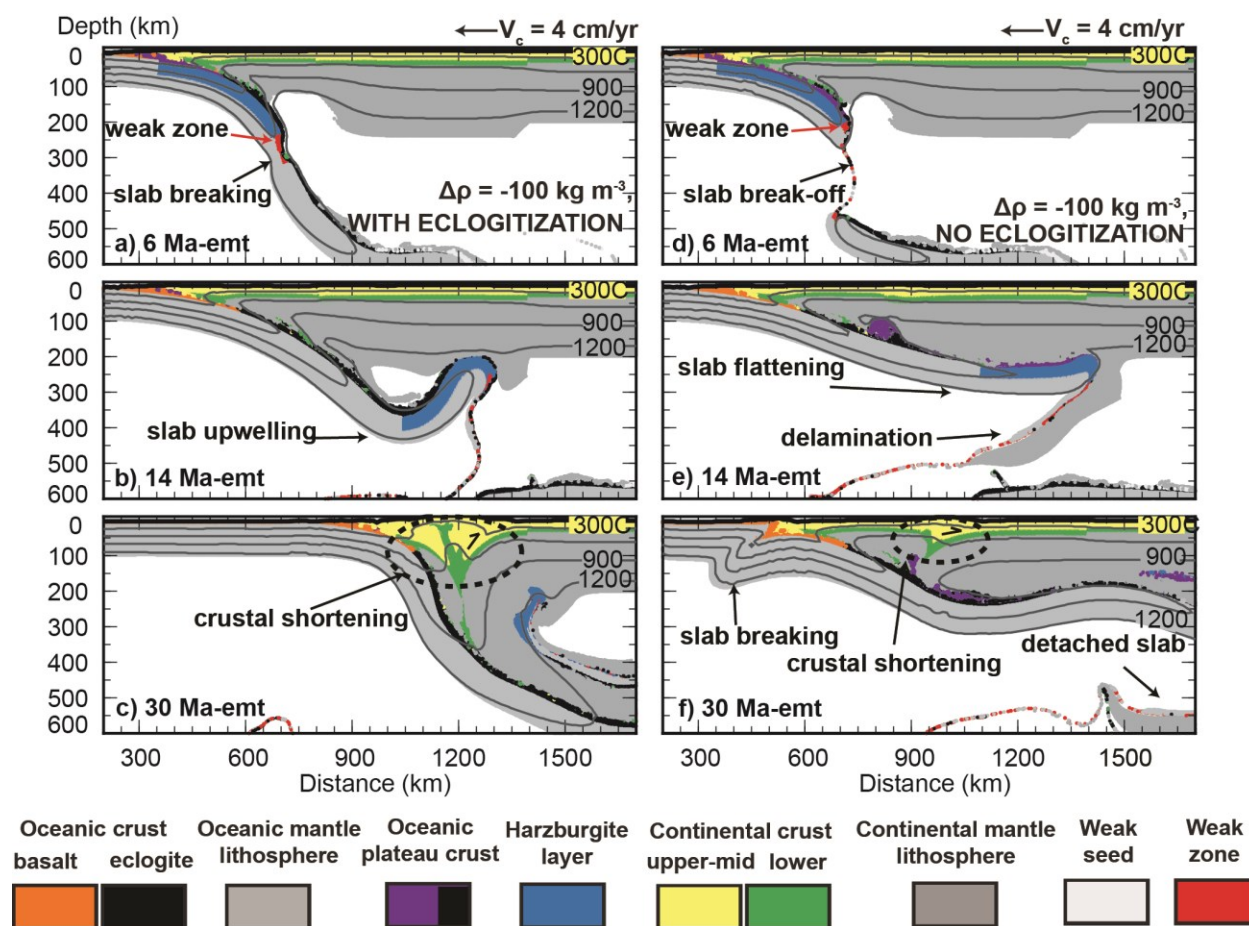
Fig. 3.24. Evolution of models that have an oceanic plateau with a harzburgite layer ($\Delta\rho$ = -100 kg m^{-3} relative to the mantle) and a weak zone in the mantle lithosphere adjacent to the plateau. The left column shows a models with oceanic plateau crust eclogitization (Model K-c) and the right column shows a model with no eclogitization (Model K-d) in oceanic plateau at: a & d) 6 Ma-emt, b & e) 14 Ma-emt and c & f) 30 Ma-emt.

In summary, the models in this section demonstrate that a weaker oceanic or the presence of a weak zone in the oceanic plate will promote slab break-off for an old, dense oceanic plate.

However, a break-off on its own is not sufficient to create flat subduction. The oceanic plate must also contain a region of abnormally low density (an oceanic plateau), which will then buoyantly lift the oceanic plate to a horizontal trajectory.

3.7 Summary

In this chapter, numerical models examine the influence of three proposed mechanisms for generating flat subduction: increased trenchward continental velocity, enhanced slab suction forces and subduction of a buoyant oceanic plateau. The investigation of the individual factors (Sections 3.2-3.4) shows that all three can produce a decrease in deep slab dip (α_d) during the evolution of the subduction zone. However, none of these are able to create a flat subduction zone on their own; multiple factors are required (Section 3.5-3.6). Table 3.3 summarizes the relative effect of each factor we investigated on the deep slab dip (α_d) and on the development of flat subduction. The models show that trenchward continental motion is the most effective at creating a rapid decrease in subduction dip angle (α_d). To create a transition to flat subduction, it is necessary to either have high mantle wedge viscosity (enhanced slab suction) or subduction of a buoyant oceanic plateau. In our models, the required mantle wedge viscosity is much higher than the observed viscosity at most subduction zones (e.g., Dixon et al., 2004). An oceanic plateau can induce flat subduction if its density is significantly less than the mantle (e.g., thick non-eclogitized crust and/or a depleted harzburgitic mantle) and if the dense frontal part of the oceanic plate is removed through a slab break-off. In the next chapter, the model results are explored in more detail.

Table 3.3. Summary of the effect of subduction parameters on the deep slab dip (α_d) and the transition to flat subduction.

Parameter	Effect on slab dip (α_d)	Flat subduction?
Continental trenchward motion (V_c)	**Main control** *Lower dip with higher V_c*	**Main control**
Thick Colorado Plateau lithosphere	Decreases slab dip *(enhanced slab suction)*	Little effect *(affects depth of flab slab)*
Mantle wedge viscosity (η_{SLM})	Lower dip with higher η_{SLM}	Great effect
Oceanic plateau with thick crust	Decreases slab dip	**Significant effect**
Plateau crust eclogitization	Increases slab dip	Hindrance
Harzburgite layer	Decreases slab dip	**Significant effect**
Width of oceanic plateau	Lower dip with larger width	Moderate effect
Location of oceanic plateau	Lower dip if plateau subducts after continent advances	Moderate effect
Slab strength	Minor effect *(weaker slabs repeatedly detach)*	Little effect
Slab break-off	Decreases slab dip	**Main control**

CHAPTER 4

<hr>

Discussion

4.1 How to get flat subduction?

Geological observations for the western US indicate a change in continental tectonics in the Late Cretaceous (Fig. 1.5). These include the development of the continental-scale Western Interior Seaway, shutdown of the Sierra Nevada volcanic arc, and initiation of the Laramide orogeny. As discussed in Section 1.3, it is widely accepted that these events mark a transition in Farallon Plate geometry from a steep-angle trajectory to flat (subhorizontal) subduction. This placed the slab at a depth of 100-200 km and in contact with the western US lithosphere for 100's of km inboard of the trench.

The models in the previous chapter examine the dynamics of subduction for an old, dense oceanic plate in a situation analogous to the Cretaceous western US. Specifically, the models investigate the effects of trenchward continental motion, the slab suction force, and subduction of an oceanic plateau. It is found that the inferred Farallon Plate geometry is obtained for only a narrow range of conditions that involved combinations of the proposed factors. These successful models can be divided into three groups (Fig. 4.1):

GROUP A: Combination of V_c and high-viscosity mantle wedge. With trenchward motion of the continental plate (V_c), the dip of the subducting slab gets progressively shallower over time (e.g., Fig. 3.2). Slab shallowing can be further enhanced if the mantle wedge viscosity is relatively high, as this increases the upward force on the slab that is generated by mantle wedge flow. The combination of trenchward V_c and a high viscosity mantle wedge can produce a flat slab that is in contact with the continental lithosphere at a depth of ~250 km (e.g., Fig. 3.10c). However, in our models, an additional effect of the high mantle viscosity is that it limits the

ability of the slab to descend into the deep mantle. The slab "piles up" under the continental lithosphere and undergoes internal deformation. We do not believe that this model is reasonable, as observational data suggests that mantle wedge viscosities are fairly low (10^{18}-10^{19} Pa s) because of fluids associated with dehydration of the subducting plate (e.g., Manea and Gurnis, 2007). Xenolith data are consistent with a hydrated western US mantle wedge (e.g., Dixon et al., 2004). Therefore, this type of model is unlikely to explain the origin of the flat Farallon Plate.

GROUP B: Combination of V_c and an oceanic plateau (OP) with harzburgite layer. In this group, the OP contains a region of thick crust with an underlying layer of depleted, harzburgitic mantle. Continental trenchward motion (V_c) induces a low-angle subduction. As the plateau subducts, the subducting plate experiences tension due to the competing effects of the low-density buoyancy OP and high-density frontal slab at the leading edge of the plateau. This causes the frontal slab to break-off and sink. The plateau then buoyantly pulls the slab upward and creates a flat geometry as the slab contacts the continental lithosphere. A fairly buoyant slab is needed to create a flat slab immediately below the continental lithosphere (100-200 km depth). The OP in our successful models includes an 18-km thick metastable basaltic crust and a 36-km thick harzburgite layer that is 100 kg m^{-3} less dense than the surrounding mantle (at the same temperature). A key requirement is that the basaltic crust cannot undergo eclogitization.

GROUP C: Combination of V_c and an OP with no harzburgite layer. This group is related to Group B models. Again, V_c creates a low-angle slab, which evolves to a flat geometry as a buoyant OP is subducted and the frontal slab is removed through a break-off. In this case, the buoyancy of the plateau comes only from its thick, metastable crust, and therefore it is less buoyant than that in Group B. However, it is buoyant enough to induce flat subduction if the OP is either wider or located further from the trench than in the Group B models. With a wider plateau, the long duration of OP subduction is sufficient to allow a break-off to develop, and the plateau is deflected to sub-horizontal trajectory. The case with an OP further from the trench corresponds to the situation where continental advance (V_c) occurs before the OP starts to subduct. The earlier onset of V_c allows for low-angle subduction to initiate before OP break-off. In addition, the frontal slab is longer, and therefore its greater negative buoyancy triggers the break-off event. In this case, the break-off occurs when the slab has a relatively low angle (due to

the longer duration of continental motion), and therefore the transition to flat subduction can be induced with a plateau that is less buoyant than in the Group B models.
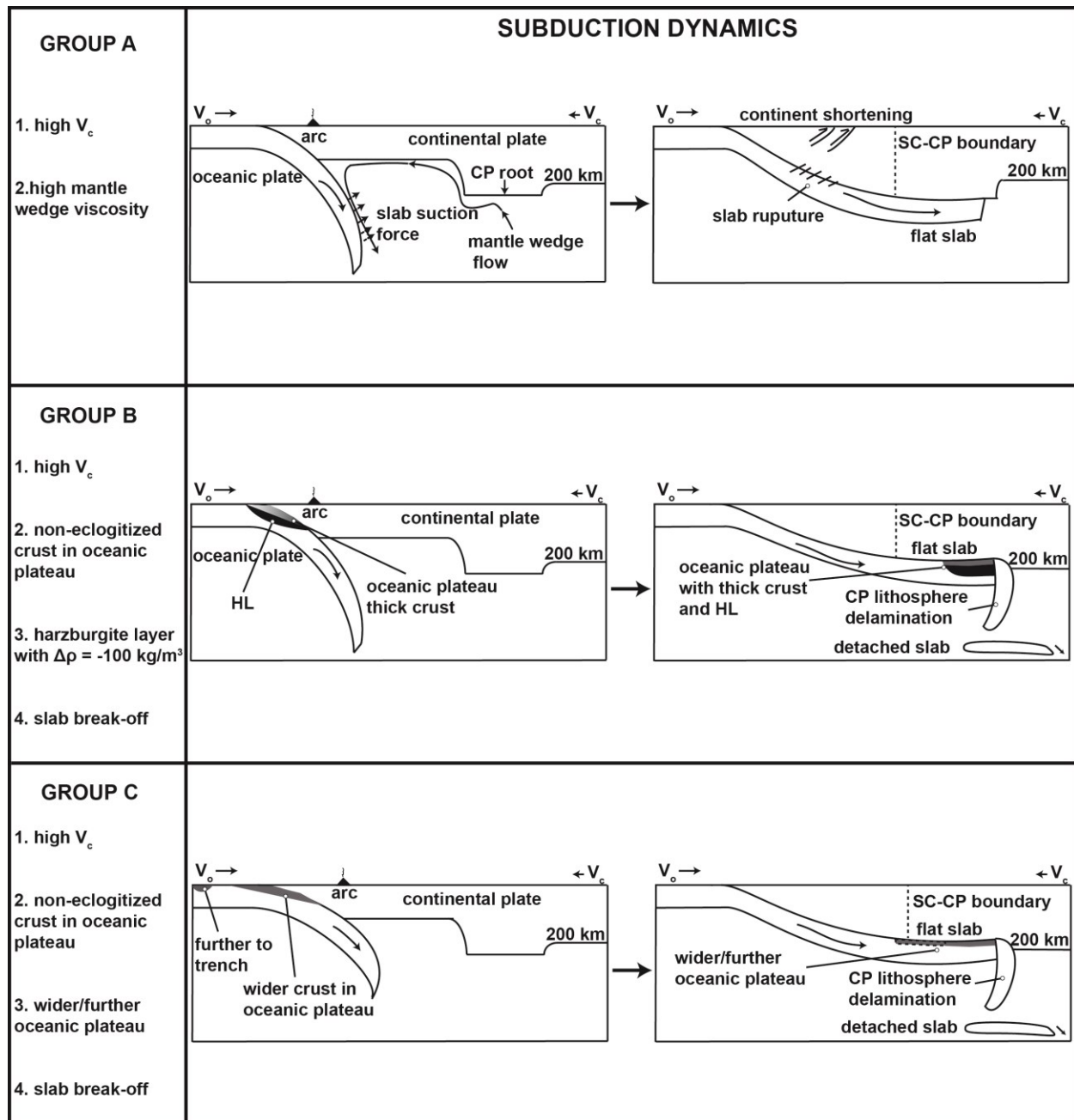
Fig. 4.1. Schematic representation of three groups of flat slab models in this study. V_o and V_c are absolute velocities of the oceanic plate and continent plate. SC, CP and HL denote the South California block, Colorado Plateau region and harzburgite layer, respectively.

In summary, we consider Group B and C to be the most plausible for producing Laramide-style flat-slab subduction. The main control is the continental trenchward velocity, which creates a low-angle subduction zone. Once this is formed, the transition to a flat/sub-horizontal trajectory requires: (1) subduction of a low-density oceanic plateau, and (2) a break-off event that removes the dense frontal slab. These two factors increase the buoyancy of the subducting plate, such that it can obtain a subhorizontal trajectory. If the plateau has only a moderately low density, the flat slab segment occurs in the deep upper mantle (400-500 km depth). A much lower density allows the flat segment to be in contact with the continental plate. In this case, the depth of the flat slab is determined by the thickness of the continental lithosphere. With no thick Colorado Plateau lithosphere, the flat slab depth is ~100 km (e.g., Fig. 3.13), but with a Colorado Plateau, the depth is ~200 km (e.g., Fig. 3.18, Fig. 3.24).

4.2 Dip angle analysis

One of the objectives of this thesis is to assess how the geometry of a subducting plate is affected by continental plate motion, slab suction (due to the presence of thick Colorado Plateau lithosphere), and oceanic plateau subduction. This section provides a quantitative comparison of the model results to demonstrate the relative influence of these factors on slab geometry.

For this, the geometry of the subducting plate is parameterized according to slab dip. At most subduction zones, the oceanic lithosphere appears to bend continuously, with a gradual increase in slab dip from the trench to a depth of 80-150 km (Lallemand et al., 2005). At greater depths, slabs tend to straighten out to an almost constant dip (Turcotte and Schubert, 2002). Lallemand et al. (2005) proposed an approach that describes slabs according to their mean dip at different depths. We adopt their method to calculate the dip angles of slabs in our models. The dip angle is calculated for two parts of the slab: (1) the shallow dip (α_s) is the mean dip between the trench and 100 km depth and (2) the deep dip (α_d) is between 100 and 200 km depth (Fig. 4.2). In both calculations, the law of tangents is used to calculate the mean dip for the top of the oceanic plate.
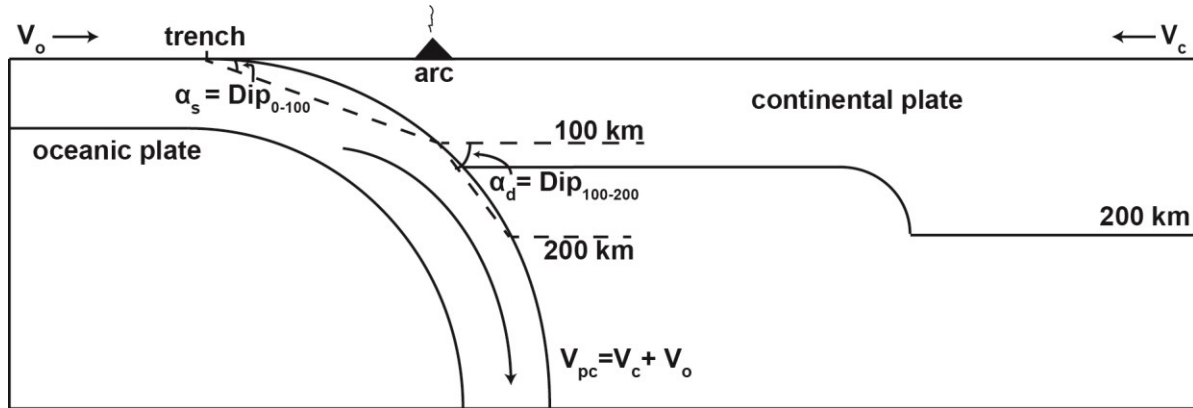
Fig. 4.2. Schematic representation of the parameters used for dip measurement in models. V_o and V_c are the absolute velocities of the oceanic plate and continent plate and the sum of them is plate convergence velocity (V_{pc}). α_s and α_d denote the angle of shallow dip and deep dip, respectively.

Table 4.1 shows the calculated dip angle for all models in our study at 14 Ma-emt (see Tables 3.1 and 3.2 for the parameters used in each model). We chose this time, as it is long enough after the start of Phase III for the slab behavior to be captured. This is also the time at which flat subduction has developed in most of the models that exhibit this behavior. Further, the development of a flat Farallon plate is inferred to have occurred over 10-30 Ma, and therefore the slab geometry at 14 Ma-emt is a good indication of whether the model may be applicable for Farallon plate dynamics. Note that in some models, the subduction zone has failed in the trench area at this time (similar to the breakage seen in Fig. 3.5), and hence the slab dips are excluded from the analysis (e.g., Model B2c in Table 4.1).

Table 4.1. The list of two different dips in above model groups at 14 Ma-emt.

Model group		α_s (°)	α_d (°)	Figure #	Model group		α_s (°)	α_d (°)	Figure #
	a	23.5	55.0			a	18.4	48.0	
A1	b	22.6	48.3		A2	b	17.4	35.5	
	c	21.8	41.2			c	16.4	32.0	
	a	21.2	50.6	3.3b		a	17.9	39.6	3.5b
B1	b	19.3	44.3		B2	b	16.4	30.5	
	c	18.2	39.0	3.9b		c	-	-	3.10
	a	20.3	53.2	3.6b		a	21.0	51.4	3.6e
C1	b	19.1	44.4		C2	b	18.9	42.3	
	c	18.2	38.7	3.11b		c	17.7	36.5	3.11e
	a	19.8	50.3	3.7b		a	19.5	47.6	3.8b
	b	20.0	47.6	3.7e		b	19.6	42.3	3.8e
C3	c	18.5	39.8		C4	c	15.9	10.1	
	d	17.9	37.2	3.12b		d	17.0	35.5	3.13b
	e	17.4	35.5	3.12e		e	15.1	9.3	3.13e
	a	19.5	45.6	3.15a		a	18.8	43.6	3.15b
D1	b	18.3	38.7		D2	b	18.0	32.0	
	c	17.3	34.8	3.16e		c	16.8	29.1	3.17e
	a	17.9	33.7	3.15c		a	18.6	43.1	
D3	b	15.4	10.2		E1	b	17.6	36.8	3.16b
	c	14.5	11.8	3.18e					
	a	18.2	41.1			a	17.3	36.9	
E2	b	17.1	35.1	3.17b	E3	b	16.4	32.0	3.18b
	a	17.9	35.9			a	16.7	34.6	
F1	b	15.1	9.8		F2	b	17.4	42.3	
						c	11.7	10.4	
	a	13.4	32.2			a	19.7	43.0	
F3	b	11.4	32.8		G	b	19.1	40.3	
	c	11.2	31.8			c	18.2	38.4	3.22b
	a	16.2	36.5	3.14b		a	15.0	18.9	
H	b	19.7	27.8	3.14e	J	b	12.5	11.8	
						c	15.5	23.0	
	a	17.5	35.9	3.22e		a	17.3	34.4	3.23c
I	b	17.1	35.5		K	b	16.8	32.8	
	c	16.8	33.7			c	15.5	10.4	3.24b
	d	16.6	32.8			d	15.1	8.6	3.24e

We first examine the slab geometry for models that specifically test the effects of V_c, the Colorado Plateau (CP) and the oceanic plateau (OP) (Model Groups A1, B1, C, D, and E in Table 3.1). Fig. 4.3 shows the measured α_s and α_d of these models. The horizontal axis corresponds to a grouping of models based on the subducting plate density structure, with the average density generally decreasing from left to right. This is obtained by sorting models into three groups: (1) no OP – models with no oceanic plateau, (2) OP-ec – models in which the OP crust undergoes eclogitization, and (3) OP-noec – models with no eclogitization of the OP crust. Groups (2) and (3) are further subdivided by the density of the OP harzburgite layer (HL): HL-0 indicates no harzburgite layer and HL-50 and HL-100 have a density contrast relative to the mantle of -50 kg m^{-3} and -100 kg m^{-3}, respectively.

For all models, the shallow dip (α_s) has a small range (15°-25°) (Fig. 4.3a). Lower α_s is observed with increasing V_c, decreasing OP density and if the continent has a thick CP. This shows that all three factors can affect the shallow subduction geometry, but the effect is relatively small.

The deep dip (α_d) ranges from <10° to >50° (Fig. 4.3b). This plot demonstrates the strong effect of V_c on the slab geometry. With no continental plate motion (V_c = 0 cm/yr), α_d is 45° or more; the only exception is the case with a highly buoyant OP (OP-noecl-HP-100: α_d=42.3°). Slab dip decreases with increasing V_c. With V_c = 3 or 4 cm/yr, the majority of models are concentrated in the region of low-angle dip (15°<α_d<45°). Therefore, we conclude that continental trenchward motion is the primary factor needed to create low-angle subduction. The plot also shows the secondary effects of the Colorado Plateau and oceanic plateau. Models with a CP have a slightly (generally <5°) lower dip angle than those without a CP, which is attributed to the enhanced slab suction force. Subduction of a buoyant oceanic plateau also causes a decreased dip angle. The dip angle appears to be most sensitive to the density of the harzburgite layer (HL) in the OP. This is probably because the HL remains intact during subduction, whereas the upper part of the crust detaches if it is metastable (OP-noec models), and the slab loses this source of buoyancy. Finally, the plot shows that in order to create flat/subhorizontal subduction (α_d<15°), multiple factors are required. All models with a flat slab include a high V_c (3 or 4 cm/yr) and subduction of a buoyant OP (non-eclogitized crust and a HL with $\Delta\rho$ = -100 kg m^{-3}. The development of a flat slab is less sensitive to the presence of the Colorado Plateau, although as noted above, the thickness of the continental lithosphere will affect the depth of the flat slab.
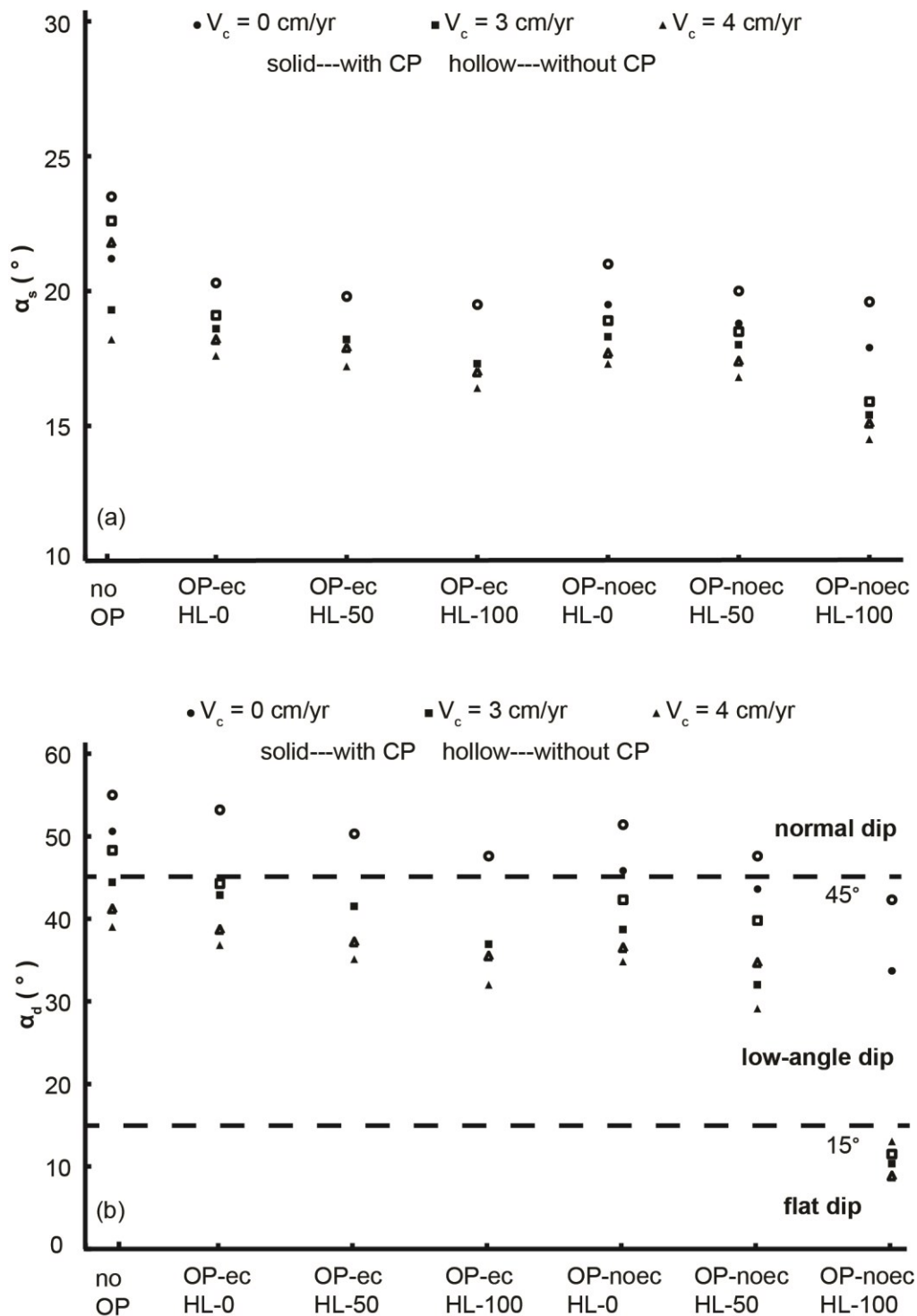
Fig. 4.3. (a) The shallow dip angle (α_s) and (b) the deep dip angle (α_d) at 14 Ma-emt for variations in continental velocity (V_c), whether the continent contains thick Colorado plateau lithosphere (CP) and the structure of the oceanic plateau (OP). The density of the subducting plate decreases from left to right; see text for an explanation.

It is also useful to examine the temporal variation in the slab geometry. Fig. 4.4 shows the evolution of the shallow (α_s) and deep (α_d) dip over the duration of the model run for several models. The shallow dip shows a gradual decrease with time for all models, but the range of dips is relatively small. There is a much greater variation in the deep dip. The effect of continental velocity can be observed in Fig 4.4c. With a CP but no OP, the model with V_c=0 cm/yr (red line) maintains a steep dip throughout the model run, whereas the model with V_c=4 cm/y continually shallows (black line). If an OP with non-eclogitized crust is included, the dip angle is further decreased, but still remains as low-angle subduction at 30 Ma-emt (blue line). If the models were run for longer, it is possible that the slab may evolve to a flat geometry, but this is outside of the time window inferred for Farallon plate flattening (see Chapter 1). Finally, the model with a low-density HL (green line) shows a rapidly decrease in dip between 6 and 14 Ma-emt. In this model, the frontal slab detaches at 6 Ma-emt and a flat geometry is obtained by 14 Ma-emt (Fig. 3.24e), followed by subduction zone failure at 26 Ma-emt.

Fig 4.4d shows the models in which the width and location of the OP are varied. These models have V_c=4 cm/yr and a CP. The OP has non-eclogitized crust only (no HL). The model with the narrow OP (200 km wide; black line) evolves to a low-angle geometry, with a dip angle that is steeper than the model with a 400 km wide plateau (black line in Fig. 4.4c). In contrast, the model with an 800 km wide OP (blue line) undergoes a slab breakoff and develops a fairly shallow geometry by ~12 Ma-emt. Later by 14 Ma-emt, this slab trajectory transits to flat below the continent. When the OP is 300 km closer to the trench (green line), the initial dip angle is slightly lower than in the other models because the plateau enters the trench prior to the start of the experiment. However, this model exhibits low-angle subduction over the duration of the model run. If the OP starts 600 km further from the trench (red line), the initial dip is higher owing to the greater length of the dense frontal slab. However, the dip shallows by the trenchward motion of continent, and at the time of the slab break-off (16 Ma-emt), the OP is buoyant enough to induce flat subduction. Flat subduction persists until the subduction zone fails at ~28 Ma-emt.
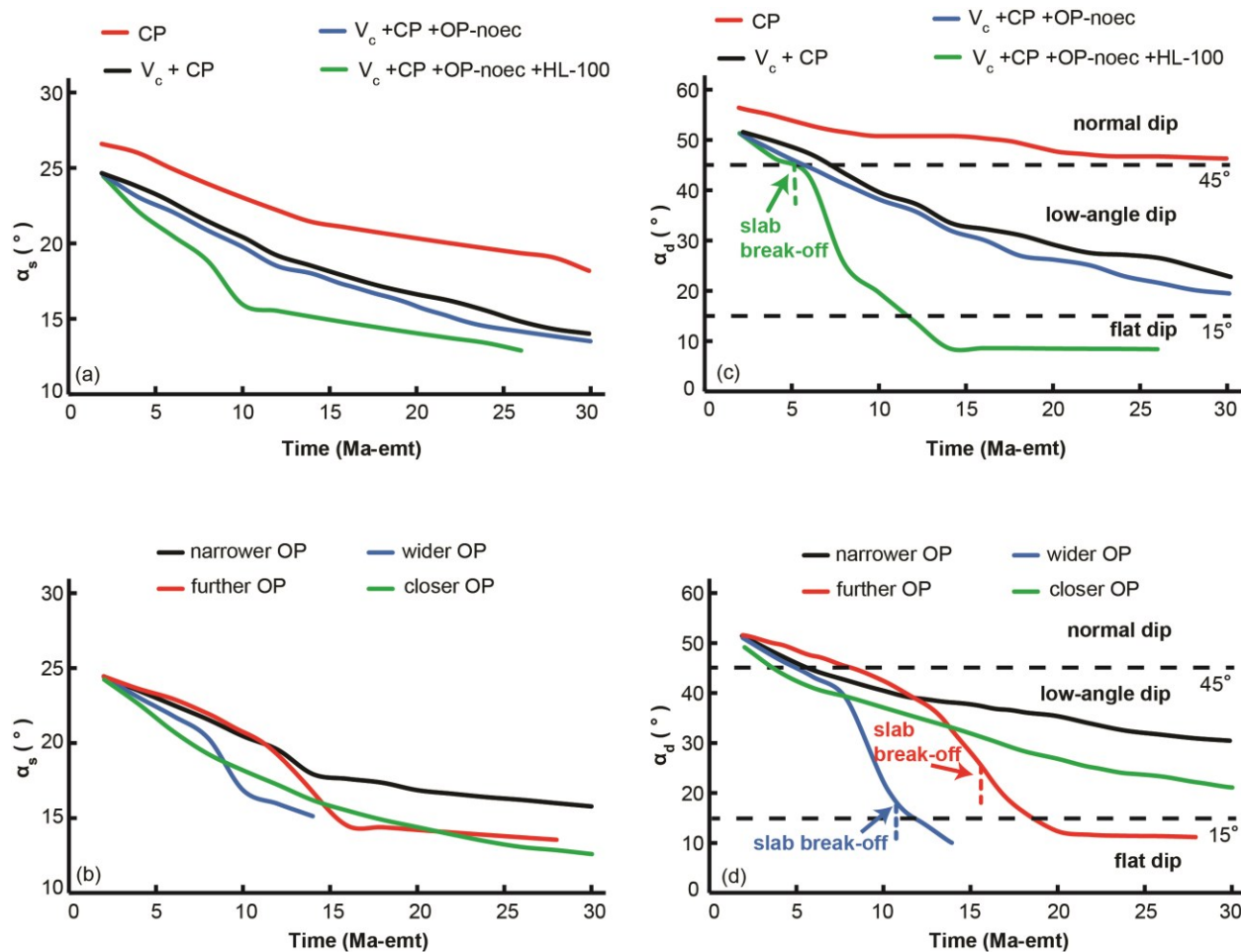
Fig. 4.4. The evolution of slab dip for selected models. (a) and (c) are α_s and α_d for models that test the effects of V_c (0 cm/yr for red line; 4 cm/yr for all others), the Colorado Plateau (CP), and an oceanic plateau (OP) with no eclogitization and with or without a harzburgite layer (HL; $\Delta\rho$ = -100 kg m^{-3}). (b) and (d) are α_s and α_d for models with variations in the OP geometry (width and location relative to trench); models have CP V_c=4 cm/yr, there is a CP, and the OP has basaltic crust but no HL.

4.3 Buoyancy analysis

In our models, subduction of a low-density oceanic plateau is required for subduction to evolve to a subhorizontal trajectory. In addition, the dense frontal slab must be removed through a slab-break off. In this section, we present a first-order analysis of the buoyancy of a subducting slab with an oceanic plateau to show how the slab geometry is related to slab density. This should be

considered as only an approximate calculation, as it does include the evolving thermal structure of the slab, the effects of slab strength on bending, or dynamic effects (e.g., slab suction force).

For the analysis, we calculate the average density contrast between the oceanic plate and the shallow sublithospheric mantle. Oceanic plate density depends on both its composition and temperature. The oceanic plate consists of two regions: 1) the frontal slab (9 km thick eclogitized crust and 81 km thick mantle lithosphere), and 2) the oceanic plateau (18 km crust (either basalt or eclogite), 36 km harzburgite layer, and 36 km mantle lithosphere). Reference densities for each unit are given in Table 2.1; the density of the harzburgite layer is 0, 50 or 100 kg m^{-3} less than that of mantle lithosphere (at the same temperature). We make the assumption that the vertical thermal structure corresponds to the 1D geotherm for an old oceanic plate. In reality, the plate is conductively headed as it subducts, which will decrease its density; therefore the densities calculated here are upper limits.

Given the composition and thermal structure, the vertical density profile ($\rho(z)$) of the oceanic plateau and frontal slab can be calculated (Fig. 4.5). Note that the density of the sublithospheric mantle (SLM) at the base of the oceanic plate is 3250 kg m^{-3}. In comparison to SLM, the mantle lithosphere is denser (negatively buoyant) owing to its low temperatures. The thermal density can be offset by the compositional effects of a harzburgite layer (HL). For harzburgitic mantle to be positively buoyant, the HL needs to have a compositional density contrast that is approximately -100 kg m^{-3} less than mantle. In addition, for the densities used in our models, eclogitized crust is denser than mantle as it is cool, but metastable basaltic crust is less dense and therefore positively buoyant.
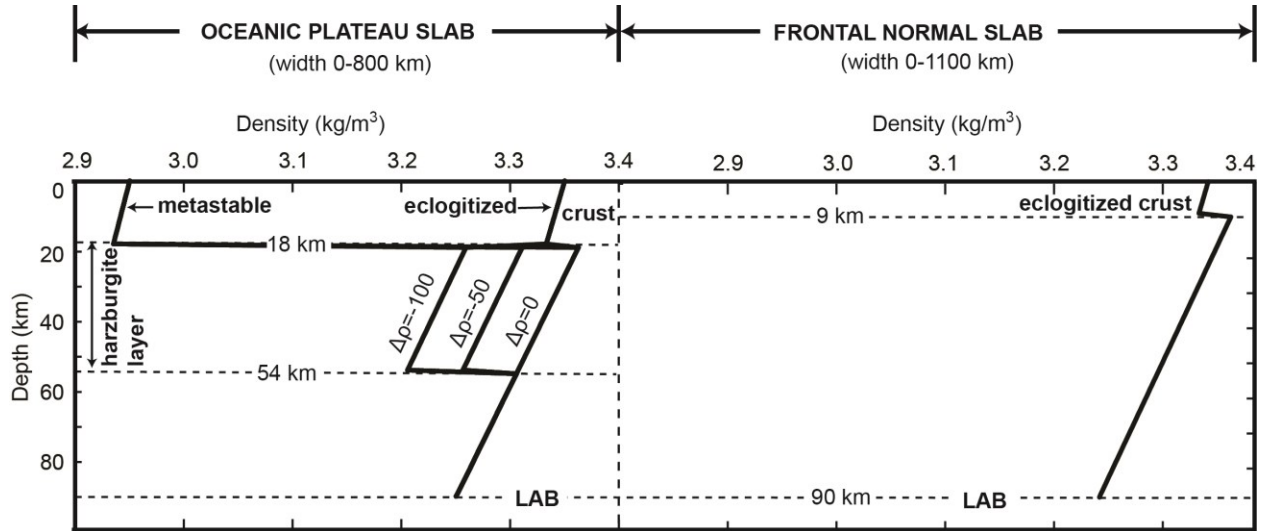
Fig. 4.5. Vertical density profiles for an oceanic plateau (left side) and the frontal slab with normal-thickness crust (right side). Normal oceanic crust is eclogite and metastable oceanic crust remains basaltic. $\Delta\rho$ is the compositional density difference (kg m^{-3}) between the harzburgite layer and standard mantle. LAB is the boundary between oceanic lithosphere and asthenosphere (sublithospheric mantle) at 90 km depth.

We use these density profiles and assume different widths (W) of the frontal slab and/or oceanic plateau to calculate the average density contrast of an oceanic plate relative to the SLM ($\Delta\rho_{avg}$):

$$\Delta\rho_{avg} = \frac{W_{fs} \int \rho_{fs}(z)dz + W_{op} \int \rho_{op}(z)dz}{90(W_{fs}+W_{op})} - \rho_{SLM} \qquad (4.1)$$

where the subscripts "fs" and "op" correspond to the frontal slab and oceanic plateau region, respectively. The integration is carried out over the thickness (z) of the oceanic lithosphere (90 km), and the last term (ρ_{SLM}) is the density of the SLM at the base of the oceanic plate (3250 kg m^{-3}). Equation 4.1 can be used to see how different widths of frontal slab and/or oceanic plateau affect the overall buoyancy of the oceanic plate. If $\Delta\rho_{avg}$ is positive, the oceanic plate is denser than mantle and it will tend to sink; a negative $\Delta\rho_{avg}$ indicates a positively buoyant plate.

From the density profiles in Figure 4.5, it can be seen that normal oceanic crust is always negatively buoyant. Negative buoyancy is also observed for an oceanic plateau with eclogitized crust, even with a HL compositional density contrast of -100 kg m^{-3}. Thus, a buoyant oceanic plate (negative $\Delta\rho_{avg}$) requires an oceanic plateau with basaltic (metastable) crust.

Figure 4.6 shows where $\Delta\rho_{avg} = 0$ kg m^{-3} for different harzburgite layer densities and widths of the frontal slab and oceanic plateau. In most models, the oceanic plateau width is 400 km, and the frontal slab width is 500 km, which gives an overall negative buoyancy ($\Delta\rho_{avg}<0$). If the frontal slab is removed through a break off, the overall buoyancy becomes positive. With no harzburgite layer, the remaining slab is only slightly positively buoyant. A highly depleted harzburgite layer (-100 kg m^{-3}) has a greater buoyancy, and in our models, this is sufficient to flatten the slab trajectory. We also observe a flat slab with an 800 km wide plateau comprised only of metastable crust (Fig. 3.19). The greater plateau width increases the buoyancy of the slab, and this is enough for flat subduction to develop following break-off of the frontal slab.
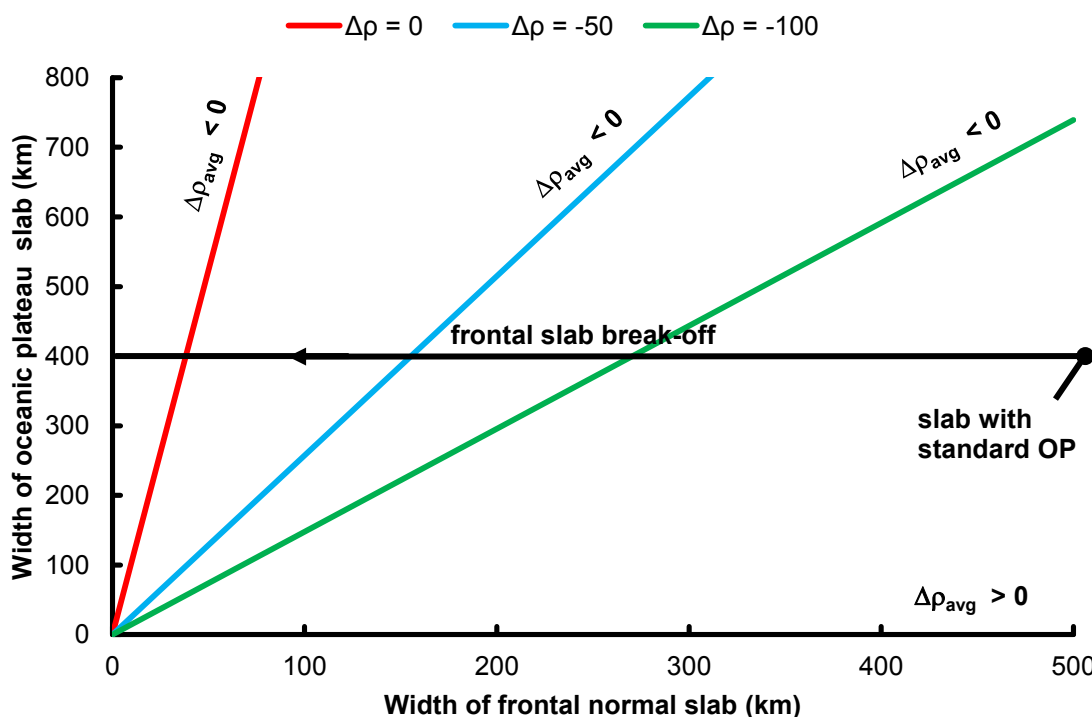
Fig. 4.6. Slab buoyancy calculations for different widths of the oceanic plateau (OP) and frontal normal slab, assuming a basaltic OP crust. The lines show where $\Delta\rho_{avg}=0$ kg m^{-3} for different compositional densities of the harzburgite layer ($\Delta\rho$ in kg m^{-3}). The slab is positively buoyant above the lines and negatively buoyant below them.

Overall, these first-order calculations confirm the results of the numerical models. In order to create a flat slab, the oceanic plate must be more buoyant than mantle so that it will upwell and bend into a sub-horizontal trajectory. This requires removal of the dense frontal slab, as well as the presence of a low-density oceanic plateau with basaltic crust.

4.4 Comparison to previous flat-slab models

There have only been a few previous numerical modeling studies of the development of flat subduction, and none of these have addressed the detailed dynamics of the Farallon plate. The models in our study show both similarities and differences to these earlier studies.

As in our study, previous work (e.g., van Hunen et al., 2004) has concluded that a necessary condition for flat subduction is a high trenchward velocity of the upper plate. The mantle wedge viscosity has also been shown to be important. Manea and Gurnis (2007) demonstrated that a flat slab can be created if the mantle wedge has a viscosity of 10^{21} Pa s or greater at a depths of <200 km. We also observe this, although a viscosity of 10^{22} Pa s is required in our models; this may be due to the fact that our models use a cooler (denser) oceanic plate. As argued in Chapter 3, these viscosities are probably too high if the mantle wedge is hydrated.

A further requirement for flat subduction in our models is the presence of a buoyant oceanic plateau, in which the oceanic plateau crust remains less dense than sublithospheric mantle during subduction. In our models, we allowed complete metastability of basaltic plateau crust. Others have also found that thick oceanic crust can induce flat subduction, as long as its density remains low due to either a kinetic delay in the basalt to eclogite transition (e.g., Pennington, 1984; van Hunen et al., 2004) or if there is only partial eclogitization (Arrial and Billen, 2013). The common conclusion is that an oceanic plateau can not be extensively eclogitized if it is to induce flat subduction. Therefore the phase transformation must be hindered as the crust enters the eclogite stability field (Figure 2.2). One possibility is that there is not sufficient water within the plateau to trigger this metamorphic phase change (e.g., Leech 2001).

An additional source of buoyancy for the oceanic plateau can be a harzburgite layer immediately below the crust, created by high degrees of mantle melting. A harzburgite layer was tested by

van Hunen et al. (2002; 2004) and they showed that flat subduction could arise if the harzburgite density if 77 kg m^{-3} less than undepleted mantle, which is similar to the 50-100 kg m^{-3} density difference tested in our models. We also found that flat subduction could be created without a harzburgite layer, if the plateau was 800 km wide. This result is consistent with that of Arrial and Billen (2013) who conclude that the width of a plateau strongly affects the slab dip angle.

The most important difference between our work and previous studies is that we have focused on subduction of an old (>100 Ma) oceanic plate. Previous studies have used much younger plates, such as 30 Ma (Manea and Gurnis, 2007), 40-60 Ma (Arrial and Billen, 2013), 44 Ma (van Hunen et al., 2002a, 2002b) and 22-45 Ma (van Hunen et al., 2004). A young oceanic plate will be warmer and therefore less dense. The lower density means that it may be easier for the slab to be deflected into a flat geometry. In addition, the warmer slab will be weaker, which will make it easier to bend upward. As a result, the geometry of a younger slab may be more sensitive to the slab suction force (due to a high mantle wedge viscosity), as concluded in earlier work (van Hunen et al, 2002b, 2004; Manea and Gurnis, 2007). In contrast, we find that the slab suction force has a relatively minor effect on an old, dense slab, unless the mantle wedge viscosity is unreasonably high. An additional effect that was tested in our models was the enhanced suction force due to thick Colorado Plateau lithosphere. O'Driscoll et al. (2009) proposed that this may induce flat subduction, but our models show that it can only produce a small decrease in slab dip.

Overall, in order to create flat subduction of an old oceanic plate, the slab buoyancy must be low. This depends on the structure of the oceanic plateau and the geometry of the frontal slab. Our models show that flat subduction is hindered if there is a long dense slab that has been subducted in front of the plateau. A transition to flat subduction requires that removal of this slab through a break-off. As far as we are aware, our study is the first to demonstrate the importance of a slab break-off in creating flat subduction. Arrial and Billen (2013) also observed a slab break-off and a transition to flat subduction in models with a wide, and thick oceanic plateau, but this was not a necessary condition for flat subduction. In addition, van Hunen (2002a, 2002b, 2004) found that an oceanic plateau could create flat subduction of a young oceanic plate, without a slab break-off.

4.5 Preferred model for Farallon Plate subduction dynamics

Several of the numerical models in this study show the development of flat slab subduction. Of these, we have chosen Model K-d (Table 3.2; Fig. 3.24d-f) as our preferred model, as it best fits the geological observations for the western US (Fig. 4.7). In this model, the oceanic plateau is 400 km wide with 18 km thick metastable crust (i.e., basaltic) and underlying 36-km-thick harzburgite layer with 100 kg m^{-3} less dense than ambient mantle. It also includes a weak zone (red block) at the front of plateau (red block), which aids in the slab break-off process.

Fig. 4.7a shows the model as the oceanic plateau enters the trench. We take this as 90 Ma in geological time, based on plate reconstructions which show that this is the time that the Shatsky Ridge conjugate plateau entered the subduction zone (Liu, et al., 2010). At this time, the slab still has a relatively steep dip, which is consistent with observations of an active Sierran volcanic arc (Chen and Moore, 1982). With a continental velocity of 4 cm/yr, the slab dip decreases. Over the next 6 Ma, slab shallowing causes the arc front (defined by the 1200°C isotherm in the models) to migrate landward at ~15 km/Myr (Fig. 4.7b). This is similar to the rate of arc migration inferred from the geological record (e.g., Coney and Reynolds, 1977). At this point, the numerical models exhibit a slab break-off, which aids in further slab shallowing. The mantle wedge below California is progressively shrinks, and the models predict that overlying continental lithosphere is cooled and that California arc would have completely shut down by 80 Ma (Fig. 4.7c). This agrees with the time of the Sierran arc shut down from isotopic dating (Chen and Moore, 1982). In addition, thermochoronogic data record a decrease in shallow crustal temperatures across the western US in the Late Cretaceous (Dimitru et al., 1991).

At 80 Ma, the slab encounters the edge of the Colorado plateau (Fig. 4.7c) and by 76 Ma; a subhorizontal geometry develops (Fig. 4.7d). At this time, the oceanic plateau is located beneath the Colorado Plateau, which matches the reconstructed position of the Shatsky conjugate at this time (e.g., Liu, et al., 2010). The model predicts that the flattening slab shears off the lower ~40 km of the Colorado Plateau lithosphere. At 70 Ma, the slab tip advances 400 km to fully underlie the Rocky Mountain foreland (Fig. 4.7e). This is less than the expected 600 km of advance expected based on a convergence velocity of 10 cm/yr. It appears that some convergence has resulted in thickening of the slab tip, as well as ~100 km of shortening at the seaward side of the

Colorado plateau. In the geological record, this time corresponds with the Laramide orogeny, which resulted in basement-involved thrusts in the Rocky Mountain foreland (e.g. Dickinson and Snyder, 1979; Bird, 1988). In the models, there is no deformation in this region; this is likely because the materials in the models have a strong rheology.

Overall, the models show the evolution of Farallon plate subduction from a steep angle (Fig. 4.7a) to flat subduction (Fig. 4.7d) over 20 Ma, and the models are consistent with geological observations for the western US in the Late Cretaceous. The flat slab segment underthrusts the continent at ~200 km depth, extending >1500 km inboard of the trench and coincident with the location of the Laramide orogeny. Therefore, the models have been successful in demonstrating the feasibility of a Farallon flat slab at the time of the Laramide orogeny. Further work is needed to understand how flat slab subduction could have triggered Laramide-style deformation in the continent.

Another interesting topic is the evolution of the western US following the Laramide orogeny. Fig. 4.7f shows a schematic diagram of how the subduction zone could have evolved in the Cenozoic (<65 Ma). The most dramatic feature is the removal of the flat slab. This must have happened since 70 Ma because seismic tomography images show that the western US upper mantle has anomalously slow velocities and a relatively thin lithosphere (<100 km thick) at present-day (e.g., Sigloch et al., 2008). In addition, the western US experienced widespread magmatism between 50 and 20 Ma, as well as regional uplift and extension (e.g., Humphreys, 1995). The magmatism may be the result of rapid heating of the continental lithosphere following removal of a flat slab. The degree of melting could have been enhanced if the continental lithosphere had been hydrated by fluids released from the Farallon plate. Additional numerical models are needed to study the dynamics of the removal process. For example, did the flat slab break below California and fall sub-vertically in the mantle (Fig. 4.7f) or did the flat slab progressively detach from the continental lithosphere through "roll back" in which the slab remained coherent (e.g., Fan and Carrapa, 2014). Also, what triggered the removal of the flat slab? One possibility is that the metastable oceanic plateau crust underwent eclogitization, which caused a rapid increase in the density of the flat slab.
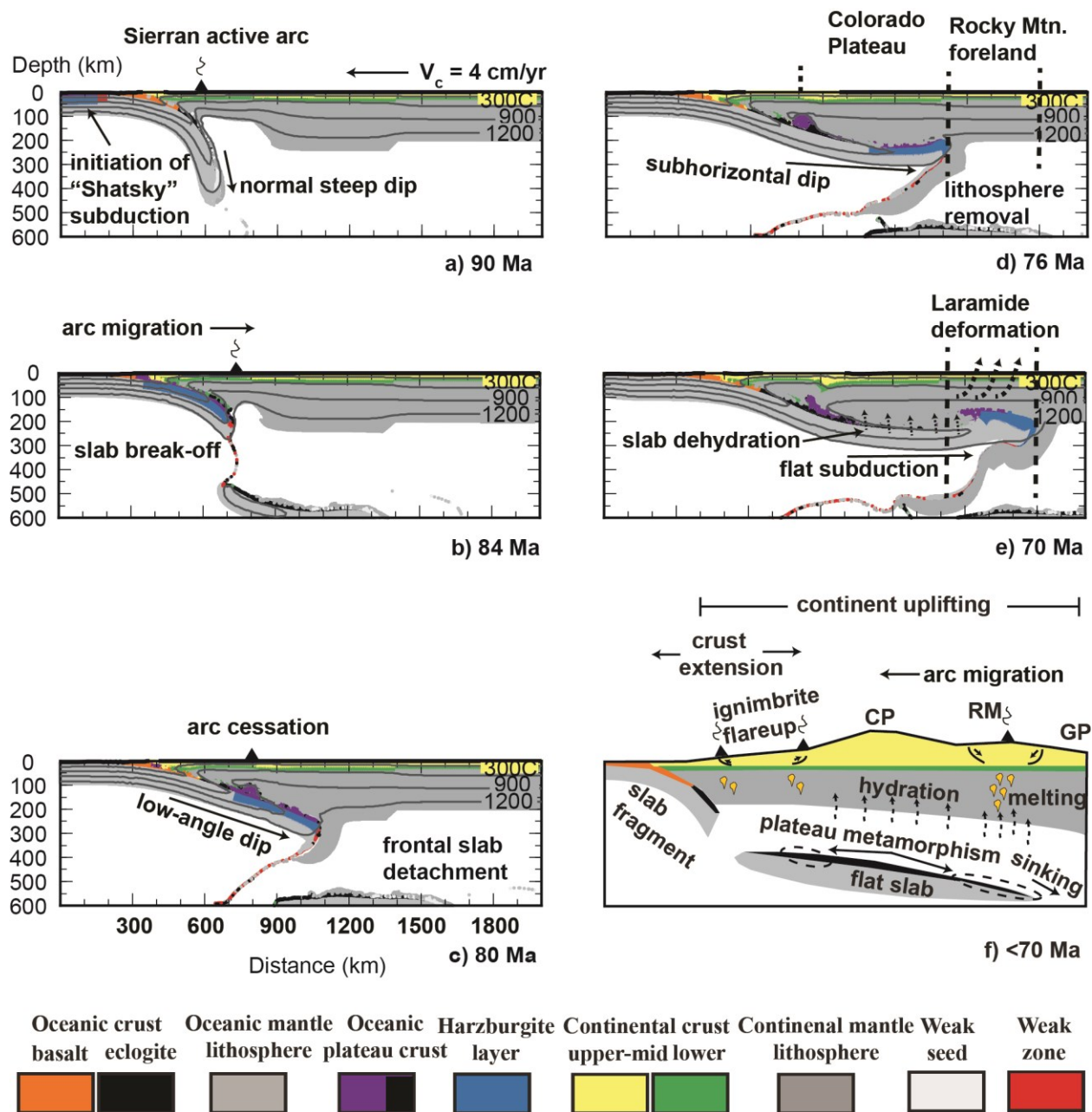
Fig. 4.7. Evolution of preferred model (Model K-d, Table 3.2) at geological time: a) 90 Ma, b) 84 Ma, c) 80 Ma, d) 76 Ma, and e) 70 Ma. (f) a schematic cross-section of Farallon plate removal in the Cenozoic (<65 Ma).

4.6 Model limitations

The main conclusions in this study are derived from a series of numerical models. Although the modeling approach uses established methods and parameters for studying lithosphere dynamics,

it is important to recognize that numerical models are simplifications of the real world. For example, the model results depend on the assigned material properties, which are often only approximately known and which may not reflect the complexity that occurs in nature (e.g., the entire 25 km thick upper crustal block has the same material properties, whereas real upper crust contains significantly heterogeneities). Four additional limitations in the numerical models are:

Constant parameters. The age of the oceanic plate and the oceanic and continental plate velocities are held constant for the duration of each numerical experiment. However, plate reconstructions show that these parameters varied through the Cretaceous and Paleocene (e.g., Engebretson et al., 1984; Figure 1.5). In particular, the rate of North America motion increased and the age of the Farallon plate decreased. Both factors may accelerate the process of slab shallowing. In addition, the North America plate had a westward velocity of ~1.5 cm/yr in the Early Cretaceous (prior to slab shallowing), whereas the numerical models have no continental plate motion in Phase II. Therefore the initial geometry of our oceanic plate may be too steep. If the actual plate motions and oceanic plate age were used, flat subduction may be observed for a wider parameter range (e.g., oceanic plateau density) than we have found. This should be tested in future work. In addition, the use of the actual velocities will allow a more direct comparison between the timing of model events and the geological record.

2D model geometry. All the numerical models use a 2D model domain with the assumption of plane strain. This means that the subduction zone is assumed to have an infinite extent perpendicular to the model plane. This is probably a suitable for the Cretaceous Farallon subduction margin, which had an along-strike length >10,000 km (Schellart et al., 2010). However, this may not be reasonable for oceanic plateau subduction, as most oceanic plateaus have an along strike width <1000 km (Arrial and Billen, 2013). For our study region, Saleeby et al. (2003) suggest that the width of the Shatsky Ridge conjugate plateau was 500 km. Three-dimensional analog (water tank) models show that a narrow plateau may not be able to induce flat subduction, as this buoyant region is pulled downward by the denser plate on either side (Martinod et al., 2005). To date, this is the only 3D study of flat subduction, and therefore much more work is needed to understand this process in 3D.

Closed bottom boundary. The bottom of the model domain is a closed boundary at 660 km depth. Thus, the oceanic plate remains in the upper mantle, and the models show that if it encounters the bottom boundary at a near-vertical angle, the slab folds on itself. We did not observe a large change in the dip angle at depths <200 km, but it is still not clear whether this boundary creates some unwanted effects on slab dynamics. In many real subduction zones, the subducting slab penetrates into the lower mantle (Turcotte and Schubert, 2002). Seismic tomography observation also indicates that parts of the Farallon plate currently reside in the lower mantle under eastern North America (e.g., Bunge and Grand, 2000). The effect of a lower mantle should be examined in future models. Such models should also include phase changes within the mantle transition zone, as these affect the viscosity and density structure of the mantle.

Stationary upper mantle. In our models, the oceanic and continental plates are assumed to be moving relative to a stationary upper mantle. In reality, the upper mantle is undergoing convection (e.g., Turcotte and Schubert, 2002). Although it is generally believed that subduction corresponds to a down-welling current, there could be cases where the subducting plate cuts through a large-scale current. The net motion between the lithosphere and upper mantle creates a "mantle wind". If the mantle wind is in the direction of subduction, it will push on the bottom of the oceanic plate, which may help create flat subduction (Fig. 4.8).
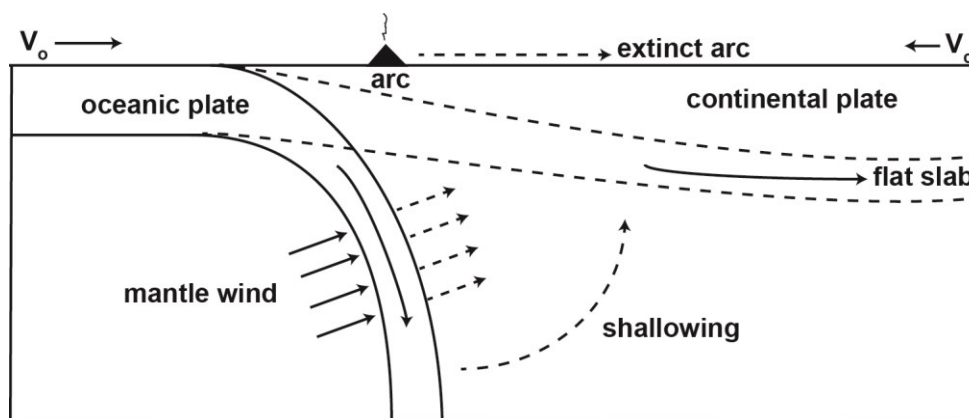
Fig. 4.8. Sketch of the mantle wind hypothesis. V_o and V_c are absolute velocities of the oceanic plate and continent plate (relative to an assumed stationary lower mantle). Motion of the upper mantle to the right (relative to the lower mantle) creates a mantle wind which acts to shallow the oceanic plate.

CHAPTER 5

Conclusions

5.1 Evolution of Farallon Plate subduction

Farallon Plate subduction has played a key role in the geological evolution of the Western United States (US) over the last 180 Ma. This thesis addresses Farallon Plate dynamics in the Late Cretaceous. At this time, the geological record shows a change in continental deformation, distribution of volcanism and subsidence of western North America (e.g., Dickinson, 2004; DeCelles, 2004). In particular, this marks the initiation of the Laramide orogeny in the continental interior. These events are interpreted to reflect a change in Farallon Plate geometry from a normal (steep) angle to flat (sub-horizontal) (e.g., Dickinson and Snyder, 1978; Bird, 1988). Throughout this transition, the Farallon plate age was >100 Ma, meaning that it was cold and thus denser than the mantle. Three factors have been proposed for causing the subduction geometry to evolve from steep to flat: (1) an increase in the westward (trenchward) velocity of the North America plate, (2) slab suction forces enhanced by the presence of thick Colorado Plateau (CP) lithosphere, and (3) subduction of a low-density oceanic plateau. The numerical models in this study systematically investigate the effect of these factors on the subduction geometry and assess the conditions needed to create flat subduction. The main conclusions are:

1. **Controls on subduction angle.** All three factors cause the subduction angle to decrease over time. The trenchward continental velocity (V_c) has the greatest effect on deep slab dip (α_d), with a negative correlation between α_d and V_c. The effect of enhanced slab suction due to a thick continental lithosphere (i.e., CP) is relatively minor in the models. This is likely because the mantle wedge viscosity is ~10^{19} Pa s, and therefore the dynamic pressure is insufficient to overcome the negative buoyancy of the slab. To

significantly decrease the dip, a viscosity of 10^{22} Pa s or greater is needed. This is inconsistent with observations that indicate a low mantle viscosity in most subduction zones (e.g., Dixon et al., 2004). Oceanic plateau subduction produces a slight decrease in subduction angle, but this is short-lived owing to the transient nature of this feature. The amount of shallowing increases slightly for a more buoyant oceanic plateau (for example, if the basaltic plateau crust is metastable or there is a low-density layer of depleted mantle (harzburgite) below the plateau crust).

2.   Transition to flat subduction. None of the individual factors can create flat subduction within 30 Ma on their own; multiple factors are required. In the successful models of flat subduction, the subduction zone evolves in two stages. First, the slab develops a low-angle geometry. The most effective way to do this is with trenchward continental plate motion. Second, the slab undergoes a break-off and then transitions to a flat geometry. This is induced by subduction of an oceanic plateau containing thick basaltic crust and/or a harzburgite layer. As the plateau is subducted, a break-off occurs at its landward side due to the competing buoyancy forces of the low-density plateau (which tends to float) and high-density frontal slab (which tends to sink). The break-off removes the dense frontal slab, and the subduction zone then evolves into flat subduction if the plateau (which now forms the slab tip) is buoyant enough to pull the slab upward to a subhorizontal trajectory. The required buoyancy depends on the slab depth and dip angle at the time of the break-off; a low-angle slab requires a less buoyant plateau.

3.   Depth of the flat slab. Flat subduction is observed at depths of 100-400 km in the models. The depth depends on both the buoyancy of the oceanic plateau and the thickness of the overlying continental lithosphere. If the oceanic plateau is much more buoyant than the mantle, it will upwell until it encounters the base of the strong continental lithosphere (100-200 km depth). The slab displaces the lower 20-40 km of the continental lithosphere as it flattens but is prevented from further shallowing by the strong rheology used in the models.

4.   Application to the western US. The models in this study demonstrate that it is possible that the old, dense Farallon Plate developed flat-slab geometry in the Late

Cretaceous. This requires: (1) trenchward continental motion, (2) subduction of a buoyant oceanic plateau in which the thick crust does not undergo eclogitization, and (3) a slab break-off at the landward side of the plateau. The first two points are consistent with plate reconstructions which show that North America accelerated to the west in the Late Cretaceous (Engebretson et al., 1984) and that a region of thick oceanic crust (the Shatsky conjugate) subducted below the proposed flat-slab region between 90 and 70 Ma (Liu et al., 2010). The third point is a model prediction. Some support for Farallon plate fragmentation comes from seismic tomography images which show that the subducted Farallon plate is not a continuous body at present-day (e.g., Sigloch et al., 2008; Sigloch and Mihalynuk, 2013).

5.2 Future work

Section 4.5 presents our preferred model for Farallon flat-slab subduction, which matches the key geological events in the western US to first order (Fig. 4.7). A more detailed comparison between the model predictions and geological observations is needed. For example, the evolving thermal structure of the models should be compared with thermochronologic data shows that the lithosphere below California and the Colorado Plateau was cooled from the Late Cretaceous to Early Tertiary (Dimitru et al., 1991). The model thermal structure could also be used to predict where hydrous phases within the oceanic plate will break down and release fluids into the overlying material. This has implications for the hydration state of the North American lithosphere and the spatial distribution of hydration-induced magmatism (e.g., Humphreys et al., 2003). In addition, the numerical models have a free top surface and therefore they can be used to examine the evolution of surface topography during slab flattening. This should be compared with the geological record of surface subsidence in the Western Interior Seaway (e.g., DeCelles, 2004).

In Section 4.6, several limitations of the models were noted, including the fact that the models use an impermeable boundary at 660 km depth and constant plate parameters

(oceanic and continental velocity, oceanic plate age). Future studies should examine the effect of these assumptions by constructing models that extend into the lower mantle (with a realistic viscosity/density structure for the mantle) and that use temporal variations in plate parameters based on plate reconstructions (e.g., Fig. 1.4). Full three-dimensional models that include a convecting mantle should also be considered.

This study has focused on the development of Farallon flat subduction, which is proposed to be the cause of the enigmatic Laramide Orogeny (Dickinson and Snyder, 1978; Bird, 1988). Although the models are successful in creating Farallon flat subduction, there is little deformation in the Southern Rocky Mountain foreland crust in the models (e.g., Fig. 4.6). This is because the models use a strong rheology for the continental lithosphere. The next generation of models should investigate variations in continental rheology, in order to explore how stresses along the subduction interface may be transmitted into the continental interior during slab flattening. Will this create Laramide-style deformation?

Finally, the modeling approach used here can be applied to modern subduction zones with a flat slab (e.g., Peru, central Chile and central Mexico; Fig. 1.3). This would involve modifying the plate velocities and the structure of the oceanic and continental plates to create site-specific models for each region. One key difference between these areas and the western US study area is that the oceanic plate is much younger (20-50 Ma vs. >100 Ma). As a result, the oceanic plate will be warmer and therefore more buoyant and weaker, which may enable flat subduction to develop more easily.

Bibliography

Abers, G.A., van Keken, P.E., Kneller, E.A., Ferris, A., and Stachnik, J.C., (2006), The thermal structure of subduction zones constrained by seismic imaging: implications for slab dehydration and wedge flow, *Earth Planet Sci. Lett.*, *241*, 387-397.

Arrial P.A., and Billen, M.I., (2013), Influence of geometry and eclogitization on oceanic plateau subduction, *Earth Planet. Sci. Lett.*, *363*, 34-43.

Austrheim, H., (1991), Eclogite formation and dynamics of crustal roots under continental collision zones, *Terra Nova*, *3*, 492–499.

Austrheim, H., Erambert, M., and Engvik, A.K., (1997), Processing of crust in the root of the Caledonian continental collision zone: the role of eclogitization, *Tectonophysics*, *273*, 129–153.

Bally, A.W., Scotese, C.R., and Ross, M.L., (1989), North America; Plate-tectonic setting and tectonic elements, in Bally, A.W., and Palmer, A.R., eds., *The Geology of North America- An overview,* Boulder, Colorado, Geological Society of America, The Geology of North America, v. A., USA.

Beaumont, C., Kamp, P.J.J., Hamilton, J., and Fullsack, P., (1996), The continental collision zone, South Island, New Zealand: Comparison of geodynamical models and observations, *J. Geophys. Res.*, *101*, 3333-3359.

Beaumont, C., Nguyen, M., Jamieson, R., and Ellis, S., (2006), Crustal flow modes in large hot orogens. In: Law, R.D., Searle, M.P., Godin, L. (Eds.), *Crustal Flow, Ductile Extrusion and Exhumation in Continental Collision Zones,* Geol. Soc. Spec. Publ., 268, 91-145.

Billen, M.I., and Gurnis, M., (2001), A low velocity wedge in subduction zones, *Earth Planet. Sci. Lett.*, *193*, 227-236.

Bird, P., (1979), Continental delamination and the Colorado Plateau, *J. Geophys. Res.*, *84*, 7561-7571.

Bird, P., (1988), Formation of the Rocky Mountains, western United States: a continuum computer model. *Science*, *239*, 1501-1507.

Bousquet, R., Goffé, B., Henry, P., Le Pichon, X., and Chopin, C., (1997), Kinematic, thermal and petrological model of the Central Alps: lepontine metamorphism in the upper crust and eclogitization of the lower crust, *Tectonophysics*, *273*, 105-127.

Buiter, S.J.H., Babeyko, A.Y., Ellis, S., Gerya, T.V., Kaus, B.J.P., Kellner, A., Schreurs, G., and Yamada, Y., (2006), The numerical sandbox: comparison of model results for a shortening and an extension experiment. In: Buiter, S., Schreurs, G. (Eds.), *Analogue and Numerical Modelling of Crustal Scale Processes*, Geological Society of London, Special Publication, 253, 29–64.

Bunge, H.-P., and Grand, S.P., (2000), Mesozoic plate-motion history below the northeast Pacific Ocean from seismic images of the subducted Farallon slab, *Nature*, *405*, 337-340.

Chapman, D.S., (1986), Thermal gradients in the continental crust, The Nature of the Lower Continental Crust, J. B. Dawson, et al., *Geol. Soc. Spec. Publ.*, *24*, 63-70.

Chen, J.H., and Moore, J.G., (1982), Uranium-lead isotopic ages from the Sierra Nevada batholith, California, *J. Geophys. Res.*, *87*, 4761-4784.

Christensen, U.R., (1996), The influence of trench migration on slab penetration into the lower mantle, *Earth Planet. Sci. Lett., 140*, 27-39.

Cloos, M., (1993), Lithospheric buoyancy and collisional orogenesis: subduction of oceanic plateaus, continental margins, island arcs, spreading ridges and seamounts, *Geol. Soc. Am. Bull.*, *105*, 715-37.

Coney, P.J., (1978), Mesozoic-Cenozoic Cordilleran plate tectonics, Cenozoic Tectonics and regional geophysics of western Cordillera, *Geol. Soc. Am. Mem.*, *152*, 33-50.

Coney, P.J., and Reynolds, S.J., (1977), Cordilleran Benioff zones, *Nature*, *270*, 403-406.

Craig, C.F., and McKengie, D., (1986), The experience of a thin low-viscosity layer beneath the lithosphere, *Earth Planet. Sci. Lett.*, *78*, 420-426.

Cross, T.A., and Pilger JR, R.H., (1978), Tectonic controls of Late Cretaceous sedimentation, western interior, U.S.A., *Nature*, *274*, 653-657.

Currie, C.A., (2004), The thermal structure of subduction zones and backarcs, Ph.D. thesis, *Chapter 3: Backarc Thermal Structure I- The Cascadia Subduction Zone*, University of Victoria, Victoria, British Columbia, Canada.

Currie, C.A., and Hyndman, R.D., (2006), The thermal structure of subduction zones back arcs, *J. of Geophys. Res.*, *111*, B08404, doi: 10.1029/2005JB004024.

Currie, C.A., Beaumont, C., and Huismans, R.S., (2007), The fate of subducted sediments: A case for backarc intrusion and underplating. *Geology*, *35*, 1111-1114.

Currie, C.A., and Beaumont, C., (2011), Are diamond-bearing Cretaceous kimberlites related to low-angle subduction beneath western North America? *Earth Planet. Sci. Lett.*, *303*, 59-70.

Dahlen, F.A., (1984), Noncohesive critical Coulomb wedges: An exact solution, *J. Geophys. Res.*, *89*, 10125-10133.

Dalziel, I.W.D., (1992b), On the organization of American plate in the Neoproterozoic and the breakout of Laurentia: *GSA Today*, *2* (11), 237-241.

Davies, G.F., and Richards, M.A., (1992), Mantle convection, *J.Geol.*, *100*, 151-206.

DeCelles, P.G., (2004), Late Jurassic to Eocene evolution of the Cordilleran thrust belt and foreland basin system, western U.S.A., *Am. J. Sci.*, *304*, 105-168.

DeCelles, P.G., Ducea, M.N., Kapp, P., and Zandt, G., (2009), Cyclicity in Cordilleran orogenic systems, *Nat. Geosci., 2*, 251-257.

Dumitru, T.A., (1991), Effects of Subduction Parameters on Geothermal Gradients in Forearcs, With an Application to Franciscan Subduction in California, *J. Geophys. Res.*, *96*, 621-641.

Dumitru, T.A., Gans, P.B., Foster, D.A., and Miller, E.L., (1991), Refrigeration of the western Cordilleran lithosphere during Laramide shallow-angle subduction, *Geology*, *19*, 1145-1148.

Dickinson, W.R., (2002), The Basin and Range Province as a composite extensional domain, *Int. Geol. Rev.*, *44*, 1-38.

Dickinson, W.R., (2004), Evolution of the North American Cordillera, *Annu. Rev. Earth Planet. Sci.*, *32*, 13-45.

Dickinson, W.R., and Snyder, W.S., (1978), Plate tectonics of the Laramide orogeny. In: Matthews, V. (Ed.), Laramide folding associated with basement block faulting in the western United States: *Geol. Soc. Am. Mem.*, *151*, 355-366.

Dixon, J.E., Dixon, T.H., Bell, D.R., and Malservisi, R., (2004), Lateral variation in upper mantle viscosity: role of water, *Earth Planet. Sci. Lett.*, *222*, 451-467.

Engebretson, D.C., Cox, A., and Thompson, G.A., (1984), Correlation of plate motions with continental tectonics: Laramide to Basin-range, *Tectonics*, *3*(2), 115-119.

English, J.M., and Johnston, S.T., (2004), The Laramide Orogeny: What Were the Driving Forces? *Int. Geol. Rev.*, *46*, 833-838.

English, J.M., Johnston, S.T., and Wang, K., (2003), Thermal modelling of the Laramide orogeny: testing the flat-slab subduction hypothesis, *Earth Planet. Sci. Lett.*, *214*, 619-632.

Erslev, E.A., (1993), Thrusts, back-thrusts, and detachment of Rocky Mountain foreland arches, in Schmidt, C.J., Chase, R.B., and Erslev, E.A., eds., *Laramide Basement Deformation in the Rocky Mountain Foreland of the Western United States*: Boulder, Colorado, Geological Society of America Special Paper 280 Edited by: Schmidt, C. J., Chase, R. and Erslev, E. A., 339-358.

Erslev, E.A., (2005), 2D Laramide geometries and kinematics of the Rocky Mountain region, in Karstrom, K.E., and Keller, G.R., eds., *The Rocky Mountain Region- An Evolving Lithosphere*: Tectonics, Geochemistry and Geophysics, Washington, D.C., American Geophysical Union, 7-20.

Fan M., and Carrapa, B., (2014), Late Cretaceous-early Eocene Laramide uplift, exhumation, and basin subsidence in Wyoming: Crustal responses to flat slab subduction, *Tectonics*, *33*, 509-529, doi: 10.1002/2012TC003221.

Figge, J., (2009), Evolution of the Pacific Northwest: An introduction to the Historical Geology of Washington State and Southern British Columbia, North Seattle Community College, USA: The Northwest Geological Institute.

Fullsack, P., (1995), An arbitrary Lagrangian-Eulerian formulation for creeping flows and its application in tectonic models, *Geophys. J. Int.*, *120*, 1-23.

Gerya T.V., S and toeckhert, B., (2002), Exhumation rates of high pressure metamorphic rocks in subduction channels: the effect of Rheology. *Geophys. Res. Let.*, *29*(8), doi: 10.1029/2001GL014307.

Gleason, G.C., and Tullis, J., (1995), A flow law for dislocation creep of quartz aggregates determined with the molten salt cell, *Tectonophysics*, *247*, 1-23.

Grand, S.P., and Helmberger, D., (1984), Upper mantle shear structure of North America, *Geophys. J. R. Astron. Soc.*, *76*, 499-438.

Griffin, W.L., O'Reilly, S.Y., Doyle, B.J., Pearson, N.J., Coopersmith, H., Kivi, K., Malkovets, V., and Pokhilenko, N., (2004), Lithosphere mapping beneath the North American plate, *Science*, *77*, 873-922

Grove, T. L., Chatterjee, N., Parman, S. W., and Medard, E., (2006), The influence of H_2O on mantle wedge melting, *Earth Planet. Sci. Lett.*, *249*, 74-89.

Goes, S., (2013), Western North America's jigsaw, *Nature, 496*, 35-37.

Guillou-Frottier, L., Buttles, J., and Olson, P., (1995), Laboratory experiments on the structure of subducted lithosphere, *Earth Planet. Sci. Lett., 133*, 19-34.

Gutscher, M.A., Spakman,W., Bijwaard,H., and Engdahl,E.R., (2000), Geodynamics of flat subduction: seismicity and tomographic constraints from the Andean margin. *Tectonics*, *19*, 814-833.

Hacker, B.R., Abers,G.A., and Peacock,S.M., (2003), Subduction factory 1. Theoretical mineralogy, densities, seismic wave speeds, and H_2O contents, *J. Geophys. Res.*, *108* (B1), 2029, doi: 10.1029/2001JB001127.

Henderson, L.J., Gordon, R.G., and Engebretson, D.C., (1984), Mesozoic aseismic ridges on the Farallon plate and southward migration of shallow subduction during the Laramide orogeny, *Tectonics*, *3*, 121-132.

Hirth, G., and Kohlstedt, D.L., (2003), Rheology of the upper mantle and the mantle wedge: a view from the experimentalists, in Inside the Subduction Factory, ed. J. Eiler, *Geophysical Monograph American Geophysical Union, Washington, D.C., 138*, 83-105.

Huismans, R., and Beaumont, C.H., (2003), Symmetric and asymmetric lithospheric extension; relative effects of frictional-plastic and viscous strain softening, *J. Geophys. Res., 108*, doi:10.2029/2002JB002026.

Humphreys, E.D., (1995), Post-Laramide removal of the Farallon slab, western United States, *Geology*, *23* (11), 987-990.

Humphreys, E.D., (2009), Relation of flat subduction to magmatism and deformation in the western United States, *Geol. Soc. Am. Mem.*, *204*, 85-98.

Humphreys, E.D., Hessler, E., Dueker, K., Erslev, E., Farmer, G.L., and Atwater, T., (2003), How Laramide-age hydration of North America by the Farallon slab controlled subsequent activity in the western U.S., *Int. Geol. Rev.*, *45*, 575-595.

Ito, G., and Clift, P.D., (1998), Subsidence and growth of Pacific Cretaceous plateaus, *Earth Planet. Sci. Lett.*, *161*, 85-100.

Jaupart, C., and Mareschal, J. C., (2003), Constraints on crustal heat production from heat flow data, *Treatise on Geochemistry, The Crust*, edited by Holland, H.D., and Turekian, K.K., vol. 3, 65-84, Elsevier, New York,.

Jarrard R.D., (1986), Relations among subduction parameters, *Rev. Geophys.*, *24*, 217–284, doi: 10.1029/RG024i002p00217.

Jones, C.H., Farmer, G.L., Sageman, B., and Zhong, S.J., (2011), Hydrodynamic mechanism for the Laramide orogeny, *Geosphere*, *7*, 183-201, doi: 10.1130/GES00575.1.

Jull, M., and Kelemen, P. B., (2001), On the conditions for lower crustal convective instability, *J. Geophys. Res.*, *106*, 6423-6446.

Kanamori H., and Cipar, J.J., (1974), Focal process of the great Chilean earthquake, May 22, 1960, *Phys. Earth Planet. Inter.*, *9*, 128-136.

Kárason, H., and van der Hilst, R.D., (2000), Constraints on mantle convection from seismic tomography, in The History and Dynamics of Global Plate Motion, edited by M. A. Richards, R. Gordon, and R. D. van der Hilst, AGU, Washington, D. C., *Geophys. Monogr. Ser.*, *121*, 277–288,

Kanda, H., (2007), Laminar-turbulent transition: Calculation of minimum critical Reynolds number in channel flow, RIMS (Research Institute for Mathematical Science, Kyoto Univ.), Kokyuroku, Bessatsu B1, 199-217.

Karato, S.I., and Wu, P., (1993), Rheology of the upper mantle: a synthesis, *Science*, *260*, 771-778.

Katsura, T., and Ito, E., (1989), The system Mg_2SiO_4 - Fe_2SiO_4 at high pressures and temperatures: precise determination of stabilities of olivine, modified spinel and spinel, *J. Geophys. Res.*, *94*, 15663–15670.

Kay, S.M., and Abbruzzi, J.M., (1996), Magmatic evidence for Neogene lithospheric evolution of the central Andean "flat-slab" between 30°S and 32°S, *Tectonophysics*, *259*,15-28.

Kearey, P., Klepeis, K.A., and Vine, F., (2008), *Global Tectonics*, third edition, Blackwell Science, Oxford.

Kundu, P.J., Cohen, I.M., and Dowling, D.R., (2011), *Fluid Mechanics*, Fifth Edition, Elsevier Academic Press, Waltham, USA, 920 pp., doi: 10.1016/B978-0-12-382100-3.10018-6.

Krystopowicz, N.J., and Currie, C.A., (2013), Crustal eclogitization and lithosphere delamination in orogens, *Earth Planet. Sci. Lett.*, *361*, 195-207

Lallemand, S., Heuret, A., and Boutelier, D., (2005), On the relationships between slab dip, back-arc stress, upper plate absolute motion, and crustal nature in subduction zones, *Geochem. Geophys. Geosyst.*, *6*, Q09006, doi:10.1029/2005GC00917.

Lay, T., Kanamori, H., Ammon, C.J., Nettles, M., Ward, S.N., Aster, R.C., Beck, S.L., Bilek, S.L., Brudzinski, M.R., Bulter, R., DeShon, H.R., Ekström, G., Satake, K., and Sipkin, S., (2005), The great Sumatra-Andaman earthquake of 26 December 2004, *Science*, *308*, 1127-1133.

Leech, M.L., (2001), Arrested orogenic development: eclogitization, delamination, and tectonic collapse, *Earth Planet. Sci. Lett.*, *185*, 149-159.

Li, Z.-X.A., Lee, C.-T.A., Peslier, A.H., Lenardic, A., and Mackwell, S.J., (2008), Water contents in mantle xenoliths from the Colorado Plateau and vicinity: Implications for the mantle rheology and hydration-induced thinning of continental lithosphere. *J. Geophys. Res.*, *113*, B09210, doi: 10, 1029/2007JB005540.

Liu, L., Gurnis, M., Seton, M., Saleeby, J., Müller, R.D., and Jackson, J.M., (2010), The role of oceanic plateau subduction in the Laramide orogeny, *Nature Geosci.*, 3, 353-357.

Livaccari, R.F., Burke, K., and Sengor, A.M.C., (1981), Was the Laramide orogeny related to subduction of an oceanic plateau? *Nature*, *289*, 276-278.

Livaccari, R.F., and Perry, F.V., (1993), Isotopic evidence for preservation of Cordilleran lithospheric mantle during the Sevier-Laramide orogeny, western United States, *Geology*, *21*, 719-722.

Mackwell, S.J., Zimmerman, M.E., and Kohlstedt, D.L., (1998), High temperature deformation of dry diabase with application to tectonics on Venus, *J. Geophys. Res.*, *103*, 975-984.

Manea, V., and Gurnis, M., (2007), Subduction zone evolution and low viscosity wedges and channels, *Earth Planet. Sci. Lett.*, *264*, 22-45.

Manea, V., Pérez-Gussinyé, M., and Manea, M., (2012), Chilean flat slab subduction controlled by overriding plate thickness and trench rollback, *Geology*, *40*, 35-38.

Mann, P., and Taira, A., (2004), Global tectonic significance of the Solomon Islands and Ontong Java Plateau convergent zone, *Tectonophysics*, *389*, 137-190.

Martinod, J., Funiciello, F., Faccenna, C., Labanieh, S., and Regard, V., (2005), Dynamical effects of Subducting ridges: insights from 3-D laboratory models, *Geophys. J. Int.*, *163*, 1137-1150.

Maxson, J., and Tikoff, B., (1996), Hit-and-run collision model for the Laramide orogeny, western United States, *Geology*, *24*, 968-972.

Mitrovica, J.X., Beaumont, C., and Jarvis, G.T., (1989), Tilting of continental interiors by the dynamical effects of subduction, *Tectonics*, *8*, 1079-1094.

Mooney, W.D., and Weaver, C.S., (1989), Regional crustal structure and tectonics of the Pacific Coastal States; California, Oregon, and Washington, In: Pakiser L.C., Mooney W.D. eds., Geophysical framework of the continental United States, *GSA Mem.*, *172*, 129-162.

Morgan, P., and Swanberg, C. A., (1985), On the Cenozoic uplift and tectonic stability of the Colorado Plateau, *J. Geodyn.*, *3*, 39-63.

Oldow, J.S., Bally, A.W., Ave Lallemant, H.G., and Leeman, W.P., (1989), Phanerozoic evolution of the North American Cordillera; United States and Canada, in Balley, A.W., and Palmer, A.R., eds., *The Geology Society of America-An overview:* Bolder, Colorado, Geological Society of America, The Geology of North America, v. A., USA

O'Driscoll, L.J., Humphreys, E.D., and Saucier, F., (2009), Subduction adjacent to deep continental roots: Enhanced negative pressure in the mantle wedge, mountain building and continental motion, *Earth Planet. Sci. Lett.*, *280*, 61-70.

Oxburgh, E.R., and Parmentier, E.M., (1977), Compositional and density stratification in oceanic lithosphere-causes and consequences, *Jounral* o*f the Geological Society of London*, *133*, 343-355

Ozawa, S., Nishimura, T., Suito, H., Kobayashi, T., Tobita, M., and Imakiire, T., (2011), Coseismic and postseismic slip of the 2011 magnitude-9 Tohoku-Oki earthquake, *Nature*, *475*, 373-376, doi: 10.1038/nature10227.

Parsons, T., McCarthy, J., Kohler,W.M., Ammon, C.J., Benz, H.M., Hole, J.A., and Criley, E.E., (1996), Crustal structure of the Colorado Plateau, Arizona: application of new long-offset seismic data analysis techniques, *J. Geophys. Res.*, *101*, 11173-11194.

Pennington, W.D., (1984), The effect of oceanic crustal structure on phase changes and subduction, *Tectonophysics*, *102*, 377-398.

Phinney, E.J., Mann, P., Coffin, M.F., and Shipley, T.H., (2004), Sequence stratigraphy, structural style, and age of deformation of the Malaita accretionary prism (Solomon Arc– Ontong Java Plateau convergent zone), *Tectonophysics*, *389* (3-4), 221-246.

Poudjom Djomani, Y.H., O'Reilly, S.Y., Grifdin, W.L., and Morgan, P., (2001), The density structure of subcontinental lithosphere: Constraints on delamination models, *Earth Planet. Sci. Lett.*, *184*, 605-621.

Pysklywec, R.N., and Beaumont, C., (2004), Intraplate tectonics: feedback between radioactive thermal weakening and crustal deformation driven by mantle lithosphere instabilities, *Earth Planet. Sci. Lett.*, *221*, 275-292.

Pysklywec, R.N., Beaumont, C., and Fullsack, P., (2002), Lithospheric deformation during the early stages of continental collision: Numerical experiments and comparison with South Island, New Zealand, *J. Geophys. Res.*, *B 107*, doi: 10.1029/2001JB000252.

Ranalli, G., (1987), *Rheology of the Earth*, Deformation and flow processes in geophysics and geodynamics, Allen & Unwin, Boston, 386 pp.

Roth, E., Wiens, D., and Zhao, D., (2000), An empirical relationship between seismic attenuation and velocity anomalies in the upper mantle, *Geophys. Res. Lett.*, *27*, 601-604.

Roy, M., Jordan, T. H., and Pederson, J., (2009), Colorado Plateau magmatism and uplift by warming of heterogeneous lithosphere. *Nature*, *459*, 978-982.

Saleeby, J., (2003), Segmentation of the Laramide slab-evidence from the southern Sierra Nevada region. *Geol. Soc. Am. Bull.*, *115*, 655-668.

Saleeby, J., Ducea, M., and Clemens-Knott, D., (2003), Production and loss of high-density batholithic root, southern Sierra Nevada, California, *Tectonics*, *22*(6), 1064, doi:10.1029/2002TC001374.

Schellart, W.P., (2005), Influence of the subducting plate velocity on the geometry of the slab and migration of the subduction hinge, *Earth Planet. Sci. Lett., 231*, 197-219.

Schellart, W.P., (2008), Subduction zone trench migration: slab driven or overriding-plate-driven? *Phys. Earth Planet. Inter.*, *170*, 73-88.

Schellart, W.P., Stegman, D.R., Farrington, R.J., Freeman, J., and Moresi, L., (2010), Cenozoic tectonics of Western North America controlled by evolving width of Farallon slab, *Science*, *329*, 316-319, doi: 10. 1126/science. 1190366.

Schmidt, M.W., and Poli, S., (1998), Experimentally based water budgets for dehydrating slabs and consequences for arc magma generation, *Earth Planet. Sci. Lett.*, *163*, 361-379.

Sigloch K., McQuarrie N., and Nolet G., (2008). Two-stage subduction history under North America inferred from multiple-frequency tomography, *Nature Geosci.*, *1*, 458-462, doi: 10.1038/ngeo231.

Sigloch, K., and Mihalynuk, M.G., (2013), Intra-oceanic subduction shaped the assembly of Cordilleran North America, *Nature*, *496*, 50-56.

Skinner, S.M., and Clayton, R.W., (2011), An Evaluation of proposed mechansims of slab flattening in central Mexico, *Pure Appl. Geophys.*, 168, 1461-1474.

Spencer, J. E., (1996), Uplift of the Colorado Plateau due to lithospheric attenuation during Laramide low-angle subduction, *J. Geophys. Res.*, *101*, 13595-13609.

Stein, C.A., and Stein, S., (1992), A model for the global variations in oceanic depth and heat flow with lithospheric age, *Nature*, *359*, 123–129, doi:10.1038/359123a0.

Stern, R.J., (2002), Subduction zones, *Rev. Geophys.*, *40*(4), 1012, doi: 10.1029/2001RG000108.

Stevenson, D.J., and Turner, S.J., (1977), Angle of subduction, *Nature*, *270*, 334-336.

Strak, V., and Schellart, W.P., (2014), Evolution of 3-D subduction-induced mantle flow around lateral slab edges in analogue models of free subduction analysed by stereoscopic particle image velocimetry technique, *Earth Planet. Sci. Lett., 403*, 368-379.

Smith, D., and Griffin, W.L., (2005), Garnetite xenoliths and mantle-water interactions below the Colorado Plateau, southwestern United States, *J. Petrol.*, *46*, 1902-1924.

Smith, A.G., Smith, D.G., and Funnell, B.M., (1994), *Atlas of Mesozoic and Cenozoic Coastlines*, Cambridge University Press, New York. 99 pp.

Syracuse, E.M., and Abers, G.A., (2006), Global compilation of variations in slab depth beneath arc volcanoes and implications, *Geochem. Geophys. Geosyst.*, *7*, Q05017, doi:10.1029/2005GC001045.

Tarduno, J. A., McWilliams, M., Debiche, M. G., Sliter, W. V., and Blake Jr, M. C., (1985), Franciscan Complex Calera limestones: Accreted remnants of Farallon Plate oceanic plateaus, *Nature, 317*, 345-347.

Turcotte, D. L., and Schubert, G., (2002), *Geodynamics* (second edition): Cambridge, UK, Cambridge University Press, 456 p.

van Hunen, J., van den Berg, A.P., and Vlaar, N.J., (2002a), The impact of the South-American plate motion and the Nazca Ridge subduction on the flat subduction below South Peru, *Geophys. Res. Lett.*, *29*(14), doi: 10.1029/2001GL014004.

van Hunen, J., van den Berg, A.P., and Vlaar, N.J., (2002b), On the role of subducting oceanic plateaus in the development of shallow flat subduction, *Tectonophysics*, *352*, 317-333.

van Hunen, J., van den Berg, A.P., and Vlaar, N.J., (2004), Various mechanisms to induce present-day shallow flat subduction and implications for the younger Earth: a numerical parameter study, *Phys. Earth Planet. Inter.*, *146*, 179-194

Wada, I., Rychert., C.A., and Wang, K., (2011), Sharp thermal transition in the forearc mantle wedge as a consequence of nonlinear mantle wedge flow, *Geophys. Res. Lett.*, *38*, L13308, doi: 10.1029/2011GL047705.

Ward, P.L., (1995), Subduction cycles under western North America during the Mesozoic and Cenozoic eras, in Miller, D.M., and Busby, C., *Jurassic Magmatism and Tectonics of the North American Cordillera*: Boulder, Colorado, Geological Society of America Special Paper 299.

Warren, C.J., Beaumont, C., and Jamieson, R.A., (2008), Formation and exhumation of ultra-high-pressure rocks during continental collision: Role of detachment in the subduction channel, *Geochem. Geophys. Geosyst.*, *9*, Q04019, doi: 10.1029/2007GC001839.

White, R. S., McKenzie, D., and O'Nions, R. K., (1992), Oceanic crustal thickness from seismic measurements and rare earth element inversions, *J. Geophys. Res.*, *97*, 19,683-19,715.

Willett, S.D., (1999), Rheological dependence of extension in wedge models of convergent orogens, *Tectonophysics*, *305*, 419-435.

Wilson, D., Aster, R., Ni, J., Grand, S., West, M., Gao, W., Baldridge, W. S., and Semken, S., (2005), Imaging the seismic structure of the crust and upper mantle beneath the Great Plains, Rio Grande Rift, and Colorado Plateau using receiver functions, *J. Geophys. Res*., *110*, B05306, doi: 10.1029/2004JB003492.

Wolf, L.W., and Cipar, J.J., (1993), Through thick and thin: A new model for the Colorado Plateau from seismic refraction data from Pacific to Arizona crustal experiment, *J. Geophys. Res.*, *98*, 19881-19894.

Wortel, M.J.R., Remkes, M.J.N., Govers, R., Cloetingh, S.A.P.L., and Meijer, P.T., (1991), Dynamics of the lithosphere and the intraplate stress field. *Philos. Trans. R. Soc. Lond.*, *337*, 111-126.

Zandt, G., Myers, S.C., and Wallace, T.C., (1995), Crust and mantle structure across the Basin and Range-Colorado Plateau boundary at 37°N latitude and implication for Cenozoic extensional mechanism, *J. Geophys. Res.*, *100*, 10529-10548.